Interactions between the PII protein and its receptors revealed by NanoBiT technology

Dissertation

der Mathematisch-Naturwissenschaftlichen Fakultät
der Eberhard Karls Universität Tübingen
zur Erlangung des Grades eines
Doktors der Naturwissenschaften
(Dr. rer. nat.)

vorgelegt von
Rokhsareh Rozbeh
aus Neyshaboor/Iran

Tübingen
2024

Gedruckt mit Genehmigung der Mathematisch-Naturwissenschaftlichen Fakultät der Eberhard Karls Universität Tübingen.

Tag der mündlichen Qualifikation:	23.07.2024
Dekan:	Prof. Dr. Thilo Stehle
1. Berichterstatter:	Prof. Dr. Karl Forchhammer
2. Berichterstatterin:	Prof. Dr. Christiane Wolz

Contents

ABBREVIATIONS

2-OG	2-oxoglutarate
ADP	adenosine diphosphate
amtB	ammonia transporter protein
AR	adenyl-removing
AT	adenyltransferase
ATase	adenylyltransferase
ATP	adenosine triphosphate
BLI	biolayer interferometry
CCM	CO2 concentrating mechanism
FRET	Forster resonance energy transfer
GS	glutamine synthetase
GST	glutathione S-transferase
IFs	Inactivating Factors
LB	Luria–Bertani broth
MSX	L-Methionine sulfoximine
NAG	N-acetylglutamate
NAGK	N-acetyl-L-glutamate kinase
NAG-P	N-acetyl-L-glutamyl 5-phosphate
NanoBiT	NanoLuc Binary Technology
Ni-NTA	nickel-nitrilotriacetic acid
Nluc	NanoLuc
NsiR4	nitrogen stress-induced RNA 4
NtcA	Nitrogen control transcription factor
OAC	ornithine-ammonia cycle
OUC	ornithine-urea cycle (OUC)
PCA	protein-fragment complementation assay
PEPC	Phosphoenolpyruvate carboxylase
PGAM	phosphoglycerate mutase
PirA	PII interacting regulator of arginine synthesis
PirC	PII-interacting regulator of carbon metabolism
PII-NG	PII-New Group
PII-UMP	uridylylated PII
SPR	Surface-Plasmon-Resonance
TSS	transcriptional start site
WT	wild type

I. ZUSAMMENFASSUNG

Die PII-Proteine sind bemerkenswerte Mitglieder einer großen und alten Protein-Familie, die an der Signalübertragung beteiligt sind. Diese Moleküle sind in allen lebenden Organismen zu finden und sind hauptsächlich für ihre Fähigkeit bekannt, Metaboliten wie ATP, ADP und 2-Oxoglutarat (2-OG) zu erkennen. Wenn die Effektormoleküle eine Bindung eingehen, führt dies zu mehreren strukturellen Veränderungen in den PII-Proteinen, insbesondere in ihren flexiblen T-Schleifen, die als dynamische Module für Protein-Protein-Interaktionen dienen. Die Interpretation der von PII gesendeten metabolischen Daten hängt vom Bindungszustand der Metaboliten und der resultierenden Konformation der PII-Rezeptoren ab. Um die komplexen Interaktionen zwischen PII und Zielproteinen gründlich zu untersuchen, sind analytische Methoden erforderlich, die das natürliche zelluläre Milieu aufrechterhalten. Angesichts der Einschränkungen bei alternativen Methoden wie der Immobilisierung auf Sensoroberflächen in der Surface-Plasmonen-Resonanz (SPR) und der Biolayer-Interferometrie (BLI) sowie der Verwendung großer Fluoreszenzproteine beim Förster-Resonanz-Energieübertragung (FRET) konzentrierten sich unsere Forschungsbemühungen auf die Entwicklung eines innovativen NanoBiT-Sensors. Der Schwerpunkt dieses Sensors liegt auf der Interaktion des PII-Proteins aus *Synechocystis* sp. PCC6803 mit dem PII-interagierenden Protein X (PipX), der N-Acetyl-L-Glutamat-Kinase (NAGK) und dem PII-interagierenden Regulator der Argininsynthese (PirA). Mit der NanoBiT-Technologie haben wir ein fortgeschrittenes Verständnis erlangt, das die Berechnung von K_D-Werten für die PII-NAGK- und PII-PipX-Komplexe ermöglicht, die zuvor nicht beschrieben wurden. Der Test zeigte auch ein erhöhtes Maß an Empfindlichkeit, was die Erkennung von Interaktionen mit geringer Affinität ermöglichte, wie sie zwischen der PII-S49E-Variante und NAGK beobachtet wurde. Die Studie erbrachte auch erstaunliche Beweise dafür, dass die Bildung des PII-NAGK-Komplexes durch die Anwesenheit von ADP beeinflusst wird, welches die Affinität verringelt. Zusätzliche Analysen durch die NanoBiT-Methode und enzymatische Assays lieferten weitere Belege dafür, dass der PII-NAGK-Komplex spezifische Feed-Forward-Aktivierung zeigt, die auf steigende Konzentrationen von NAG reagiert. Diese beiden Sensoren wurden ebenfalls eingesetzt, um die metabolischen Schwankungen in Echtzeit in Reaktion auf Stickstoffanhebungs- oder Stickstoffentzugsbehandlungen zu untersuchen.

Unsere Forschung erstreckte sich auch auf ein kleines Protein, das vom *ssr0692*-Gen in *Synechocystis* sp. PCC 6803 codiert wird. Dieses Protein reguliert den Fluss in den Ornithin-Ammonium-Zyklus (OAC), einen entscheidenden Mechanismus für die Anreicherung und Umverteilung von Stickstoff in Cyanobakterien. Die Regulation in diesem Kontext ergibt sich aus der Verbindung zwischen dem PII-Protein und dem OAC-Zyklus. PII reguliert traditionell das Schlüsselenzym NAGK, das die Produktion von Arginin katalysiert. Das Ssr0692-Protein konkurriert mit NAGK um die Bindung an PII, was zu einer Hemmung der NAGK-Aktivierung und einer daraus resultierenden Verringerung der Argininsynthese führt. Aufgrund seiner Funktion haben wir es als den PII-Interagierenden Regulator der Argininsynthese (PirA) benannt. Die Interaktion zwischen PirA und PII hängt von der Anwesenheit von ADP ab und wird durch Mutationen in PII, die die Struktur der T-Schleife beeinflussen, behindert. Daher schlagen wir vor, dass PirA als wichtiger Vermittler wirkt, der den Fluss in Stickstoffspeicher-Verbindungen lenkt, indem er sowohl die Verfügbarkeit von Stickstoff als auch den Energiezustand der Zelle berücksichtigt.

II. SUMMARY

The PII proteins are notable members of a vast and ancient protein family involved in signal transduction. These molecules are found in all living organisms and are primarily recognized for their ability to sense metabolites such as ATP, ADP, and 2-oxoglutarate (2-OG). When the effector molecules are non-covalently bound by PII, they cause several structural changes in PII proteins, particularly in their flexible T-loops, which serve as dynamic modules for protein-protein interactions. The interpretation of metabolic data sent by PII is dependent on the binding state of metabolites and the resulting conformation of PII receptors. To thoroughly investigate the complex interactions between PII and target proteins, analytical methods that maintain the natural cellular milieu are needed.

In light of the limitations inherent in alternative methodologies such as immobilization on sensor surfaces in Surface-Plasmon-Resonance (SPR) and Biolayer Interferometry (BLI), as well as the reliance on sizable fluorescence proteins in Förster Resonance Energy Transfer (FRET), our research endeavors focused on the development of an innovative NanoBiT sensor. The focus of this sensor is on the interaction of the PII protein derived from *Synechocystis* sp. PCC6803 with the PII-interacting protein X (PipX), N-acetyl-L glutamate kinase (NAGK) and the PII-interacting regulator of arginine synthesis (PirA). Using the NanoBiT technology, we have attained an advanced comprehension, enabling the calculation of K_D values for the PII-NAGK and PII-PipX complexes, which have not been previously reported. The test also demonstrated an increased level of sensitivity, allowing for the detection of low-affinity interactions, such as the one seen between the PII-S49E variant and NAGK. The study also highlights astounding proof indicating that the development of the PII-NAGK complex is impacted by the presence of ADP, which reduces the complex affinity. Additional analysis by the NanoBiT method and enzymatic assays provided further evidence that the PII-NAGK complex exhibits specific feed-forward activation in response to increasing concentrations of NAG. These two sensors were also applied to investigate the real time metabolic fluctuations in response to nitrogen upshift or nitrogen depletion treatments.

Furthermore, our exploration extended to a small protein encoded by the *ssr0692* gene in *Synechocystis* sp. PCC 6803. The protein regulates the flux into the ornithine-ammonia cycle (OAC), a pivotal mechanism for the accumulation and redistribution of nitrogen in cyanobacteria. The regulation described in this context arises from the connection between the PII protein and the OAC cycle. PII traditionally regulates the key enzyme NAGK, which catalyzes arginine production. The Ssr0692 protein competes with NAGK for PII binding, resulting in the inhibition of NAGK activation and a consequent reduction in arginine synthesis. In light of its function, we have identified it as the PII Interacting Regulator of Arginine Synthesis (PirA). The interaction between PirA and PII depends on the presence of ADP and is hindered by mutations in PII that affect the structure of the T-loop. Therefore, we propose that PirA serves as a crucial mediator, directing flux into nitrogen storage compounds by considering both the availability of nitrogen and the energy level of the cell.

III. PUBLICATIONS

1. Accepted publications

Publication 1: Research article

Rozbeh, R., & Forchhammer, K. (2021). Split NanoLuc technology allows quantitation of interactions between PII protein and its receptors with unprecedented sensitivity and reveals transient interactions. *Scientific reports, 11*(1), 12535.

Publication 2: Research article

Bolay, P., **Rozbeh, R**., Muro-Pastor, M. I., Timm, S., Hagemann, M., Florencio, F. J., Forchhammer, K., Klähn, S. (2021). The novel PII-interacting protein PirA controls flux into the cyanobacterial ornithine-ammonia cycle. *Mbio, 12*(2), 10.1128/mbio. 00229-00221.

Publication 3: Research article

Rozbeh, R., & Forchhammer, K. (2024). In vivo Detection of Metabolic Fluctuations in Real Time Using the NanoBiT Technology Based on PII Signaling Protein Interactions, *International Journal of Molecular Sciences, 25*(6), 3409.

2. Declaration of author contribution

Publication 1: *"Split NanoLuc technology allows quantitation of interactions between PII protein and its receptors with unprecedented sensitivity and reveals transient interactions"*

Under the supervision of Prof. Karl Forchhammer, I developed the NanoBiT sensors, performed in vitro assays and prepared all the figures. Prof. Forchhammer and I analyzed the data and prepared the manuscript.

Publication 2: *"The Novel PII-Interacting Protein PirA Controls Flux into the Cyanobacterial Ornithine-Ammonia Cycle"*

I performed measurements to assess the interaction between PirA and PII and characterization of PirA in PII-NAGK complex formation. I prepared Figures 5 and 6 and edited the manuscript text under the supervision of Prof. Karl Forchhammer.

Publication 3: *"In vivo Detection of Metabolic Fluctuations in Real Time Using the NanoBiT Technology Based on PII Signaling Protein Interactions"*

Under the supervision of Prof. Karl Forchhammer, I performed the NanoBiT experiments, prepared all the figures, data analysis and wrote the preliminary drafts. Prof. Forchhammer conducted the data analysis and wrote the manuscript.

IV. INTRUDUCTION

1. PII Signal Transduction Proteins

Protein PII was discovered in the late sixties of the last century by Bennett Shapiro (Stadtman, 2001), when *Escherichia coli* glutamine synthetase (GS), the central enzyme of bacterial nitrogen metabolism, was found to be regulated by the adenylylation and deadenylylation of one tyrosine residue per GS subunit. Through gel filtration to purify the enzyme that participated in the deadenylylation of GS, two components, PI and PII, were identified (Shapiro, 1969). PI interacts with the bifunctional enzyme adenylyltransferase (ATase), which is responsible for adenylylates or deadenylylates GS while the activity of the ATase is controlled by the PII subunit (Jiang et al., 2007).

We now know that PII proteins are one of the most widely distributed signal transduction proteins in nature and are applied to transduce energy, carbon, and nitrogen abundance signals in all domains of life (Kinch & Grishin, 2002; Sant'Anna et al., 2009).

The proteins of the PII family have been classified into three main subgroups based on two criteria: genetic linkage and similarity of amino acid sequence. They include *glnB*, *glnK,* and *nifI* (Arcondéguy et al., 2001). The *glnB* and *glnK,* two paralogous genes with diverse functions in *E. coli*, show rather common homologues. *glnB* genes are found under the control of GS, and *glnK* genes are linked to the ammonia transporter protein (amtB) (Leigh & Dodsworth, 2007). In archaea and certain anaerobic bacteria, *nifI* is associated with nitrogenase genes, namely *nifH, nifD*, and *nifK* (Ehlers et al., 2002). There is also an uncharacterized group of PII subfamilies called the PII-New Group (PII-NG). These groups of PII might be involved in the regulation of heavy metal transporters, but PII-NG proteins up to date have not been more explored (Sant'Anna, et al., 2009).

By binding PII proteins to target molecules, including channels, enzymes, or molecules responsible for gene regulation, and through functional modification of these targets, PII proteins enable monitoring of ammonia entry, nitrogen metabolism, and gene expression (Forchhammer, 2008; Llácer et al., 2008).

The cyanobacterial PII protein was first discovered in the non-diazotrophic strain *S. elongatus* PCC 6301 (Harrison et al., 1990). The biochemical properties of the PII proteins in cyanobacteria are about 50–65% the same as those of the PII proteins in Proteobacteria. There is only one gene that encodes a PII protein in most cyanobacterial genomes, which is the *glnB* gene (Forchhammer, 2004). Although the similarity of PII homologues is high in some strains, their physiological function should still be still explained (Laichoubi et al., 2011). On the other hand, the genomic studies of PII proteins revealed the availability of these proteins in a multitude of prokaryotes, including bacterial and archaeal genomes and plasmids, while studies of 2783 Genbank files displayed 291 bacterial species and 36 archaeal species that do not encode PII proteins at all (Huergo et al., 2013).

1.1 The structure of PII-mediated Signal Transduction

The X-ray crystallography of bacterial PII proteins revealed a unified picture with a homotrimeric structure of 112 amino acids. Each monomer contains two-helices and four β-strands that construct a double βαβ motif linked by a large loop of 19 amino acids (Son & Rhee, 1987). The loop was designed as the T-loop first identified in *E. coli* with the site for post-translational modification (Cheah et al., 1994). Another loop with a smaller size, which is placed between the second α-helix and fourth β-strands, is named B-loop. The third loop, which is entitled the C-loop, is located at the C-terminus of amino acids. The combination of the T loop and B loop from one monomer with the C loop from an adjacent monomer makes the inter-subunit cleft, which is well-known as a ligand binding site. The T loop's flexible structure is suited to the binding of effector molecules and interaction with PII target proteins. The stability of PII trimers, with a melting temperature ranging from 60 to 70 °C, makes them robust molecules. Consequently, purifying PII is made simpler due to this heat stability (Moure et al., 2012).

1.2 Binding of effector molecules to PII proteins

The PII trimer has three effector nucleotide binding sites that are characterized by binding to the effector molecules ATP, ADP, and 2-oxoglutarate (2-OG). These effector molecules bind to the intersubunit clefts of the PII protein, with ATP and ADP competing for the same site. Generally, in the presence of Mg^{2+}-ATP in the binding pocket, up to three 2-OGs can bind to each trimer. However, in *Arabidopsis thaliana* the PII protein can bind to 2-OG in the presence of ADP (Smith et al., 2003). The Mg^{2+} ion is coordinated by three phosphate oxygens of ATP together with 2-oxo moiety of 2-OG at the base of the T loop (Radchenko et al., 2013). Furthermore, 2-OG is able to create a salt bridge to a Lys residue placed at the posterior end of the T-loop. The binding of 2-OG leads to a conformational change in the T-loop of the proteins by making them more tightly folded. This conformational change favors or disfavors the PII's binding to its target proteins (Schubert, 2021).

1.3 Post translational modification of PII Proteins

The interaction between PII and its targets is not solely determined by bound metabolites; a second layer of regulation occurs through covalent modification of PII. The important layer of PII regulation takes place by post-translational modification at the T-loop that was first recognized in many Proteobacteria, like *E. coli*, in the regulatory cascade of the GS as uridylylation of Tyr51 under nitrogen-deficient conditions. Thus, in the GS-regulating cascade, PII is uridylylated with low glutamine concentrations and deuridylylated with high glutamine concentrations. The uridylylated PII (PII-UMP) activates the GS deadenylylating activity of ATase (Grau et al., 2021; Jiang, et al., 2007). This uridylylation has also been reported in Proteobacteria, Actinobacteria, and an Archaeon (Merrick, 2015; Pedro-Roig et al., 2013). Cyanobacteria with the conserved Tyr51 are not uridylylated, whereas under nitrogen starvation, the serine 49 region in the T loop is phosphorylated in *S. elongatus* PCC 7942 and *Synechocystis* sp. with an unknown mechanism (Forchhammer & Tandeau de Marsac,

1994). However, the phosphorylation has not been reported in other cyanobacteria, such as *Prochlorococcus* and *Anabaena* (Forchhammer, 2004). In addition, there is also no data for post-translational modification of P_{II} in plants (Smith et al., 2004). Nevertheless, when modification takes place, it significantly impacts the regulation of PII's targets by inhibiting its interaction with the majority of them.

1.4 Regulatory Targets of PII

As mentioned earlier, PII proteins can control targets such as transcription factors, membrane transporters, and enzymes, contingent on the availability of specific metabolites. These interactions can activate, inhibit, or prevent the targets from interacting with other proteins, and ongoing research continues to identify new PII targets. This section provides an overview of some extensively studied PII interaction partners.

1.4.1 Ammonium Channel AmtB

AmtB, one of the targets of PII regulation, is a stable homotrimeric ammonium channel in the cytoplasmic membrane that is conserved in all domains of life (Forchhammer et al., 2022; Javelle et al., 2004). The three hydrophobic pores in AmtB are used for the transportation of ammonia gas into the cell (Khademi et al., 2004; Zheng et al., 2004). To regulate an undesirable overflow of intracellular ammonium, the *E. coli* PII homolog GlnK makes a membrane-bound complex with AmtB (Javelle & Merrick, 2005). In addition, the function of GlnK is defined by the localization of its gene in one operon with *amtB*, a gene encoding an ammonium transporter (Thomas et al., 2000). Hence, GlnK in the form of a complex with AmtB inactivates it under nitrogen-excess conditions (Coutts et al., 2002; Javelle, et al., 2004).

The mechanism is applied by inserting the tips of non-uridylylated T-loops of the PII protein into the ammonium channels to block the pores of the transporter (Conroy et al., 2007; Gruswitz et al., 2007). In this complex, ADP is bound to the nucleotide binding site of GlnK. In contrast, 2OG inhibits GlnK binding to the ammonia channel due to the occupation of the binding sites with Mg^{2+}-ATP plus 2-OG. It leads to the bending outwards of the T-loops, avoiding their topographical correspondence with the three holes of the trimer associated with ammonia channels and uridylylation of GlnK's Tyr51, which prevents the complex formation with AmtB (Forcada-Nadal et al., 2018). In addition, the T-loops of PII protein in complex with Mg^{2+}-ATP/2OG displayed different flexed conformations, so binding 2OG alone does not determine a particular T-loop conformation (Forcada-Nadal, et al., 2018). In cyanobacteria, the Amt1 permease is predominantly responsible for ammonium uptake. The interaction of this protein with PII is similar to the studied interaction of GlnK from heterotrophic bacteria with AmtB (Watzer et al., 2019).

1.4.2. N-Acetyl-Glutamate Kinase

N-acetyl-glutamate kinase (NAGK) was first discovered as a PII interacting protein in *S. elongatus* PCC 7942 through yeast two-hybrid analysis (Burillo et al., 2004; Heinrich et al., 2004). NAGK is an enzyme that controls

the ornithine/arginine pathway and is encoded by the *argB* gene. NAGK catalyzes the rate-limiting step in arginine biosynthesis by converting N-acetyl-L-glutamate to N-acetyl-L-glutamyl phosphate. A high intracellular arginine level is also used as N-storage in the form of the polymer cyanophycin in cyanobacteria and plants (Maheswaran et al., 2006; Uhrig et al., 2009). NAGK activity is subject to strong feedback inhibition by arginine. Under high nitrogen and energy supply conditions, represented by low 2OG and high ATP concentrations, the regulatory protein PII interacts with NAGK. In the PII-NAGK complex, two PII trimers at the poles can sandwich one NAGK hexameric (Llácer et al., 2007). Each PII subunit interacts via its T and B loops with each NAGK subunit. This interaction increases the activity of NAGK and relieves it from arginine feedback inhibition. When there is not enough energy or nitrogen, however, and there are high levels of ADP or 2OG, the PII proteins bind ADP or ATP+2OG, which change the shape of PII and breaks up the PII-NAGK complex. NAGK alone is feedback inhibited by arginine; thus, at spare energy or nitrogen supplies, no excess arginine is produced as N-storage. The phosphorylation of the T-loop in the PII-S49E variant strongly blocks the PII-NAGK interaction (Llácer, et al., 2007; Lüddecke & Forchhammer, 2013a), whereas the PII-I86N variant, as a hyperactive NAGK binder, overproduces arginine and cyanophycin (Fokina et al., 2010a; Watzer et al., 2015).

1.4.3. The Transcriptional Coactivator PipX

PII-interacting protein X (PipX), a small protein with 89 amino acids, interacts with both PII and the global transcription factor NtcA (Espinosa et al., 2006; Espinosa et al., 2007). NtcA is a homodimer with around 50 kDa subunits that belong to the CRP/FNR family of transcriptional regulators and consist of N- and C-terminal domains. NtcA has been found to be the key element for the regulation of nitrogen-controlled gene expression in all cyanobacteria. Therefore, it competes with PII to bind to PipX (Domínguez-Martín et al., 2018; Llácer et al., 2010; Luque & Forchhammer, 2008; Weber & Steitz, 1987). In the PII-PipX complex, three PipX monomers bind to the extended T-loops of one PII trimer that is close to the core of the protein (Llácer, et al., 2010; Zhao et al., 2010). This complex is stabilized in vitro by ADP, while it is dissociated in the presence of Mg^{2+} ATP and high 2-OG (Fokina et al., 2011; Llácer, et al., 2010). In contrast, under N-limiting conditions and high 2-OG concentrations, one active NtcA dimer binds to two PipX monomers (Espinosa et al., 2006, Muro-Pastor et al., 2001). On the other hand, the phosphorylation of the T loop's tip, which has a significant role in many interactions, does not affect the PII binding to PipX or NtcA. Hence, the S49 phosphorylation site of the PII protein does not hinder the PII-PipX interaction, which explains the importance of the adenylate energy charge for binding (Espinosa, et al., 2006; Fokina, et al., 2011; Llácer, et al., 2010).

1.4.4. Glutamine synthetase

1.4.4.1 E. coli

GS was originally identified as the first target of PII regulation in *Escherichia coli* (Stadtman & Ginsburg, 1974). The protein involved in GS regulation in *E. coli* and other gram-negative bacteria is termed GSI, which consists

of two hexameric rings with 12 active sites and corresponds to the *glnA* gene (Haskett et al., 2022; Jiang & Ninfa, 2007). A bifunctional enzyme named GlnE controls GSI at both the transcriptional and post-transcriptional levels. The adenyltransferase (AT) activity is at the C-terminus of GlnE, and the adenyl-removing (AR) activity is at the N-terminus of the nucleotidyl transferase domains (Haskett, et al., 2022; Jiang & Ninfa, 2007). In *E. coli*, the regulation of GlnE is under the control of GlnB and GlnK, but the participation of GlnB is much more efficient than that of GlnK in vitro (Atkinson & Ninfa, 1998, 1999; Van Heeswijk et al., 1996; van Heeswijk et al., 2000).

When there is not enough nitrogen, the amount of ammonium outside the cell goes up, and the form of GlnB that is uridylylated and bound to Mg^{2+} ATP/2-OG interacts with the AT domain and makes the adenylyl-removing (AR) activity stronger. This leads to the activation of GS. On the other hand, when there is enough nitrogen, the deuridylylated form of GlnB that is mainly bound to ADP interacts with the AR domain. This makes the AT domain more active and turns off adenylylated GS (Ninfa & Atkinson, 2000; Reitzer, 2003). Furthermore, the interaction of GlnE with GlnB is mediated by the PII T-loop region (Jiang & Ninfa, 2007; Jiang et al., 1997a). Additionally, one T-loop in the trimer is needed for interaction since heterotrimers, including one wild-type subunit, and two T-loop deleted subunits are able to regulate GlnE (Jiang et al., 1997b).

1.4.4.2 Cyanobacteria

The GS pathway in cyanobacteria has unique characteristics. The functioning of GS is regulated by its interaction with the protein inhibitors IF7 and IF17, encoded by the *gifA* and *gifB* genes, respectively (García-Domínguez et al., 1999; García-Domínguez et al., 2000; Saelices et al., 2011). The transcription of these genes is orchestrated by NtcA, a transcriptional regulator that is conserved globally. In contrast to the regulatory mechanism seen in *glnA*, NtcA has the opposite effect on the expression of *gifA* and *gifB* (Herrero et al., 2001; Reyes et al., 1997). NtcA, a member of the CRP/FNR regulator family, exhibits dual functionality as an enhancer or suppressor, depending on its binding location relative to the transcriptional start site (TSS) of the genes it regulates (Herrero, et al., 2001). In conditions characterized by a lack of nitrogen, the protein NtcA plays a role in promoting the simultaneous upregulation of many genes associated with nitrogen metabolism, such as *glnA* and *ntcA* itself (Ohashi et al., 2011; Vázquez-Bermúdez et al., 2002). The activity of NtcA is further enhanced by its interaction with the transcriptional auxiliary protein PipX, which 2-OG modulates (Espinosa, et al., 2006) (Forcada-Nadal et al., 2014). Increased levels of 2-OG, in conjunction with the coactivator protein PipX under nitrogen limitation, enhance the DNA-binding ability of NtcA (Espinosa, et al., 2006). Nevertheless, under conditions of low 2-OG, PipX exhibits a preference for binding with PII, resulting in the inhibition of PipX-mediated activation of NtcA (Klähn et al., 2018). Simultaneously, in the presence of limited nitrogen, NtcA facilitates the transcription of the *glnA* gene, increasing the levels of glutamine synthetase (GS) and enhancing the rates of ammonium assimilation. Concurrently, increasing the affinity between NtcA and DNA leads to the suppression of *gifA* and *gifB* transcription, resulting in decreased production of IFs: IF7 and IF17

(García-Domínguez, et al., 2000). This mechanism guarantees a harmonious equilibrium between the nitrogen requirements and the metabolic demands associated with the ATP-intensive glutamine synthetase (GS) process (Bolay et al., 2018). Cyanobacteria exhibit an additional level of glutamine regulation facilitated by a diminutive regulatory RNA known as NsiR4 (nitrogen stress-induced RNA 4), which is subject to regulation by NtcA. The interaction between NsiR4 and the 5′UTR of *gifA* mRNA is responsible for regulating the expression of glutamine synthetase inactivating factor IF7. Through a comprehensive analysis, it was determined that this particular interaction had a detrimental effect on the synthesis of IF7 protein, hence resulting in an adverse influence on GS activity (Bolay, et al., 2018). Additionally, the presence of the glutamine binding aptamer located in the 5'UTR of *gifB* gene has an impact on the production of IF17. The process of glutamine binding elicits conformational alterations in the RNA element, enhancing protein synthesis and characterizing it as a riboswitch. Hence, non-coding RNA plays a crucial role in regulating nitrogen assimilation in cyanobacteria (Klähn, et al., 2018).

In addition to *gifA* and *gifB*, NtcA also negatively regulates a number of other genes. Upon additional investigation in the unicellular model of *Synechocystis* sp. strain PCC 6803, the gene *ssr0692* was identified as a possible target of NtcA suppression (Giner-Lamia et al., 2017). The gene encodes a small protein consisting of 51 amino acids. This protein is characterized by its high content of nitrogen and positively charged residues, which are crucial for facilitating protein interactions, as shown by observations in GS IFs (Saelices, et al., 2011) (Figure 1). Like well-known GS IFs, this entity has unique properties that suggest it plays a big role in controlling nitrogen as a modulator of metabolic pathways.

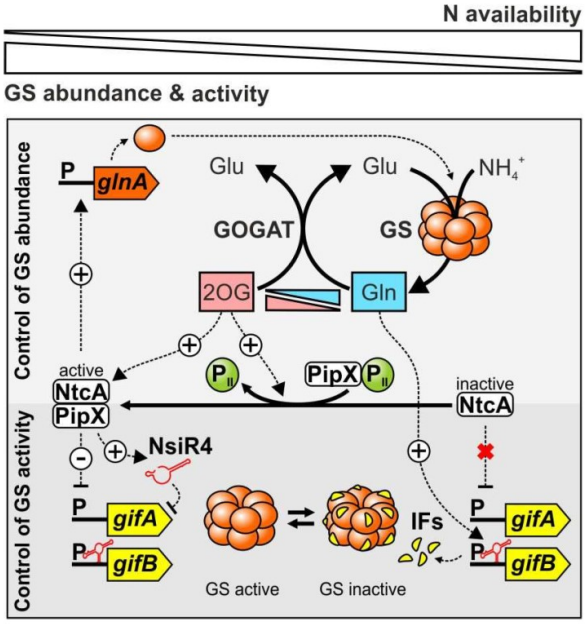

Figure 1. Regulatory network of GS in *Synechocystis* sp. PCC 6803. Picture was taken from (Bolay, et al., 2018)

1.4.5. Phosphoenolpyruvate carboxylase (PEPC)

Phosphoenolpyruvate carboxylase (PEPC), a catalytic enzyme that carboxylates phosphoenolpyruvate to deliver oxaloacetate, (Chollet et al., 1996; Forchhammer, et al., 2022; Svensson et al., 2003) is another target of PII regulation. Like most of PII's interacting partners, the flexible structural element, T-loop, is responsible for PII-PEPC interaction (Scholl et al., 2020). In addition, phosphorylation of the T-loop attenuates the binding of PEPC to PII. ATP and, to a lower degree, ADP can inhibit the activity of PEPC, while PII in the form of a complex with PEPC can relieve the inhibitory effect of ATP and stabilize the enzyme by making a stable complex. In comparison, PII is not capable of relieving PEPC from ADP inhibition. In contrast, in the presence of 2-OG, PEPC stays in the bound form of PII. Therefore, it leads to the conformational modification of the complex, which moderates the activation of PEPC (Forchhammer, et al., 2022; Scholl, et al., 2020).

In nitrate growth cells, when CO2 supply is high, PII is phosphorylated (Forchhammer & Tandeau de Marsac, 1995), while at low levels of CO2 supply, when PII is almost non-phosphorylated, PEPC is activated by binding to PII. (Burnap et al., 2015). As PEPC is a key component in the carbon fixing reaction, its significant boosting activity could assist the CO2 concentrating mechanism (CCM). On the other hand, in cells with low nitrogen concentrations, 2-OG amounts grow, and then PII gets phosphorylated. Hence, the completely phosphorylated PII simply leaves the PEPC in a non-activated state. As a result, the carbon stream towards the tricarboxylic acid (TCA) cycle should decline (Qian et al., 2018). Further, in non-phosphorylated PII conditions, ATP can stimulate PEPC. This condition correlates to a nitrogen-sufficient status that accelerates the growth rate. In these conditions, PEPC activation could contribute to speeding up anabolic reactions, which lead to the fixation of up to 25% of the carbon in *Synechocystis* by the synthesis of 2-OG (Yang et al., 2002).

1.4.6. PII-interacting regulator of carbon metabolism (PirC)

Another novel PII interactor, PII-interacting regulator of carbon metabolism (PirC), is a protein of 112 amino acids encoded by the *sll0944* gene. This protein regulates the carbon flux in cyanobacteria through interaction with either PII or 2,3-phosphoglycerate-independent phosphoglycerate mutase (PGAM), the enzyme that changes the direction of newly fixed CO2 into lower glycolysis. The binding of PirC to PII is weak in the absence of effector molecules, while it greatly increases in the presence of ATP and ADP. The metabolite 2-OG, which accumulates in nitrogen starvation, is in charge of tuning the binding of PirC to PII or PGAM. In the case of sufficient nitrogen supply, when 2-OG levels are low, PII can interact with PirC, but it is not able to bind to PGAM. The active PGAM is responsible for catalyzing the conversion of 3-PGA to 2-PGA to guide the newly fixed carbon in the direction of amino acid and fatty acid synthesis. Only a minor amount of fixed carbon is applied to the glycogen pathway. On the other hand, in nitrogen-starved cells, 2-OG binds to PII, which leads to the dissociation of PII–PirC (Forchhammer, et al., 2022; Orthwein et al., 2021). Consequently, PirC binds to PGAM and inhibits its enzymatic activity. The blocked activity of PGAM suppresses the conversion of 3-PGA to 2-PGA and increases the quantity of 3-PGA to work in the glycogen direction. As a consequence of adapting

the cellular metabolism to a restricted nitrogen supply, the flux in the direction of amino acid synthesis is reduced. In addition, 3-PGA activates the GlgC enzyme, which is responsible for catalyzing the preliminary and regulated steps of the glycogen pathway (Preiss, 1984). Thus, PirC regulates PGAM inhibition by reducing lower glycolysis and inducing glycogen accumulation through the activation of GlgC. The increase in glycogen is followed until up to 50% of the dry weight of chlorotic cells is filled with it (Klotz et al., 2016). The accumulation of glycogen reaches its maximum right after 24 hours of nitrogen starvation and the amounts stay high during chlorosis (Koch et al., 2019).

2. Protein-protein interactions

Proteins are essential components for the main physiological processes of living cells by making interactive networks that are responsive to evolving conditions such as environmental circumstances, the activity of drugs, stress, or pathological situations. The interactions are affected by a complicated interplay of structural conformations, associations with effector molecules, and microenvironmental surroundings (Dixon et al., 2016). Considering the significance of PII in adjusting metabolic activities by binding to numerous targets, analytical methods are required that do not disrupt the native cellular framework. In order to provide an overview, a selection of well-studied analytical methods is explained in the subsequent sections.

2.1 Surface plasmon resonance (SPR)

Surface plasmon resonance (SPR) is a remarkably effective technology that allows for the determination of the entire process associated with the target molecules' binding reaction in a label-free environment. Accordingly, the development of SPR sensors was rapidly promoted. These sensors are potent instruments for real-time supervision of molecular interactions in the fields of chemistry and biology analysis (Bedford et al., 2012; Shalabney & Abdulhalim, 2011; Wang et al., 2017).

This technique is broadly applied as a transducer for affinity-based biosensors, which consist of receptor molecules or ligands immobilized at the metal surface of a SPR transducer. Once the target molecules or analytes within the solution phase bind to the receptor molecules, changes take place in the refractive index close to the metal surface. These changes lead to a shift in the SPR angle, which can be applied to gain information like the binding quantity and the rate of association and dissociation constants (Wang, et al., 2017; Wei et al., 2022).

As already reported in earlier literature, the PII-PipX and PII-NAGK complex formations in cyanobacteria were analyzed by SPR. To do these, NAGK and PipX with an attached His_6 tag were immobilized on a Ni-NTA sensor chip, while PII variants were injected sequentially (Selim et al., 2019a).

Although this technique has numerous advantages, such as a label-free environment, real-time and continuous measurement of interactions, high sensitivity, and quick testing, it also has some disadvantages, like immobilization effects of ligand on binding, non-specific binding to the sensor surfaces, mass transport limitations for nonspecific surface sites, and the existence of low affinity.

2.2 Biolayer interferometry technique

Another way to study the PPI is with the biolayer interferometry (BLI) technique. It is an optical biosensing technique that measures interference patterns from white light reflected by an internal reference layer and a biomolecular layer at the tip of a disposable biosensor (Petersen, 2017). Thus, it screens the interaction of two molecules of interest in real time while one ligand is immobilized on the surface of the biosensor and another molecule, the analyte, is in the solution. Any change in the amount of attached molecules to the biosensor tip makes a wavelength shift corresponding to binding, which can be analyzed in real-time (Barrows & Van Dyke, 2022; Petersen, 2017; Wallner et al., 2013). Since the required sample amount is in the range of nanomolar, BLI is an efficient method for challenging proteins to isolate. Additionally, it is capable of performing large numbers of experiments in parallel, which confirms it as a time-efficient technique. It is also effective to measure protein concentration in a heterogeneous crude lysate; thus, it does not impact the shift in the interference pattern. But the immobilization of the ligand on the sensor tip makes this approach less precise as well (Martin, 2011).

2.3 Förster resonance energy transfer

Another path to studying protein-protein interactions opened up with the discovery of Förster resonance energy transfer (FRET). FRET is a radiationless method that transfers energy from a donor to an acceptor fluorophore according to the dipole-dipole coupling process and causes the reduction of the donor while also enhancing the acceptor fluorescence (Wang & Wang, 2012).

FRET is a complex method that needs numerous requirements to take place, such as overlapping the emission and excitation spectra of the donor and acceptor fluorophore, energy transfer over a distance of 1–10 nM, and a suitable angle between the fluorescent proteins. These features enable FRET to be a proper system to study PPI dynamics and also intra-molecular conformational modifications in vitro and in vivo (Wang & Wang, 2013).

Although some disadvantages are inherent in the physical activity of FRET, especially the technologies employed for measurement, For instance, the changes in fluorescence properties of many proteins are sensitive to alterations in the local environment like changes in ionic concentrations, temperature, pH, refractive index, and oxidation. To measure FRET, some fluorescent labels or even proteins are applied, and any of them may represent diverse sensitivities to alterations in environmental factors. Consequently, FRET measurements could be deviated by unrecognized changes in the local environment (Piston & Kremers, 2007).

2.4 NanoLuc Binary Technology

A significantly better technique to analyze dynamic protein-protein interactions is the use of NanoLuc Binary Technology (NanoBiT), which is based on the smallest luciferase enzyme, termed NanoLuc. NanoLuc (Nluc) is an engineered luciferase derived from a deep-sea luminous shrimp. The enzyme is small, with a size of 19 kDa, stable, and emits bright and sustained luminescence. The NanoLuc luciferase is split into two subunits, a Large Bit (18 kDa polypeptide) and a Small Bit (1.3 kDa peptide), which only weakly associate, so that their assembly,

which restores luciferase activity, depends on the interaction characteristics of target proteins onto which they are fused (Figure 2). To engineer the complementation reporter, the first dissection site from 90 candidate sites of the Nluc sequence was identified. It led to an N-terminus 18 kDa fragment and a C-terminus 13-amino acid peptide with a dissociation constant of 6 μM between the fragments. While the low affinity was appropriate for the protein-fragment complementation assay (PCA), the low stability of the N-terminal fragment hindered the use of the system. The problem was solved by optimizing an N-terminal fragment from a library containing 15,000 variants. It caused a 300-fold increase in luminescence signal by interacting with two fragments. It also increased the affinity between the N and C terminal fragments (K_D = 900 nM). Optimization of the C-terminal peptide from 350 variants created an 11-amino acid peptide with low intrinsic affinity for the N-terminal fragment (K_D = 190 μM) (Dixon, et al., 2016; Ohmuro-Matsuyama & Ueda, 2019). Therefore, the weak association between the N-terminal fragment (termed LargeBiT, LgBiT) and the C-terminal fragment (termed Small BiT, SmBiT) should not affect the binding affinity of target proteins. Luminescence restoration is contingent upon the interaction between candidate proteins fused with LgBiT and SmBiT fragments. This method was applied to analyze various protein-protein interactions in mammalian cells. It was first displayed to verify the interaction between SME-1 β-lactamase and a set of inhibitor binding proteins in vivo. The remarkable functionality was achieved when LgBiT was attached to the C-terminus of SME1 and SmBiT was attached to the C-terminus of inhibitor binding proteins (Dixon, et al., 2016).

In addition, the system was validated in vitro by characterization of the interaction between bacterial transcription factors NusB and NusE and also the interaction between RNA polymerase with σA from the gram-positive organism *Bacillus subtilis.* These configurations evidently imposed minor steric constraints and easily approved the integrity of the NanoBiT method for analysis of protein-protein interaction (Tsang et al., 2019).

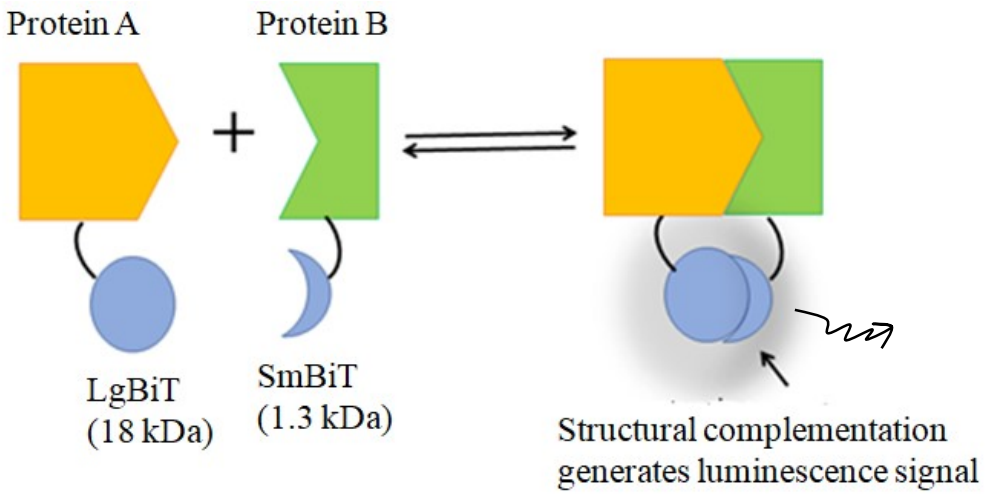

Figure 2. Structural collaboration of the two optimized subunits during the interaction between protein A and protein B in NanoBiT system

3. Aim of this work

As already mentioned, PII proteins are extremely significant sensors for the metabolic state of cells and regulators that interact with numerous target proteins. The interaction of PII with its target proteins has been investigated by different methods during the last few years. Surface plasmon resonance spectroscopy (SPR) was applied to analyze the complex formation of PII-PipX and NAGK-PII within the effects of different metabolites. Subsequently, the interaction of two various molecules in real time was screened by the biolayer interferometry technique while a ligand was immobilized on the biosensor tip surface and an analyte was in the solution. Another path was followed by the discovery of the radiationless technique of Förster resonance energy transfer (FRET), which transfers energy from a donor to an acceptor fluorophore. The first PII protein was used for the measurement of the ATP:ADP ratio. Then, after the evaluation of the 27 kDa FP-tags effect on the small PII protein, the PII-NAGK interaction and 2-OG FRET sensor were analyzed by FRET technique.

Unfortunately, all these methods have restrictions and could represent a part of PII interactions stories. For instance, in SPR and BLI methods, the ligands must be immobilized on the surface of biosensors. While it is broadly identified in the FRET sensor, the sensitivity of fluorescent proteins to changes in the local environment and the low signal-to-noise ratio. Additionally, FRET analysis for cyanobacterial samples reveals high background fluorescence from the pigments. Therefore, the NanoLuc Binary Technology (NanoBit), a novel interaction method that does not affect the native cellular context, is demanding to study protein-protein interactions. In this study, the NanoBiT sensor is developed based on the interaction of the signal transduction protein PII from *Synechocystis* sp. PCC6803 with the PII-interacting protein X (PipX), N-acetyl-L-glutamate kinase (NAGK), and the PII-interacting regulator of arginine synthesis (PirA) to gain information that is not achievable by other approaches. The efficient binding affinity is observed when Large BiT is attached at the C-terminus of the PII protein and Small BiT is attached at the C-terminus of target proteins with appropriate linker sequences. The system demonstrates remarkable sensitivity and accurate results compared to other methods such as BLI and SPR. These studies additionally represent further information regarding superior PII network interactions and read out the metabolite responses in real time.

Transitioning our attention to another aspect of this research, it is generally acknowledged, based on an extensive review of the scientific literature, that cyanobacteria hold a crucial position in the process of global oxygen synthesis and exhibit significant involvement in biogeochemical cycles, particularly as primary producers. The photosynthetic capacities of these organisms have attracted considerable interest due to their potential for sustainable fuel and high-value chemical synthesis. However, the extensive use of microbial cell factories is hindered by our inadequate understanding of metabolic flux control in these organisms. In our investigation, we have identified a novel regulatory protein, PirA that modulates nitrogen flow, particularly in arginine biosynthesis. The dual role of arginine as a proteinogenic amino acid and a precursor for cyanophycin, a storage compound for fixed nitrogen in cyanobacteria, suggests that this finding has significant implications for biotechnology. As a result, our research outcomes not only enhance our understanding of flux control in

cyanobacteria but also provide fundamental information for accurate metabolic engineering, thereby facilitating the development of novel photosynthesis-driven biotechnological initiatives.

IV. RESULTS

1. Advancement of the NanoBiT sensor system

NanoBiT has supplied a system to evaluate protein-protein interactions in real time (Dixon, et al., 2016; Schwinn et al., 2018; Yano et al., 2018). The initial step to generate the NanoBiT sensor was performed by a hybrid construct of PII fusion protein when the LgBiT fragment was fused at the C-terminus and the SmBiT fragment was on the tip of the T-loop with different sizes of linker peptides (24-aa linker, 16-aa linker, and 8-aa linker). To develop the construction, we utilized the information obtained from creating the hybrid PII-FRET sensor, as explained in Lüddecke et al.'s 2017 research (Lüddecke et al., 2017). This sensor, which merges the PII protein with FRET technology, provided useful insights into the potent interactions of biomolecules. By utilizing the knowledge acquired through its development, we were able to design and build our experimental setup with a high degree of accuracy and assurance.

During the construction of various constructs involving different size of linkers, only the one with a 16-aa linker displayed a 30% drop in NanoBiT upon effector molecule addition, which indicates that the two parts of the NanoBiT sensor moved away from each other. As a result, we decided to divide the NanoBiT fragments into two distinct polypeptides, one on the PII protein and the other on a PII-receptor protein. In our initial experiments, the SmBiT fragment was attached using a 16 amino acid linker at the C-terminus of PipX, and the LgBiT fragment was attached to the PII Strep-tag purification linker at the C-terminus (Figure 3). It's important to note that this purification linker had already been used successfully in PII-VENUS FRET construct tests (Lüddecke & Forchhammer, 2013b), giving our strategy a strong foundation. The C-termini were selected to fuse the NanoLuc proteins since they are easily available and placed in the same direction. PASK-Iba3 and pTEV5 expression vectors were used, respectively, to clone the genes for the PII-LgBiT and PipX-SmBiT constructs for the in vitro experiments. While the pACYCDuet-1 expression vector with two cloning sites for PII-LgBiT and PipX-SmBiT was used for the in vivo experiments.

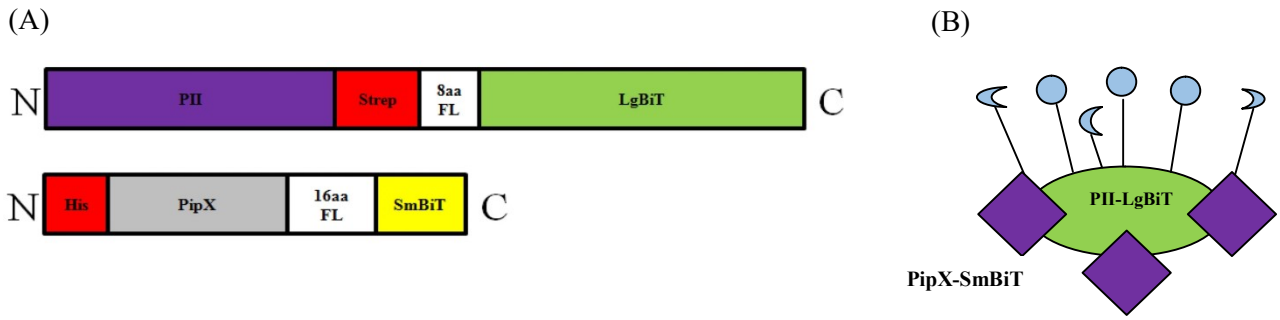

Figure 3. Schematic representation of PII-LgBiT and PipX-SmBiT fusion proteins (A, B)

When we looked at the purified individual Nanoluc sensor part, we noticed a very tiny background luminescence that measured around ~ 1×10^{-5} RLU. We removed this background light from the signals produced during complex formation in order to obtain precise measurements. This correction made sure that background noise was not affecting our data and that it accurately reflected the specific interactions and responses of the sensor.

1.1. PII-PipX NanoBiT sensor

In the in vitro preliminary tests to study the binding of PipX-SmBiT and PII-LgBiT in optimal conditions in the presence of 2 mM ADP, increasing concentrations of PII-LgBiT, starting at 0.33 pM, were systematically titrated with 10 nM PipX-SmBiT. The recorded luminescence signal was plotted against the respective PII-LgBiT concentration. Low concentrations of PII-LgBiT showed a linear increase in luminescence signal reaching up to 1×10^{7} RLU, which is equivalent to a 10 pM PII concentration. The luminescence curve, however, started to plateau as the PII-LgBiT concentration increased beyond this point, indicating a saturation effect at higher PII-LgBiT concentrations (Figure 1b, Publication 1). This finding indicates that higher concentrations of NanoLuc cannot be detected by the assay's linear detection range. To ensure that the measurements stayed within the assay's precise detection range, we limited the concentration of PII-LgBiT to 10 pM in all subsequent tests.

Next, the impact of different effector molecules on PII-PipX complex formation was investigated by continuously measuring the luminescence. In the absence of effector molecules, an extremely small increase in luminescence signal was recorded, while by adding the adenyl-nucleotides, the luminescence signal was immediately increased. Consequently, it monitored the stimulation of PII binding to the PipX protein (Figure 2a, 2b, Publication 1).

Additionally, to find out the kinetics of PII-PipX complex formation, raising concentrations of PipX-SmBiT were titrated to the fixed concentration of PII-LgBiT (10 pM trimer) in the presence of 2 mM ATP or ADP. Subsequently, the dissociation constants in both conditions were determined by plotting the RLUs against the PipX-SmBiT concentrations. It was calculated to be 5.7 ± 0.78 nM in the presence of ADP and 52.4 ± 0.92 nM in the presence of ATP (Figure 2C and Table 1, Publication 1).

The ratio of ATP to ADP plays a pivotal role in regulating cellular energy metabolism by affecting the amount of free energy released during ATP hydrolysis and facilitating numerous biochemical activities. The maintenance of cellular energy balance is essential for both cell health and the regulation of signaling processes (Tantama et al., 2013)**.** In order to find out its effect on binding of PII to PipX through NanoBiT analysis, the increase in luminescence signal was recorded at diverse ATP/ADP ratios, while the final concentration for ADP+ATP stayed constant at 2 mM. It was shown that in the presence of 0.5 mM ADP and 1.5 mM ATP, the luminescence signal almost reached the level of 2 mM ADP alone. This signifies the powerful effect of ADP on the PII-PipX interaction and its dominance over ATP (Figure 2d, Publication 1).

2-OG is the main signal of the carbon/nitrogen balance in cyanobacteria and is sensed by the PII protein (Zhao, et al., 2010). It is considered a significant indicator of the binding of PipX to the PII protein (Espinosa, et al.,

2006). Hence, in the following step, the impact of different 2-OG concentrations on the PII-PipX interaction was analyzed in the presence of 2 mM ATP. Initially, the combinations of PII-LgBiT and PipX-SmBiT were incubated with different amounts of 2-OG in the absence of ATP. Then 2 mM ATP was added to the mixture after a 5-minute incubation period, allowing complexes to form, and this process proceeded until saturation was attained after 15 minutes (Figure 3a, Publication 1). To figure out how big the effect was, the maximum RLU values were plotted against the concentrations of 2-OG in the assay, which ranged from 0 to 5 mM. In the PII-PipX interaction, the increasing 2-OG concentrations gradually prevented the complex formation that was previously revealed by other methods like SPR analysis. The $IC_{50,}$ for the inhibition by 2-OG was 25 µM (Figure 3b, Publication 1). This value is 40% less than the average K_D of 39 µM for 2-OG binding to all three binding sites, while the K_D value for 2-OG binding to the first binding site with highest affinity in the PII trimer is around 5 µM. This implies that when 2-OG only binds to the highest affinity site, PipX can still bind to other free subunits. Only in cases of complete occupation of trimeric PII by 2-OG is PipX unable to bind PII.

Therefore, in order to investigate how 2-OG disrupts the PII-PipX complex using NanoBiT technology, 2-OG was added at different times in time-course experiments while the effector molecules were included sequentially. The complex was completely dissociated in two minutes in the presence of 2-OG and 2 mM ATP. While the dissociation took longer when 2-OG was present with 1 mM ATP and 1 mM ADP (Figure 3c, Publication 1). The result indicated that it takes only 45 seconds to dissociate half of the complex when 2-OG and ATP are the only factors present. By contrast, when 2-OG was coexisting with 1 mM ATP and 1 mM ADP, the dissociation process was significantly slowed down, indicating a strong mitigation of dissociation. Under these conditions, approximately half of the complex was dissociated for around 340 seconds, which was 7-8 times longer compared to the time during which ADP was absent.

PII-PipX NanoBiT sensor was also applied to monitor the metabolic fluctuation in the cells. To investigate this, first the response of the sensor was analyzed to ammonium upshift. The maximum response occurred at 40 mM ammonium and remained high during the measurement. In contrast, the RLU signal for 4 mM ammonium stayed consistent between 1 mM and 40 mM ammonium treatment. This sensor was also treated to two concentrations (0.1 and 1 mM) of L-Methionine sulfoximine (MSX) which inhibits the nitrogen assimilation but minimal response was observed. The response of sensor to the nitrogen starvation was characterized by the immediate decrease in RLU signal, followed by subsequent increase again to near the initial RLU ratio (Figure 5, Publication 3).

1.2. PII-NAGK NanoBiT sensor

To study the interaction of the purified proteins PII and their main interacting partner, N-acetyl-L-glutamate kinase (NAGK), by NanoBiT technology, the SmBiT fragment was fused by a 16-amino acid flexible linker to the C-terminus of NAGK (Figure 4). The formation of the PII-NAGK complex is primarily controlled by two

factors: the ratio of ATP to ADP and the occupancy of PII by Mg^{2+}-ATP-2-OG (Fokina, et al., 2011; Lapina et al., 2018a; Selim, et al., 2019a).

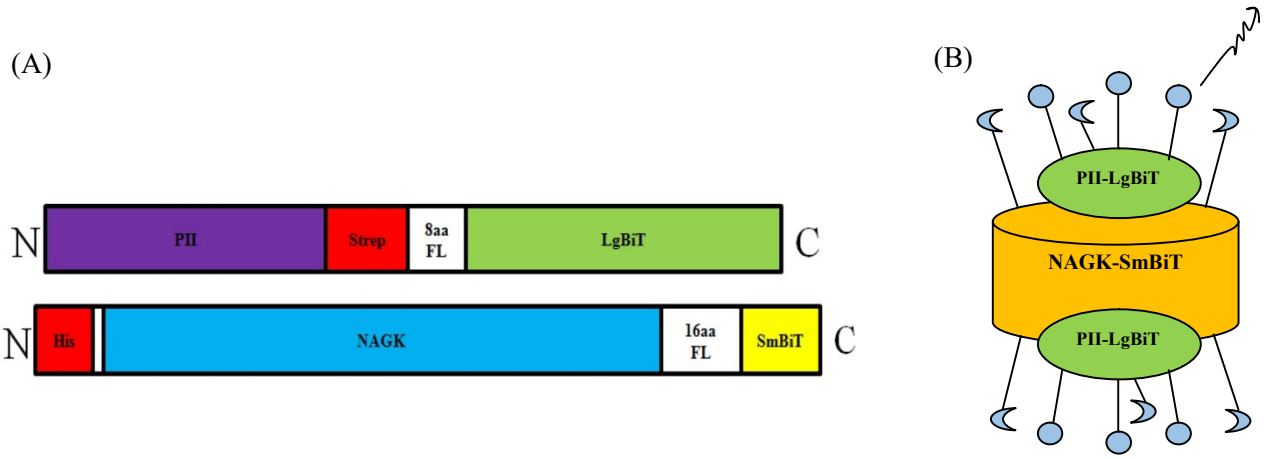

Figure 4. Schematic representation of PII-LgBiT and NAGK-SmBiT fusion proteins (A,B)

To find out how effector molecules affect the PII-LgBiT–NAGK-SmBiT complex formations, the NAGK-SmBiT fusion protein was titrated to the fixed quantity of PII-LgBiT (10 pM). These experiments were carried out under three different conditions: in the presence of 2 mM ATP, 2 mM ADP, or in a condition where no effector molecules were included (Figure 4b, Publication 1). The most successful complexes were formed in the presence of ATP and in the absence of any effector molecules, as reported previously by other methods such as SPR and BLI. The NanoBiT technology displayed complex formation even in the presence of ADP with lower affinity. This data indicates the remarkable sensitivity of this method compared to the SPR method, which was only able to detect weak and transient PII-NAGK complexes when ADP was present.

The next step was to find out the effect of 2-OG on PII-NAGK complex dissociation with NanoBiT technology. To follow this, the interaction of PII-LgBiT and NAGK-SmBiT was performed in the presence of ATP and different concentrations of 2-OG. The obtained data was plotted against the 2-OG concentrations (Figure 4c, Publication 1). The application of curve fitting led to an IC_{50} of 0.15 mM, which was perfectly aligned with previous data provided via diverse experimental methods such as FRET with an IC_{50} of 0.1 mM and SPR and enzyme assays with an IC_{50} of 0.12 mM for 2-OG.

The PII- NAGK NanoBiT sensor was also applied to monitor the metabolic changes in the cells. In the initial perturbation experiment, the response of the sensor was examined toward ammonium upshift treatment. The rapid luminescence increase was observed in 40 mM ammonium reaching an almost two fold increase after two minutes. This was followed by addition of 4 mM ammonium resulted in higher luminescence compared to untreated control. To conclude, the ammonium treatment led to the rapid reduction in 2-oxogulatarate levels which established the favourable intracellular conditions for the formation of PII-NAGK complex (Figure 3a and 3b, Publication 3). In the second perturbation experiment, the effect of two concentrations of MSX as an inhibitor of glutamine synthetase was tested. The addition of 0.1 or 1 mM MSX prompted a rapid decrease in

RLU signal, indicating a reduction of PII-NAGK NanoBiT complex formation (Figure 4a and 4b, Publication 3). In the third perturbation experiment, the investigation focused on the response toward nitrogen starvation. Upon nitrogen downshift, the RLU signal immediately decreased and reached the basal level, corresponding to the dissociation of PII-NAGK complex and an increase in the level of 2-oxogulatarate (Figure 4c and 4d, Publication 3). All these three treatments were performed on the PII-FL sensor as a part of control experiment, and the results indicated almost negligible or very minor responses (Figure 3c and 3d, Figure 4e and 4f, Publication 3).

1.3. The proteins PipX and NAGK engage in a competitive binding interaction with the protein PII

Based on the findings derived from a previous study using ultrafiltration, it became evident that PipX is able to disrupt the interactions between PII and NAGK (Llácer, et al., 2010). Hence, we further explored this experiment using the NanoBiT system to monitor the feasibility of the method in competition assays. The PipX was applied as a competitor against NAGK for PII binding. To achieve this, increasing PipX amounts were added to a fixed concentration of PII-LgBiT and NAGK-SmBiT in the presence of 2 mM ADP. It was shown the addition of PipX completely suppressed the luminescence signal of the PII-LgBiT–NAGK-SmBiT complex, which was verified by previous data with ultrafiltration. In contrast, titrating NAGK to the fixed concentration of PII-LgBiT and PipX-SmBiT in the presence of ADP had no effect on the luminescence signal of the PII-LgBiT–PipX-SmBiT binding complex (Figure 5a, Publication 1).

According to previous data, PII has a higher affinity for PipX in the presence of 2 mM ADP despite the presence of NAGK. This was also verified by the NanoBiT system when the addition of PipX completely suppressed the luminescence signal of the PII-LgBiT–NAGK-SmBiT complex. The other way around, NAGK was titrated to the fixed concentrations of PII-LgBiT and PipX-SmBiT in the presence of ADP. Surprisingly, even with increasing concentrations of NAGK, no significant change was observed in the luminescence signal of the PII-LgBiT–PipX-SmBiT binding complex. It was obviously demonstrated that in the presence of ADP and both partners, PII prefers to bind to PipX rather than NAGK. The challenging condition was noted by performing the two previous experiments in the presence of ATP. Titration of PipX to the constant concentration of PII-LgBiT and NAGK-SmBiT led to a slowly reduced luminescence signal (Figure 5b, Publication 1). This result indicated that even though the affinity of PII for NAGK is higher than that of PipX in the presence of ATP, the ratio of a 1:1 stoichiometric amount of PipX to NAGK significantly decreases the luminescence signal to around 50%. Increasing the amount of PipX can even reduce the luminescence signal. On the contrary, with the addition of increasing amounts of NAGK, even in excess amounts, to the constant concentrations of PII-LgBiT and PipX-SmBiT, the luminescence signal was only partially reduced. Albeit, it was expected that at these high NAGK concentrations, the PII would preferentially bind to NAGK. The probable evidence might be the poor interaction of PipX-SmBiT protein with PII-LgBiT–NAGK complexes. This diminished interaction might be detected by the NanoBiT sensor as a consequence of the substantial sensitivity of the reporter system.

1.4. Interaction of NAGK with two PII variants in the presence of different effector molecules

In order to analyze the complex formation of NAGK with PII variants, NAGK-SmBiT was titrated to a constant concentration of PII-S49E and PII-I86N variants in the presence of 2 mM ATP and 2 mM ADP and without effector molecules (Figure 6a-c, Publication 1). It was previously investigated that seryl residue 49 plays an important role in complex formation; therefore, impaired T loop by S49 phosphorylation abolishes interaction with NAGK (Heinrich, et al., 2004). Conversely, the PII-I86N variant with a single substitution of IIe86 to Asp86 in the B loop was recognized as a superactive NAGK binder. Although no complex formation for NAGK and PII-S49E was detected by SPR analysis, the sensitive NanoBiT assay was able to expose the low residual interaction of the PII-S49E variant with NAGK in the presence of ATP, ADP, or without effector molecules. However, the complex formation in these conditions was about 10–20 fold lower than that of wild-type PII. Further, the result from PII-I86N-LgBiT was also in agreement with the previous data for ATP conditions. Notably, it also revealed high affinity to NAGK even in the presence of ADP.

1.5. Influence of arginine on PII – NAGK complex formation

Arginine is an amino acid with a pivotal role in protein synthesis and nitrogen storage in cyanobacteria (Llácer, et al., 2008). The synthesis of arginine is controlled by the PII protein by activation of the N-acetyl glutamate kinase (NAGK) reaction. Furthermore, arginine, with its feedback inhibition effect, binds to allosteric sites in NAGK and inhibits its activity. Hence, arginine interferes with the formation of the PII-NAGK complex. PII interaction with NAGK tunes down or down regulates the arginine feedback inhibition. Probably the PII complex reduces the affinity of Arg for the allosteric binding sites of NAGK. To discover the negative effect of Arg on NAGK-SmBiT–PII-LgBiT complex formation by the NanoBiT system, increasing Arg amounts were added to PII-LgBiT–NAGK-SmBiT complexes. Arginine in extremely small concentrations could gently increase complex formation, but raising the arginine concentrations in the presence of 2 mM ATP or 1 mM ATP/1 mM ADP reduced the luminescence signal slowly to reach a constant line more than half of the initial value. While in the presence of 2 mM ADP, the luminescence signal was increased at low arginine concentrations, and it returned later to the initial value by enhancing the arginin levels. The complex reacted differently in the absence of any effector molecules; the luminescence signal could not be enhanced even at low concentrations of arginine (Figure S1, Publication 1).

To quantitatively realize the binding affinity of the PII-NAGK interaction in the presence of 2 mM Arg and 2 mM ATP, increasing NAGK-SmBiT amounts were added to the fixed concentration of the respective PII-LgBiT variants (Figure 6d, Publication 1). The presence of Arg reduced the affinity of PII around 2-fold, which was in harmony with the decreasing luminescence signal detected in the experiment of Arg titration. Apparently, complex dissociation is not the reason to suppress the activity of enzymes. Instead, it appears that PII can indeed bind to fully saturated NAGK by Arg, but the complex probably undergoes conformational variation that hinders the activity of NAGK catalytic sites by PII.

Remarkably, the effect of Arg on the binding of NAGK to PII variants was different. In wild-type PII, the affinity was gently reduced, while in the PII-S49E variant, the reduction was even stronger. Interestingly, the PII-I86N variant demonstrated substantial affinity for NAGK and much greater efficiency in relieving NAGK from arginine inhibition (Figure 6d, Publication 1). This is in agreement with the potent stimulation of arginine synthesis and accumulation of cyanophycin in *Synechocystis* strains with the PII-I86N mutation.

1.6. The impact of substrate, N-acetylglutamate (NAG), on PII–NAGK complex formation

We know from previous studies that the formation of the PII-NAGK complex boosts the affinity for the substrate NAG (Selim et al., 2020). Hence, the influence of NAG on the interaction of NAGK with PII was investigated for the first time, with the importance of discovering its relevance for in vivo situations. Increasing concentrations of NAG were titrated to the constant concentration of NAGK - PII complex binding in the presence of 2 mM ATP (Figure 7a, Publication 1). To allow the sensitive detection of changing affinity, NAGK was used at a concentration equal to half of its Km value. The result demonstrated that increasing concentrations of NAG induced a tighter PII-NAGK complex formation that was revealed by an increasing luminescence signal. 50 mM NAG, the highest substrate concentration in the luminescence assay, boosts the binding affinity of PII and NAGK under any conditions. In the presence of ATP, 50 mM NAG increases the affinity of complexes more than 10-fold compared to the same condition without NAG (Figure 7c, Publication 1). Conversely, Arg with a negative impact on PII-NAGK affinity alleviated the potent stimulating effect of NAG, as NAG could only mildly enhance the affinity of the complex in the presence of 2 mM Arg (Figure S2,Publication 1).

Surprisingly, the S49E PII variant, which is not able to relieve NAGK from arginine feedback inhibition, can bind firmly to the PII protein in the presence of 50 mM NAG (Figure 7c, Publication 1). Therefore, the interaction of PII with NAGK is insufficient to relieve the enzyme from the inhibitory effect of Arg.

The binding affinity of NAGK to PII increases due to enhanced substrate concentrations. This leads to elevated kinetic activation. Hence, the coupled NAGK assay was performed with NAG titration (0–2 mM) in the presence of 1 mM ATP, 1 mM ADP, and 0.1 mM Arg, which shows the sigmoidal curve. In contrast, the standard assay was applied with increasing concentrations of NAG (0–50 mM) in the presence of 10 mM ATP (Figure 8, Publication 1). The findings displayed the strong effect of increasing concentrations of NAG on NAGK activity to enhance the binding affinity to PII.

2. The Novel PII-Interacting Protein PirA Controls Flux into the Cyanobacterial Ornithine-Ammonia Cycle

Nitrogen, a vital element for sustaining life, is subject to sophisticated regulatory mechanisms inside bacterial organisms, with a particular focus on the enzyme glutamine synthetase (GS). This regulation is primarily mediated by the proteins NtcA and PII. The discovery of the pirA gene, which bears resemblance to inhibitory components of GS, presents a novel dimension. PirA, a component of the NtcA regulon, is subject to intricate

transcriptional regulation including putative NtcA binding sites. The present study sheds light on the involvement of PirA in the process of nitrogen adaptation, hence offering valuable insights into the nitrogen metabolism of cyanobacteria and its potential implications for engineering purposes (Krysenko & Wohlleben, 2022; Luque et al., 1994; Saelices, et al., 2011). It is worth mentioning that PirA demonstrates increased expression in response to ammonium upshift, resulting in a decrease in the production of arginine. This study examines the relationship between this mechanism and PII, as demonstrated by the influence of PirA on the enzymatic mechanism of NAGK.

2.1. The dependence of PirA–PII complex formation on ADP metabolites

In recent experimental studies, the protein PirA, which was found by pulldown assays of the signaling molecule PII, (Watzer, et al., 2019) was observed to engage in direct interaction with PII. In order to validate this interaction, in vitro binding studies were performed utilizing biolayer interferometry. The immobilization of recombinant PII protein onto a sensor tip was conducted, followed by the use of GST-tagged PirA as the analyte. This analysis was performed in the presence or absence of different effector molecules (Figure 5A, Publication 2). The findings demonstrated a distinct, concentration-dependent correlation between PirA and PII in the presence of ADP. However, no correlation was observed in the presence of ATP, ATP/2-OG combinations, or in the absence of effectors (Figure 5B, Publication 2).

Further experiments with PII variants revealed that PirA interacts with PII through the T-loop structure, which exhibits a high degree of flexibility. One variant of PII (PII(I86N)) that has a preference for constitutive binding with NAGK (Fokina et al., 2010b; Zeth et al., 2012) did not show any binding with PirA. On the other hand, a phosphomimetic variant (PII(S49E)) which does not interact with NAGK (Burillo, et al., 2004; Forchhammer & Selim, 2020), still formed complexes with PirA without any noticeable effects (Figure 5D, Publication 2). This suggests a potential relationship between the conformation of the T-loop, interaction with NAGK, and binding with PirA. These findings, in conjunction with the dysregulated production of arginine in the Δ*pirA* mutant, suggest that PirA disrupts the control of NAGK by interacting with PII. This provides insight into the involvement of PirA in the complex regulatory system that governs nitrogen metabolism.

2.2. PirA antagonizes PII-dependent activation of arginine-inhibited NAGK

In a detailed enzyme assay, PirA's interaction with the PII-NAGK complex was investigated. The results obtained from the standard NAGK assays, in which ADP concentrations were kept at zero indicated that PirA did not have any effect on the PII-mediated activation of NAGK. In order to evaluate the impact of PirA in situations when ADP addition is permitted, a coupled assay was employed. This experiment involved linking NAG phosphorylation to the subsequent reduction of NADPH-dependent N-acetyl-g-glutamyl-5-phosphate (Fokina, et al., 2011; Selim et al., 2019b). In this experimental configuration, the protection of PII from arginine inhibition was observed, hence enabling the differentiation between unbound NAGK and NAGK complexed

with PII (Figure 6A, Publication 2). When the experimental procedure involved the inclusion of 0.1 mM arginine and 1 mM ATP, it was observed that varying doses of PirA did not provide any discernible impact. Nevertheless, when exposed to a concentration of 1 mM ATP and 1 mM ADP, the activity of NAGK was shown to be inhibited in a manner that was dependent on the concentration of PirA. This inhibition reached a maximum of 50%, which is consistent with the need for ADP in the interaction between PII and PirA (Figure 6B, Publication 2). As a result, PirA causes disruption of the PII-NAGK complex, resulting in the inhibition of NAGK by arginine.

V. DISCUSSION

1. Split NanoLuc technology for investigating PII's interactions with its partner proteins

PII proteins are widely present members of the signal transduction family within the prokaryotic domain. These prototypical PII signaling proteins determine the cellular metabolic status by attaching to metabolites such as ATP, ADP, and 2-oxoglutarate. PII proteins have the ability to modulate the activity of different target proteins based on their particular binding to effector molecules (Fokina, et al., 2010a; Lüddecke & Forchhammer, 2015; Shen et al., 2023). In order to comprehensively explore the complex associations between PII and its respective target proteins, it's vital to use analytical techniques that maintain the natural environment of the cell. In this work, we utilized the NanoBiT method to explore the interactions between the PII protein from *Synechocystis* sp. PCC6803, PipX, and NAGK.

1.1 The effect of metabolites on PII–PipX interactions

A review of the results obtained from the pull-downs and SPR tests, it can be inferred that the formation of a complex between the transcriptional co-activators PipX and PII is more likely to occur in the ADP-bound state. Conversely, the presence of ATP had little or no discernible impact on the binding between these two molecules (Llácer, et al., 2010; Llop Estevez et al., 2023; Selim, et al., 2019b). According to our research, the NanoBiT system has shown that the interaction between PII and PipX is also stronger when ADP is present compared to ATP. This is evident from the lower dissociation constant in the presence of ADP. It is noteworthy that the luminescence signal remains almost similar to that produced by 2 mM ADP alone, despite the simultaneous presence of both ATP and ADP. This discovery underscores the significant impact of ADP on the relationship between PII and PipX and its superiority over ATP, which is consistent with previous findings. The enhanced accuracy of this methodology further facilitates a detailed understanding of the binding strengths between PII and its specific target, PipX.

1.2 Dissociation of PII-PipX complex in the presence of 2-OG

Nevertheless, it is crucial to acknowledge that the limited association between LgBiT and SmBiT, characterized by a K_D value of up to 190μM (Dixon, et al., 2016), does not seem to influence the higher affinity of the partners they interact with. The uniqueness of the interaction between PII and its partner, PipX, becomes apparent by the rapid dissociation of their complex upon exposure to 2-OG. The binding mechanism between the PII protein and 2-OG follows a sequential approach, whereby the binding of 2-OG to one subunit leads to a reduction in its binding affinity to the remaining subunits (Fokina, et al., 2010a). It is worth mentioning that 2-OG only interacts with the binding sites that are already occupied by magnesium-adenosine triphosphate (Mg^{2+}-ATP) in PII proteins. In the presence of elevated ATP concentrations, the binding sites of all PII proteins become occupied

by Mg-ATP, resulting in the formation of PII-ATP_3 complexes. This enables the binding of a maximum of three 2-OG molecules to each PII-ATP_3 complex. This particular arrangement optimizes the level of detection sensitivity shown by the effector. The dominance of the PII-ATP_2-ADP_1 population is seen with the increase in ADP levels. The accumulation of the PII-ATP_1-ADP_2 population occurs only when the concentration of ADP exceeds that of ATP, which may be attributed to the comparatively lower binding affinity of ADP compared to ATP. In a broad sense, the mixed populations consisting of PII-ATP_2-ADP_1 and PII-ATP_1-ADP_2 have a lower number of binding sites for 2-OG in comparison to PII-ATP_3. The findings from calorimetric titration studies indicate that when the ATP:ADP ratio is 1:1, just a single molecule of 2-OG binds (Fokina, et al., 2011). The absence of identification of two 2-OG binding sites in this experimental setup implies that PII-ATP_2-ADP_1 has the capability to bind just one 2-OG molecule. Alternatively, while less probable, it is possible that PII-ATP_1-ADP_2 is selectively produced in the presence of equal amounts of ADP and ATP (Zeth et al., 2014).

Previously, it was noted that the K_D value for the binding of 2-OG to PII was lower in the presence of 2 mM ATP compared to the K_D value obtained in the presence of 1 mM ATP and 1 mM ADP (39 μM vs. 180 μM, respectively) (Fokina, et al., 2011). Using the NanoBiT method to assess the PII-PipX complex, the results showed that the disassembly of half of the complex occurred more rapidly when exposed to a concentration of 2 mM ATP, in contrast to the conditions of 1 mM ATP and 1 mM ADP. Consequently, the moderately rapid dissociation of the PII-PipX complex is consistent with PII's decreased binding affinity for 2-OG when exposed to 1 mM ATP/ADP. The observed quick dissociation further substantiates the notion that LgBiT and SmBiT fragments have little effect on binding affinity. Therefore, the intrinsic low affinity does not modify the affinity constants of PII with its targets. Furthermore, NanoBiT technology offers the advantage of enabling interactions within a solution, distinguishing it from other techniques like SPR or BLI analysis.

1.3 The sensitivity of NanoBiT technology

The NanoBiT sensor has remarkable sensitivity, enabling it to detect the formation of the PII-NAGK complex even in the presence of ADP, which exhibits a lower affinity. Previous methodologies, such as SPR, were limited to the detection of transient complexes between PII-NAGK complexes in ADP's presence (Fokina, et al., 2010b). It was also demonstrated by the NanoBiT assay a high level of accuracy in detecting subtle residual contacts between the PII-S49E variant and NAGK, irrespective of the presence or absence of ATP, ADP, or any other effector molecules. Nevertheless, this particular interaction exhibited much lower strength, perhaps 10-20 times less potent than the typical PII. Conventional techniques such as SPR and BLI failed to detect these nuanced interactions, but only FRET analysis successfully identified the weak interaction of PII S49 variant (PII-S49G) (Lüddecke & Forchhammer, 2013b, 2015; Scholl, et al., 2020). Previous research had hinted at this "encounter complex" between PII and NAGK mutants (Fokina, et al., 2010a). The use of NanoBiT has provided valuable insights into the affinity of this complex and has shown that the formation of the complex is not facilitated by adenyl-nucleotide binding to PII, as evidenced by the observed variations in dissociation rates in the presence of

different effectors. The PII-S49E variant exhibits characteristics similar to those of a phosphorylated form of PII. Under situations of limited nitrogen availability, the canonical PII protein undergoes phosphorylation at residue S49. The altered version under consideration does not possess the capability to activate NAGK; hence, it is reasonable to hypothesize that phosphorylated PII may exhibit the same behavior. However, the research conducted by NanoBiT suggests that the intricate structure of the complex stays partially intact, suggesting that phosphorylation of PII leads to a loose connection between the proteins. Under certain conditions, the dephosphorylation of PII might lead to the rapid reformation of the PII-NAGK complex. In contrast, PII-I86N-LgBiT exhibited significant affinity for NAGK in the presence of ADP, while the previous data by SPR only detected the PII(I86N)–NAGK binding complex in the low concentration of ADP (25 Mm) (Fokina, et al., 2010b).

1.4 The calculation of K_D value for the interactions between PII and its interacting partners

In previous studies on cyanobacterial PII protein interactions using SPR, no K_D values were reported for the interactions between cyanobacterial PII protein and NAGK, as well as PII and PipX. These tests were focused on investigating the comparative influence of effector molecules on PII interactions (Fokina, et al., 2010b; Zeth, et al., 2014). The K_D value for the PII-NAGK complex was determined only by ultrafiltration experiments, which were carried out in a setting characterized by significantly elevated NAGK concentrations. This indicates that the equilibrium was mostly shifted towards the complex. From the minimal quantity of free PII, a K_D of around 73 nM was derived (Llácer, et al., 2007). The resultant K_D value obtained from our NanoBiT system (K_D = 12.9 nM) shows a roughly six-fold reduction, though within a similar range. The discrepancy might perhaps be attributed to the different buffers used in these tests. In more recent times, biolayer interferometry has been used for the evaluation of PII interactions. The evaluation of the PII-NAGK interaction was conducted as a prominent illustration of the approach. As a result, we proceeded to review the binding curves and reassess them, using the Octet data analysis HT software (ForteBio) to analyze the association and dissociation kinetics. The further assessment resulted in a calculated K_D value of 11.7±0.005 nM (Supplementary material in Scholl et al.) (Scholl, et al., 2020), which closely corresponds to the K_D value of 12.9±0.65 nM obtained from the NanoBiT sensor data. This simultaneous agreement enhances the credibility of the NanoBit sensor's results.

In the case of PII-PipX complex affinity, an approximate K_D value was reported in a previous study in the range of μM (6.8±0.7 μM) (Llácer, et al., 2010) which is several orders of magnitudes higher than the K_D value that we determined by NanoBiT in the range of nM. However, this previous determination of K_D was carried out by determining the amount of non-binding PII after removing PII-PipX complexes on Ni-NTA columns. The entire experiment was performed in the absence of effector molecules. Without effectors, only a very weak interaction between PII and PipX was detected by NanoBiT system and the high affinity complex only formed after addition of ATP or ADP. So the weak association between PII and PipX in the absence of adenyl-nucleotides is in perfect agreement with the previous data.

1.5 The competition involves PipX and NAGK vying for binding to PII

The NAGK and PipX proteins compete for binding to PII, with their affinity dependent on the metabolic state. The results of the ultrafiltration experiments demonstrated that the introduction of PipX had a detrimental effect on the interaction between PII and NAGK, leading to a weakened binding (Llácer, et al., 2010). In the context of a SPR competition test, the attachment of NAGK to a sensor chip was observed. The analyte utilized in this test consisted of a combination of PII and PipX. It was observed that the creation of the PII-NAGK complex exhibited a slower rate in the presence of PipX compared to its absence. It is worth mentioning that the addition of 1 mM ADP resulted in the total inhibition of PII-NAGK binding by PipX (Zeth, et al., 2014). The results obtained from FRET analysis provided further evidence that, under conditions of high ATP/ADP ratios, PII exhibits a greater affinity for NAGK compared to PipX. As the levels of ADP increase, the competitive advantage of PipX becomes more pronounced, resulting in the displacement of NAGK in terms of PII attachment (Lüddecke & Forchhammer, 2015). The use of the PII-focused NanoBiT toolbox in investigating the competitive binding of several PII receptors has shown that PII exhibits the highest affinity towards PipX in the presence of ADP (5.7 nM), while displaying a comparatively lesser affinity towards NAGK (30.8 nM). This implies that NAGK was unable to outperform PipX in terms of PII binding in the presence of ADP. Nevertheless, in the presence of ATP, the affinity of PII for PipX decreases to 52.4 nM, but its affinity for NAGK increases to 8.8 nM. In the given conditions, the introduction of additional NAGK resulted in a reduction of the interaction between PII-LgBiT and PipX-SmBiT, mostly as a consequence of effective competition. Interestingly, despite the presence of a large quantity of NAGK, the PII-LgBiT-PipX-SmBiT signal was not negated, despite the expectation that NAGK would have mostly controlled the signal. This lingering luminescence may suggest a close proximity between PipX-SmBiT and PII-LgBiT when they are connected to NAGK. However, more research is required to fully understand the precise mechanism behind their connection (Figure 5).

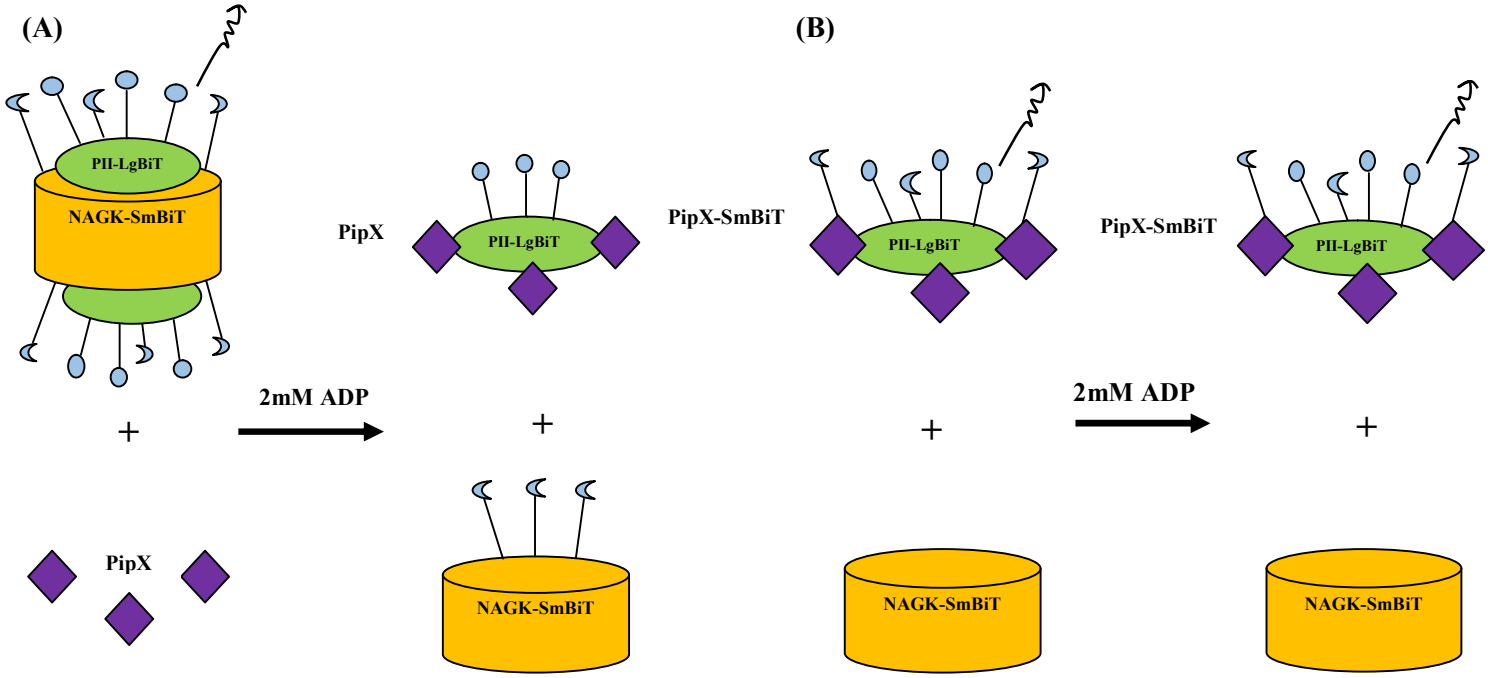

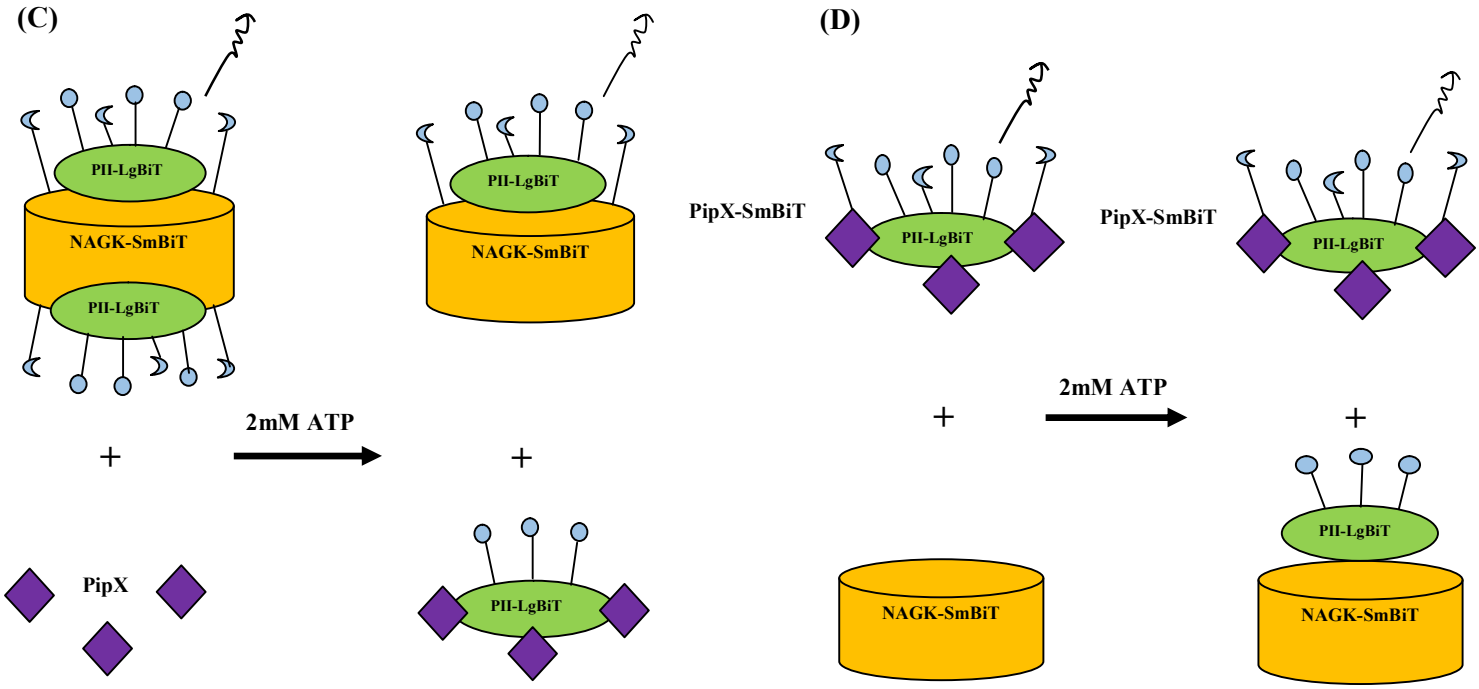

Figure 5. Schematic representation of competition among PII interaction partners to bind to PII in the presence of 2 mM effector molecules: (A) Competition between NAGK-SmBiT and PipX for PII-LgBiT binding in the presence of 2 mM ADP. (B) Competition between NAGK and PipX-SmBiT for PII-LgBiT binding in the presence of 2 mM ADP. (C) Competition between NAGK-SmBiT and PipX for PII-LgBiT binding in the presence of 2 mM ATP. (D) Competition between NAGK and PipX-SmBiT for PII-LgBiT binding in the presence of 2 mM ATP. LgBiT are shown in circle. SmBiT are shown in moon shape.

1.6 Role of arginine in modulating the PII-NAGK interaction

NAGK serves as a crucial enzyme throughout the arginine production process. Operating as a hexameric enzyme, it carries out the pivotal step within this route and is subject to regulation through feedback inhibition mediated by arginine (Vlasova et al., 2023). The interactions between the T-loop of PII and NAGK play a crucial role in defining the catalytic activity of the enzyme. When the binding of PII to NAGK occurs, it not only increases the activity of NAGK, but also mitigates the inhibitory effect provided by arginine via feedback inhibition. Nevertheless, when the cellular nitrogen levels are depleted, leading to high 2-OG concentrations, PII proteins form complexes with Mg^{2+}, ATP, and 2-OG effector molecules. The binding induces a conformational change in the T-loop, making it unfit for interactions with NAGK (Lüddecke & Forchhammer, 2013b).

The investigation conducted using the NanoBiT sensor provided insights into the impact of arginine on the interaction between PII-LgBiT and NAGK-SmBiT. It has been shown that the saturation of NAGK with arginine leads to a decrease in its binding affinity for PII. Remarkably, upon binding to its first allosteric site, arginine

exhibits a transient increase in its affinity for PII. At a dose of 2 mM, arginine significantly inhibits NAGK. It halts the enzymatic activity of free NAGK and inhibits the activity of NAGK when it forms a complex with PII by 90%. The results, mainly when combined with the luminescence data obtained from the titration studies, indicate that the decrease in enzyme activity is not attributable to the dissociation of the complex. It appears that PII may still bind to Arg-rich NAGK. However, the resultant complex may adopt a unique shape. The distinctive morphology of this structure has the potential to impede the catalytic activation of NAGK by PII.

The difficulty is further compounded by the behavior shown by the PII-I86N variant. This variant has an increased affinity for N-acetyl-L-glutamate kinase (NAGK) in the presence of arginine. The increased affinity mentioned above may explain the notable increase in arginine synthesis found in a particular strain of *Synechocystis*. In this experimental setup, the standard PII protein was replaced with the PII-I86N mutant, resulting in increased arginine synthesis and a significant accumulation of cyanophycin (Watzer, et al., 2019). This discovery strengthens the existing understanding of the complex and precise interplay between PII, its many forms, and NAGK in the control of arginine synthesis.

1.7 Effect of N-acetylglutamate (NAG) on the formation of the PII-NAGK complex

The PII proteins possess a significant evolutionary lineage associated with controlling the ornithine pathway, ultimately resulting in the synthesis of arginine and polyamine. One pivotal stage within the arginine production process is the transformation of N-acetyl-L glutamate (NAG) into N-acetyl-L-glutamyl 5-phosphate (NAG-P). The conversion method is assisted by the enzyme NAGK, whose genetic code encoded by the *argB* gene. The excessive presence of arginine has been seen to impede the activity of NAGK. However, it has been found that the unaltered PII protein, in its natural state, functions as a counteractive agent against this inhibitory effect (Heinrich, 2004; Maheswaran et al., 2004).

Our research into how NAG affects the interaction between PII and NAGK revealed that NAG acts as a stimulant, enhancing the PII-NAGK interaction regardless of the presence of ATP and ADP. Nevertheless, including Arg adds a certain level of complexity to the issue. The inhibitory effects of Arg on the affinity between PII and NAGK were seen to offset the beneficial influence of NAG, notably when the concentration of Arg reached 2mM. This suggests that the simple interaction of PII with NAGK is not enough to liberate the enzyme from the suppressive effects of Arg.

Upon further examination at the molecular level, it becomes evident that there exists a complex and complicated interaction of several forces in operation. The hydroxyl group located at position S49 forms a substantial network of hydrogen bonds, which directly interacts with the catalytic core of NAGK (Llácer, et al., 2007; Scholl, et al., 2020). The aforementioned network plays a crucial role in the modulation of NAGK's enzymatic activity. Therefore, the observed decrease in interaction between the S49E PII variant and NAGK do not affect the enzyme activity. Upon careful examination of previous metabolome data, it is evident that NAG exhibits a relatively low abundance, possibly in the low millimolar range, within the context of in vivo settings. This

observation suggests that NAG's significant stimulatory impact on the PII-NAGK complex has physiological significance.

A notable finding was seen during the analysis of the binding dynamics: increased substrate concentrations led to a corresponding increase in the binding affinity between NAGK and PII, resulting in enhanced kinetic activation. The observed activity, dependent on the substrate, exhibits a sigmoidal pattern that aligns well with a Hill slope of 1.76 ± 0.032. The significant impact of increasing NAG concentrations on enhancing the affinity between PII and NAGK highlights a distinct regulatory mechanism known as feed-forward regulation. This mechanism involves the substrate, NAG, facilitating the formation of the PII-NAGK complex. The aforementioned finding has unveiled new opportunities for comprehending the intricate control inside the arginine production pathway.

2. Metabolite fluctuation in real time experiments

The effect of 2-OG on in vivo interaction of PII-PipX NanoBiT or PII-NAGK NanoBiT sensor was also shown by different treatments. The results for ammonium upshift treatment were consistent for both sensors, with an increase in the RLU signal. The previous metabolomic analysis of E. coli cells with 10 mM NH_4Cl to nitrogen-limited cells revealed a rapid decline of 2-oxoglutarate levels, accompanied by a swift increase of glutamine levels (Yuan et al., 2009). Since the cyanobacterial PII and NAGK proteins don't respond to glutamine (Forchhammer & Lüddecke, 2016), it is reasonable to conclude that the observed increase in NanoBiT signals is indeed attributed to the reduction in 2-oxoglutarate levels, consequently increasing the interaction of PII-PipX or PII-NAGK.

The assessment of metabolic fluctuations in sensors, through the inhibition of nitrogen assimilation imposed by MSX and nitrogen starvation revealed that only PII-NAGK sensor exhibited a response to the changes. Due to the rapid increase in 2-OG levels, the dissociation of PII-NAGK occurs, leading to an immediate decline in RLU signal. However the PII-PipX NanoBiT sensor did not show any distinct decline. Prior studies demonstrated the PII-PipX interaction is remarkably sensitive to even minor changes in ADP levels. In fact, an increase in ADP levels enhances the interaction between PII and PipX (Fokina, et al., 2011; Zeth, et al., 2014). Therefore the limited dissociation efficiency of PII-PipX NanoBiT sensor may be attributed to a gradual increase in ADP concentrations, hindering the dissociation of PII-PipX complex.

3. PirA function in regulating the arginine synthesis pathway

As we have already talked about, NAGK plays a crucial role in the conversion of N-acetyl-L-glutamate (NAG) to N-acetyl-L-glutamyl-phosphate in plants and cyanobacteria. This enzymatic reaction serves as a pivotal step in the biosynthesis of ornithine and arginine (Llácer, et al., 2008; Selim, et al., 2019b). The activity of this enzyme is inhibited by feedback from Arg, but is augmented by its interaction with PII (Forcada-Nadal, et al., 2018; Forchhammer & Selim, 2020). Typically, PII teams up with NAGK to form a complex that effectively counteracts the inhibitory influences of Arg, thereby facilitating the synthesis of the desired final product (Lapina

et al., 2018b; Llácer, et al., 2007). Additionally, it has been acknowledged that the arginine metabolic process encompasses a specific dynamic loop called the ornithine-ammonia cycle (OAC). This cycle converts arginine into ornithine, and serves a crucial function in regulating nitrogen storage and remobilization machinery. This mechanism plays a crucial role in facilitating the adaptation of cyanobacterial cells to fluctuations in nitrogen concentrations within their surrounding environment (Zhang et al., 2018).

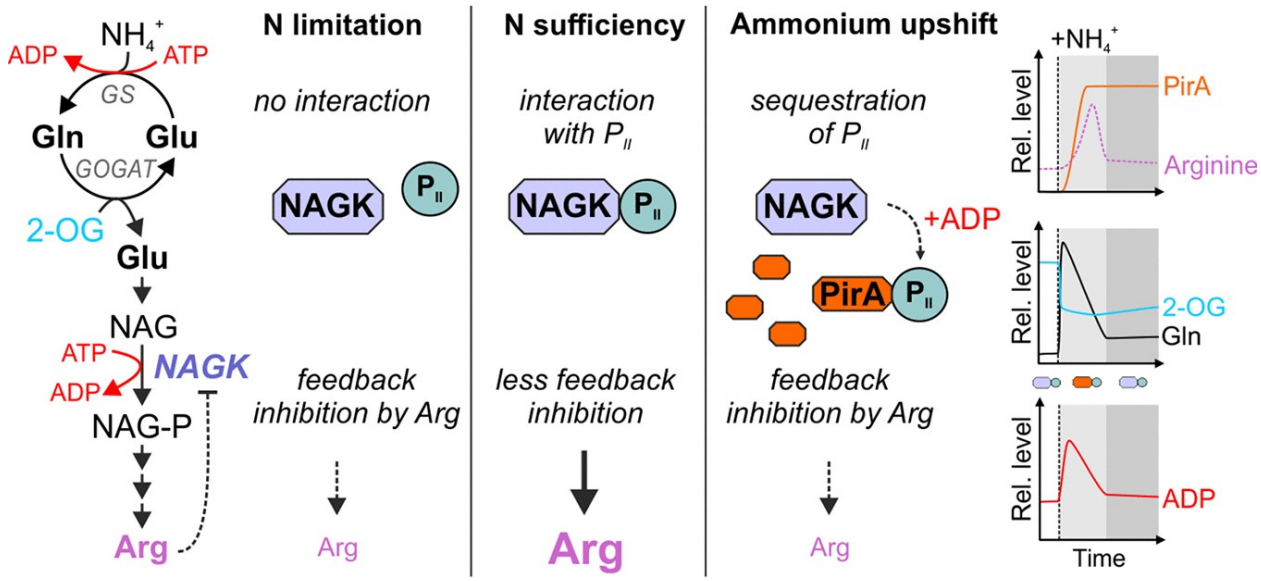

Figure 6. Predicted framework illustrating the role of PirA (from Bolay et al., 2021)

This study successfully found a novel factor that plays a role in the control of nitrogen metabolism in *Synechocystis* sp. PCC 6803. This component is a small cyanobacterial protein named PirA. This protein serves as a novel and critical regulator within the cyanobacterial arginine synthesis pathway and, consequently, the OAC. Recent findings indicate that PirA has a significant impact on the synthesis of arginine by engaging in competitive binding with NAGK for PII binding. The relationship between NAGK and the PII protein is shown to reduce the effectiveness of feedback inhibition. PirA, conversely, impedes the buildup of arginine and acts as an indirect inhibitor of NAGK (Figure 6).

3.1 The way PirA interferes with the formation of the PII-NAGK complex

In the presence of abundant amounts of ADP, the tiny protein PirA engages in competition with NAGK for PII binding, hence indicating a cellular state characterized by low energy levels. The interaction between PirA and PII is subject to substantial modulation by the levels of ADP, so establishing a link to the cellular energy status. The observed behavior resembles that of another protein, PipX, which exhibits interaction with PII and demonstrates a greater propensity for such interaction under elevated ADP concentrations (Fokina, et al., 2011; Zeth, et al., 2014). PipX enhances the functionality of the transcription factor NtcA and plays a crucial part in the process of 2-OG-driven DNA binding and subsequent activation of genes (Espinosa, et al., 2006; Espinosa, et al.,

2007; García-Domínguez, et al., 2000). When there is an excess of ADP, the regulatory protein known as PipX has a greater affinity for binding to the protein PII. The inhibition of NtcA activity leads to the indirect upregulation and increased expression of the *pirA* gene, resembling the reported pattern in the *gif* genes that encode the GS IFs (García-Domínguez, et al., 2000).

Fundamentally, the association between PII and NAGK is not only reliant on the presence of ATP; it may also take place in the presence of ADP, although with a lower degree of affinity. The findings of the NanoBiT research suggest that the creation of complexes occurs with both ADP and ATP. However, the strength of these complexes is comparatively less with ADP than with ATP (Figure 4b, Publication 1). The transient PII-NAGK complex was also shown in surface plasmon resonance (SPR) assays using ADP. Even though the presence of ADP contributes to the disengagement of NAGK from PII (Fokina, et al., 2010b; Fokina, et al., 2011). A comprehensive investigation highlights that ADP's impact on the connection between NAGK and PII is very insignificant in the presence of ATP. The critical aspect of their interaction is predicated upon the amounts of 2-OG (Fokina, et al., 2011; Lüddecke & Forchhammer, 2013b).

As has been discussed in earlier literatures, PII proteins serve the purpose of sensing the state of specific metabolites and transmitting these signals to diverse target proteins linked with PII (Selim, et al., 2020). Based on the available evidence, PirA can potentially enhance the energy-dependent signal in the PII-mediated activation of NAGK. In situations when there is a decrease in 2-OG levels and an increase in ADP levels, PirA binds to PII, perhaps causing a shift in the equilibrium of the PII-NAGK complex towards a state where NAGK is not bound to PII. This phenomenon is particularly evident when the cell experiences temporary limitations in energy availability. Given that bacteria use GS-GOGAT mostly when energy is abundant (Helling, 1998), it is plausible to suggest that the increased consumption of ATP by GS, resulting from the inflow of ammonium to nitrate-grown cells, could lead to energy deficiencies. This possible energy limitation may require the implementation of a restriction on the ATP-dependent conversion of NAGK into arginine. The coordination of a regulatory system in conjunction with the internal ADP levels inside a cell is of utmost importance, particularly considering the significant use of ATP.

NAGK is significantly influenced by the phosphorylation state of PII, which has a crucial position in the analysis of the complex structure of these components. The phosphorylation site S49 in PII establishes a hydrogen bond network with specific residues of NAGK, therefore guaranteeing the stability of their interaction (Forcada-Nadal, et al., 2018). Modifications at the S49 residue, whether induced by phosphorylation or genetic mutation, impede the collaborative interaction between NAGK and PII protein (Heinrich, et al., 2004; Lüddecke & Forchhammer, 2013b). It is noteworthy that the presence of S49 site in PII does not seem to impact its interaction with PipX. This is supported by the observation that the phosphomimic versions of PII, namely S49D, still retain their association with PipX (Espinosa, et al., 2006; Llácer, et al., 2010).

The PII variant S49E demonstrated a somewhat enhanced affinity for PirA compared to the wild type. The association between PII and PipX remains unaffected by any modifications at the Ser49 site. However, it

depends on the T-loop (Espinosa, et al., 2006). The binding site of fundamental importance is situated near the initiation point of the T-loop, whereas the terminal residue Ser49 does not participate in this binding interaction. The interaction mode between PirA and PII, being independent of Ser49, implies that PirA retains its ability to bind to a phosphorylated form of PII that is not associated with NAGK. Essentially, PII can't interact concurrently with NAGK and PirA due to their need on the T-loop, although in different conformations. This statement elucidates the in vitro effect of PirA on the activity of the PII-NAGK complex at inhibitory concentrations of arginine. When PirA competes for PII binding, it leaves NAGK free which is highly sensitive to arginine feedback inhibition. The competitive performance of NAGK and PirA is contingent upon the cellular equilibrium between ATP and ADP.

The interaction between PirA and PII, especially when NAGK is involved, is investigated by observing that PirA cannot attach to the PII (I86N) mutant despite the tremendous binding affinity of this variant towards NAGK. The T-loop demonstrates a higher degree of structural compaction when combined with NAGK, facilitated by forming a recently created hydrogen bond. The interaction between these two components results in the displacement of the front segment of the T-loop towards the core of PII. The presence of a salt bridge serves to reinforce the dense arrangement of atoms inside the T-loop (Fokina, et al., 2010b; Selim, et al., 2019b; Zeth, et al., 2012). Therefore, the failure of PirA to establish a complex with PII (I86N) is consistent with the observed activation of NAGK in vivo caused by this particular variant. The enhanced functionality of NAGK is attributed to its association with the non-phosphorylated variant of PII (PII (I86N)) (Heinrich, et al., 2004; Watzer, et al., 2015). To get a comprehensive understanding of the mechanisms through which PirA impacts PII signaling, it is essential to conduct thorough biochemical investigations and structural analyses.

VII. REFERENCES

Arcondéguy, T., Jack, R., & Merrick, M. (2001). PII signal transduction proteins, pivotal players in microbial nitrogen control. *Microbiology and Molecular Biology Reviews, 65*(1), 80-105.

Atkinson, M. R., & Ninfa, A. J. (1998). Role of the GlnK signal transduction protein in the regulation of nitrogen assimilation in Escherichia coli. *Molecular microbiology, 29*(2), 431-447.

Atkinson, M. R., & Ninfa, A. J. (1999). Characterization of the GlnK protein of Escherichia coli. *Molecular microbiology, 32*(2), 301-313.

Barrows, J. K., & Van Dyke, M. W. (2022). Biolayer interferometry for DNA-protein interactions. *PLoS One, 17*(2), e0263322.

Bedford, E. E., Spadavecchia, J., Pradier, C. M., & Gu, F. X. (2012). Surface plasmon resonance biosensors incorporating gold nanoparticles. *Macromolecular bioscience, 12*(6), 724-739.

Bolay, P., Muro-Pastor, M. I., Florencio, F. J., & Klähn, S. (2018). The distinctive regulation of cyanobacterial glutamine synthetase. *Life, 8*(4), 52.

Bolay, P., Rozbeh, R., Muro-Pastor, M. I., Timm, S., Hagemann, M., Florencio, F. J., . . . Klähn, S. (2021). The novel PII-interacting protein PirA controls flux into the cyanobacterial ornithine-ammonia cycle. *Mbio, 12*(2), 10.1128/mbio. 00229-00221.

Burillo, S., Luque, I., Fuentes, I., & Contreras, A. (2004). Interactions between the nitrogen signal transduction protein PII and N-acetyl glutamate kinase in organisms that perform oxygenic photosynthesis. *Journal of Bacteriology, 186*(11), 3346-3354.

Burnap, R. L., Hagemann, M., & Kaplan, A. (2015). Regulation of CO2 concentrating mechanism in cyanobacteria. *Life, 5*(1), 348-371.

Cheah, E., Carr, P. D., Suffolk, P. M., Vasudevan, S. G., Dixon, N. E., & Ollis, D. L. (1994). Structure of the Escherichia coli signal transducing protein PII. *Structure, 2*(10), 981-990.

Chollet, R., Vidal, J., & O'Leary, M. H. (1996). Phospho enol pyruvate carboxylase: a ubiquitous, highly regulated enzyme in plants. *Annual review of plant biology, 47*(1), 273-298.

Cloning, G. A. (2024). addgene.

Conroy, M. J., Durand, A., Lupo, D., Li, X.-D., Bullough, P. A., Winkler, F. K., & Merrick, M. (2007). The crystal structure of the Escherichia coli AmtB–GlnK complex reveals how GlnK regulates the ammonia channel. *Proceedings of the National Academy of Sciences, 104*(4), 1213-1218.

Coutts, G., Thomas, G., Blakey, D., & Merrick, M. (2002). Membrane sequestration of the signal transduction protein GlnK by the ammonium transporter AmtB. *The EMBO Journal, 21*(4), 536-545.

Dixon, A. S., Schwinn, M. K., Hall, M. P., Zimmerman, K., Otto, P., Lubben, T. H., . . . Kirkland, T. A. (2016). NanoLuc complementation reporter optimized for accurate measurement of protein interactions in cells. *ACS chemical biology, 11*(2), 400-408.

Domínguez-Martín, M. A., López-Lozano, A., Clavería-Gimeno, R., Velázquez-Campoy, A., Seidel, G., Burkovski, A., . . . García-Fernández, J. M. (2018). Differential NtcA responsiveness to 2-oxoglutarate underlies the diversity of C/N balance regulation in Prochlorococcus. *Frontiers in Microbiology, 8*, 2641.

Ehlers, C., Veit, K., Gottschalk, G., & Schmitz, R. A. (2002). Functional organization of a single nif cluster in the mesophilic archaeon Methanosarcina mazei strain Gö1. *Archaea, 1*(2), 143-150.

Espinosa, J., Forchhammer, K., Burillo, S., & Contreras, A. (2006). Interaction network in cyanobacterial nitrogen regulation: PipX, a protein that interacts in a 2-oxoglutarate dependent manner with PII and NtcA. *Molecular microbiology, 61*(2), 457-469.

Espinosa, J., Forchhammer, K., & Contreras, A. (2007). Role of the Synechococcus PCC 7942 nitrogen regulator protein PipX in NtcA-controlled processes. *Microbiology, 153*(3), 711-718.

Fokina, O., Chellamuthu, V.-R., Forchhammer, K., & Zeth, K. (2010a). Mechanism of 2-oxoglutarate signaling by the Synechococcus elongatus PII signal transduction protein. *Proceedings of the National Academy of Sciences, 107*(46), 19760-19765.

Fokina, O., Chellamuthu, V.-R., Zeth, K., & Forchhammer, K. (2010b). A novel signal transduction protein PII variant from Synechococcus elongatus PCC 7942 indicates a two-step process for NAGK–PII complex formation. *Journal of molecular biology, 399*(3), 410-421.

Fokina, O., Herrmann, C., & Forchhammer, K. (2011). Signal-transduction protein PII from Synechococcus elongatus PCC 7942 senses low adenylate energy charge in vitro. *Biochemical Journal, 440*(1), 147-156.

Forcada-Nadal, A., Forchhammer, K., & Rubio, V. (2014). SPR analysis of promoter binding of Synechocystis PCC6803 transcription factors NtcA and CRP suggests cross-talk and sheds light on regulation by effector molecules. *FEBS letters, 588*(14), 2270-2276.

Forcada-Nadal, A., Llácer, J. L., Contreras, A., Marco-Marín, C., & Rubio, V. (2018). The PII-NAGK-PipX-NtcA regulatory axis of cyanobacteria: A tale of changing partners, allosteric effectors and non-covalent interactions. *Frontiers in molecular biosciences, 5*, 91.

Forchhammer, K. (2004). Global carbon/nitrogen control by PII signal transduction in cyanobacteria: from signals to targets. *FEMS microbiology reviews, 28*(3), 319-333.

Forchhammer, K. (2008). PII signal transducers: novel functional and structural insights. *Trends in microbiology, 16*(2), 65-72.

Forchhammer, K., & Lüddecke, J. (2016). Sensory properties of the PII signalling protein family. *The FEBS journal, 283*(3), 425-437.

Forchhammer, K., & Selim, K. A. (2020). Carbon/nitrogen homeostasis control in cyanobacteria. *FEMS microbiology reviews, 44*(1), 33-53.

Forchhammer, K., Selim, K. A., & Huergo, L. F. (2022). New views on PII signaling: from nitrogen sensing to global metabolic control. *Trends in Microbiology*.

Forchhammer, K., & Tandeau de Marsac, N. (1994). The PII protein in the cyanobacterium Synechococcus sp. strain PCC 7942 is modified by serine phosphorylation and signals the cellular N-status. *Journal of Bacteriology, 176*(1), 84-91.

Forchhammer, K., & Tandeau de Marsac, N. (1995). Phosphorylation of the PII protein (glnB gene product) in the cyanobacterium Synechococcus sp. strain PCC 7942: analysis of in vitro kinase activity. *Journal of Bacteriology, 177*(20), 5812-5817.

García-Domínguez, M., Reyes, J. C., & Florencio, F. J. (1999). Glutamine synthetase inactivation by protein–protein interaction. *Proceedings of the National Academy of Sciences, 96*(13), 7161-7166.

García-Domínguez, M., Reyes, J. C., & Florencio, F. J. (2000). NtcA represses transcription of gifA and gifB, genes that encode inhibitors of glutamine synthetase type I from Synechocystis sp. PCC 6803. *Molecular microbiology, 35*(5), 1192-1201.

Giner-Lamia, J., Robles-Rengel, R., Hernández-Prieto, M. A., Muro-Pastor, M. I., Florencio, F. J., & Futschik, M. E. (2017). Identification of the direct regulon of NtcA during early acclimation to nitrogen starvation in the cyanobacterium Synechocystis sp. PCC 6803. *Nucleic acids research, 45*(20), 11800-11820.

Grau, F. C., Burkovski, A., & Muller, Y. A. (2021). Crystal structures of adenylylated and unadenylylated PII protein GlnK from Corynebacterium glutamicum. *Acta Crystallographica Section D: Structural Biology, 77*(3), 325-335.

Gruswitz, F., O'Connell III, J., & Stroud, R. M. (2007). Inhibitory complex of the transmembrane ammonia channel, AmtB, and the cytosolic regulatory protein, GlnK, at 1.96 Å. *Proceedings of the National Academy of Sciences, 104*(1), 42-47.

Harrison, M. A., Keen, J. N., Findlay, J. B., & Allen, J. F. (1990). Modification of a gInB-like gene product by photosynthetic electron transport in the cyanobacterium Synechococcus 6301. *FEBS letters, 264*(1), 25-28.

Haskett, T. L., Karunakaran, R., Bueno Batista, M., Dixon, R., & Poole, P. S. (2022). Control of nitrogen fixation and ammonia excretion in Azorhizobium caulinodans. *PLoS Genetics, 18*(6), e1010276.

Heinrich, A., Maheswaran, M., Ruppert, U., & Forchhammer, K. (2004). The Synechococcus elongatus PII signal transduction protein controls arginine synthesis by complex formation with N-acetyl-l-glutamate kinase. *Molecular microbiology, 52*(5), 1303-1314.

Heinrich, B. (2004). *Bumblebee economics*: Harvard University Press.

Helling, R. B. (1998). Pathway choice in glutamate synthesis in Escherichia coli. *Journal of bacteriology, 180*(17), 4571-4575.

Herrero, A., Muro-Pastor, A. M., & Flores, E. (2001). Nitrogen control in cyanobacteria. *Journal of bacteriology, 183*(2), 411-425.

Huergo, L. F., Chandra, G., & Merrick, M. (2013). PII signal transduction proteins: nitrogen regulation and beyond. *FEMS microbiology reviews, 37*(2), 251-283.

Javelle, A., & Merrick, M. (2005). Complex formation between AmtB and GlnK: an ancestral role in prokaryotic nitrogen control: Portland Press Ltd.

Javelle, A., Severi, E., Thornton, J., & Merrick, M. (2004). Ammonium sensing in Escherichia coli: role of the ammonium transporter AmtB and AmtB-GlnK complex formation. *Journal of Biological Chemistry, 279*(10), 8530-8538.

Jiang, P., Mayo, A. E., & Ninfa, A. J. (2007). Escherichia coli glutamine synthetase adenylyltransferase (ATase, EC 2.7. 7.49): Kinetic characterization of regulation by PII, PII-UMP, glutamine, and α-ketoglutarate. *Biochemistry, 46*(13), 4133-4146.

Jiang, P., & Ninfa, A. J. (2007). Escherichia coli PII signal transduction protein controlling nitrogen assimilation acts as a sensor of adenylate energy charge in vitro. *Biochemistry, 46*(45), 12979-12996.

Jiang, P., Zucker, P., Atkinson, M. R., Kamberov, E. S., Tirasophon, W., Chandran, P., . . . Ninfa, A. J. (1997a). Structure/function analysis of the PII signal transduction protein of Escherichia coli: genetic separation of interactions with protein receptors. *Journal of Bacteriology, 179*(13), 4342-4353.

Jiang, P., Zucker, P., & Ninfa, A. J. (1997b). Probing interactions of the homotrimeric PII signal transduction protein with its receptors by use of PII heterotrimers formed in vitro from wild-type and mutant subunits. *Journal of Bacteriology, 179*(13), 4354-4360.

Khademi, S., O'Connell III, J., Remis, J., Robles-Colmenares, Y., Miercke, L. J., & Stroud, R. M. (2004). Mechanism of ammonia transport by Amt/MEP/Rh: structure of AmtB at 1.35 A. *Science, 305*(5690), 1587-1594.

Kinch, L. N., & Grishin, N. V. (2002). Evolution of protein structures and functions. *Current opinion in structural biology, 12*(3), 400-408.

Klähn, S., Bolay, P., Wright, P. R., Atilho, R. M., Brewer, K. I., Hagemann, M., . . . Hess, W. R. (2018). A glutamine riboswitch is a key element for the regulation of glutamine synthetase in cyanobacteria. *Nucleic acids research, 46*(19), 10082-10094.

Klotz, A., Georg, J., Bučinská, L., Watanabe, S., Reimann, V., Januszewski, W., . . . Forchhammer, K. (2016). Awakening of a dormant cyanobacterium from nitrogen chlorosis reveals a genetically determined program. *Current Biology, 26*(21), 2862-2872.

Koch, M., Doello, S., Gutekunst, K., & Forchhammer, K. (2019). PHB is produced from glycogen turn-over during nitrogen starvation in Synechocystis sp. PCC 6803. *International journal of molecular sciences, 20*(8), 1942.

Krysenko, S., & Wohlleben, W. (2022). Polyamine and ethanolamine metabolism in bacteria as an important component of nitrogen assimilation for survival and pathogenicity. *Medical Sciences, 10*(3), 40.

Laichoubi, K. B., Beez, S., Espinosa, J., Forchhammer, K., & Contreras, A. (2011). The nitrogen interaction network in Synechococcus WH5701, a cyanobacterium with two PipX and two PII-like proteins. *Microbiology, 157*(4), 1220-1228.

Lapina, T., Selim, K. A., Forchhammer, K., & Ermilova, E. (2018a). The PII signaling protein from red algae represents an evolutionary link between cyanobacterial and Chloroplastida PII proteins. *Scientific Reports, 8*(1), 1-14.

Lapina, T., Selim, K. A., Forchhammer, K., & Ermilova, E. (2018b). The PII signaling protein from red algae represents an evolutionary link between cyanobacterial and Chloroplastida PII proteins. *Scientific Reports, 8*(1), 790.

Leigh, J. A., & Dodsworth, J. A. (2007). Nitrogen regulation in bacteria and archaea. *Annu. Rev. Microbiol., 61*, 349-377.

Llácer, J. L., Contreras, A., Forchhammer, K., Marco-Marín, C., Gil-Ortiz, F., Maldonado, R., . . . Rubio, V. (2007). The crystal structure of the complex of PII and acetylglutamate kinase reveals how PII controls the storage of nitrogen as arginine. *Proceedings of the National Academy of Sciences, 104*(45), 17644-17649.

Llácer, J. L., Espinosa, J., Castells, M. A., Contreras, A., Forchhammer, K., & Rubio, V. (2010). Structural basis for the regulation of NtcA-dependent transcription by proteins PipX and PII. *Proceedings of the National Academy of Sciences, 107*(35), 15397-15402.

Llácer, J. L., Fita, I., & Rubio, V. (2008). Arginine and nitrogen storage. *Current opinion in structural biology, 18*(6), 673-681.

Llop Estevez, A., Bibak, S., Cantos, R., Salinas, P., & Contreras, A. (2023). The ribosome assembly GTPase EngA is involved in redox signaling in cyanobacteria.

Lüddecke, J., & Forchhammer, K. (2013a). From P II Signaling to Metabolite Sensing: A Novel 2-Oxoglutarate Sensor That Details P II-NAGK Complex Formation. *PLoS One, 8*(12), e83181.

Lüddecke, J., & Forchhammer, K. (2013b). From PII signaling to metabolite sensing: a novel 2-oxoglutarate sensor that details PII-NAGK complex formation. *PLoS One, 8*(12), e83181.

Lüddecke, J., & Forchhammer, K. (2015). Energy sensing versus 2-oxoglutarate dependent ATPase switch in the control of Synechococcus PII interaction with its targets NAGK and PipX. *PLoS One, 10*(8), e0137114.

Lüddecke, J., Francois, L., Spät, P., Watzer, B., Chilczuk, T., Poschet, G., . . . Forchhammer, K. (2017). PII protein-derived FRET sensors for quantification and live-cell imaging of 2-oxoglutarate. *Scientific Reports, 7*(1), 1-13.

Luque, I., Flores, E., & Herrero, A. (1994). Molecular mechanism for the operation of nitrogen control in cyanobacteria. *The EMBO Journal, 13*(12), 2862-2869.

Luque, I., & Forchhammer, K. (2008). Nitrogen assimilation and C/N balance sensing. *The cyanobacteria: molecular biology, genomics and evolution*, 335-382.

Maheswaran, M., Urbanke, C., & Forchhammer, K. (2004). Complex formation and catalytic activation by the PII signaling protein of N-acetyl-L-glutamate kinase from Synechococcus elongatus strain PCC 7942. *Journal of Biological Chemistry, 279*(53), 55202-55210.

Maheswaran, M., Ziegler, K., Lockau, W., Hagemann, M., & Forchhammer, K. (2006). PII-regulated arginine synthesis controls accumulation of cyanophycin in Synechocystis sp. strain PCC 6803. *Journal of Bacteriology, 188*(7), 2730-2734.

Martin, J. (2011). Harnessing Optical Label-Free on Microtiter Plates for Lead Finding: From Binding to Phenotypes. *Label-Free Technologies for Drug Discovery*, 171-187.

Merrick, M. (2015). Post-translational modification of P II signal transduction proteins. *Frontiers in Microbiology, 5*, 763.

Moure, V. R., Razzera, G., Araújo, L. M., Oliveira, M. A., Gerhardt, E. C., Müller-Santos, M., . . . Souza, E. M. (2012). Heat stability of Proteobacterial PII protein facilitate purification using a single chromatography step. *Protein expression and purification, 81*(1), 83-88.

Ninfa, A. J., & Atkinson, M. R. (2000). PII signal transduction proteins. *Trends in microbiology, 8*(4), 172-179.

Ohashi, Y., Shi, W., Takatani, N., Aichi, M., Maeda, S.-i., Watanabe, S., . . . Omata, T. (2011). Regulation of nitrate assimilation in cyanobacteria. *Journal of experimental Botany, 62*(4), 1411-1424.

Ohmuro-Matsuyama, Y., & Ueda, H. (2019). Protein-protein interaction assays using split-NanoLuc. *Bioluminescence-Analytical Applications and Basic Biology*, 1-16.

Orthwein, T., Scholl, J., Spät, P., Lucius, S., Koch, M., Macek, B., . . . Forchhammer, K. (2021). The novel PII-interactor PirC identifies phosphoglycerate mutase as key control point of carbon storage metabolism in cyanobacteria. *Proceedings of the National Academy of Sciences, 118*(6), e2019988118.

Pedro-Roig, L., Lange, C., Bonete, M. J., Soppa, J., & Maupin-Furlow, J. (2013). Nitrogen regulation of protein–protein interactions and transcript levels of GlnK PII regulator and AmtB ammonium transporter homologs in Archaea. *MicrobiologyOpen, 2*(5), 826-840.

Petersen, R. L. (2017). Strategies using bio-layer interferometry biosensor technology for vaccine research and development. *Biosensors, 7*(4), 49.

Piston, D. W., & Kremers, G.-J. (2007). Fluorescent protein FRET: the good, the bad and the ugly. *Trends in biochemical sciences, 32*(9), 407-414.

Preiss, J. (1984). Bacterial glycogen synthesis and its regulation. *Annual review of microbiology, 38*(1), 419-458.

Qian, X., Zhang, Y., Lun, D. S., & Dismukes, G. C. (2018). Rerouting of metabolism into desired cellular products by nutrient stress: fluxes reveal the selected pathways in cyanobacterial photosynthesis. *ACS Synthetic Biology, 7*(5), 1465-1476.

Radchenko, M. V., Thornton, J., & Merrick, M. (2013). PII signal transduction proteins are ATPases whose activity is regulated by 2-oxoglutarate. *Proceedings of the National Academy of Sciences, 110*(32), 12948-12953.

Reitzer, L. (2003). Nitrogen assimilation and global regulation in Escherichia coli. *Annual Reviews in Microbiology, 57*(1), 155-176.

Reyes, J., Muro-Pastor, M., & Florencio, F. (1997). Transcription of glutamine synthetase genes (glnA and glnN) from the cyanobacterium Synechocystis sp. strain PCC 6803 is differently regulated in response to nitrogen availability. *Journal of bacteriology, 179*(8), 2678-2689.

Rozbeh, R., & Forchhammer, K. (2021). Split NanoLuc technology allows quantitation of interactions between PII protein and its receptors with unprecedented sensitivity and reveals transient interactions. *Scientific Reports, 11*(1), 1-13.

Saelices, L., Galmozzi, C. V., Florencio, F. J., & Muro-Pastor, M. I. (2011). Mutational analysis of the inactivating factors, IF7 and IF17 from Synechocystis sp. PCC 6803: critical role of arginine amino acid residues for glutamine synthetase inactivation. *Molecular microbiology, 82*(4), 964-975.

Sant'Anna, F. H., Trentini, D. B., de Souto Weber, S., Cecagno, R., Da Silva, S. C., & Schrank, I. S. (2009). The PII superfamily revised: a novel group and evolutionary insights. *Journal of molecular evolution, 68*, 322-336.

Scholl, J., Dengler, L., Bader, L., & Forchhammer, K. (2020). Phosphoenolpyruvate carboxylase from the cyanobacterium Synechocystis sp. PCC 6803 is under global metabolic control by PII signaling. *Molecular microbiology, 114*(2), 292-307.

Schubert, C. (2021). *L-Aspartate is a high-quality nitrogen source of Escherichia coli: regulation and physiology.* Johannes Gutenberg-Universität Mainz.

Schwinn, M. K., Machleidt, T., Zimmerman, K., Eggers, C. T., Dixon, A. S., Hurst, R., . . . Wood, K. V. (2018). CRISPR-mediated tagging of endogenous proteins with a luminescent peptide. *ACS chemical biology, 13*(2), 467-474.

Selim, K. A., Ermilova, E., & Forchhammer, K. (2020). From cyanobacteria to Archaeplastida: new evolutionary insights into PII signalling in the plant kingdom. *New Phytologist, 227*(3), 722-731.

Selim, K. A., Haffner, M., Watzer, B., & Forchhammer, K. (2019a). Tuning the in vitro sensing and signaling properties of cyanobacterial PII protein by mutation of key residues. *Scientific reports, 9*(1), 1-11.

Selim, K. A., Haffner, M., Watzer, B., & Forchhammer, K. (2019b). Tuning the in vitro sensing and signaling properties of cyanobacterial PII protein by mutation of key residues. *Scientific Reports, 9*(1), 18985.

Shalabney, A., & Abdulhalim, I. (2011). Sensitivity-enhancement methods for surface plasmon sensors. *Laser & Photonics Reviews, 5*(4), 571-606.

Shapiro, B. M. (1969). Glutamine synthetase deadenylylating enzyme system from Escherichia coli. Resolution into two components, specific nucleotide stimulation, and cofactor requirements. *Biochemistry, 8*(2), 659-670.

Shen, F., Qin, Y., Wang, R., Huang, X., Wang, Y., Gao, T., . . . Wei, J. (2023). Comparative genomics reveals a unique nitrogen-carbon balance system in Asteraceae. *Nature Communications, 14*(1), 4334.

Smith, C. S., Morrice, N. A., & Moorhead, G. B. (2004). Lack of evidence for phosphorylation of Arabidopsis thaliana PII: implications for plastid carbon and nitrogen signaling. *Biochimica et Biophysica Acta (BBA)-Proteins and Proteomics, 1699*(1-2), 145-154.

Smith, C. S., Weljie, A. M., & Moorhead, G. B. (2003). Molecular properties of the putative nitrogen sensor PII from Arabidopsis thaliana. *The Plant Journal, 33*(2), 353-360.

Son, H., & Rhee, S. (1987). Cascade control of Escherichia coli glutamine synthetase. Purification and properties of PII protein and nucleotide sequence of its structural gene. *Journal of Biological Chemistry, 262*(18), 8690-8695.

Stadtman, E., & Ginsburg, A. (1974). 24. The Glutamine synthetase of Escherichia coli: Structure and control *The enzymes* (Vol. 10, pp. 755-807): Elsevier.

Stadtman, E. R. (2001). The story of glutamine synthetase regulation. *Journal of Biological Chemistry, 276*(48), 44357-44364.

Svensson, P., Bläsing, O. E., & Westhoff, P. (2003). Evolution of C4 phosphoenolpyruvate carboxylase. *Archives of Biochemistry and Biophysics, 414*(2), 180-188.

Tantama, M., Martínez-François, J. R., Mongeon, R., & Yellen, G. (2013). Imaging energy status in live cells with a fluorescent biosensor of the intracellular ATP-to-ADP ratio. *Nature communications, 4*(1), 2550.

Thomas, G. H., Mullins, J. G., & Merrick, M. (2000). Membrane topology of the Mep/Amt family of ammonium transporters. *Molecular microbiology, 37*(2), 331-344.

Tsang, T. F., Qiu, Y., Lin, L., Ye, J., Ma, C., & Yang, X. (2019). Simple method for studying in vitro protein–protein interactions based on protein complementation and its application in drug screening targeting bacterial transcription. *ACS Infectious Diseases, 5*(4), 521-527.

Uhrig, R. G., Ng, K. K., & Moorhead, G. B. (2009). PII in higher plants: a modern role for an ancient protein. *Trends in plant science, 14*(9), 505-511.

Van Heeswijk, W. C., Hoving, S., Molenaar, D., Stegeman, B., Kahn, D., & Westerhoff, H. V. (1996). An alternative PII protein in the regulation of glutamine synthetase in Escherichia coli. *Molecular microbiology, 21*(1), 133-146.

van Heeswijk, W. C., Wen, D., Clancy, P., Jaggi, R., Ollis, D. L., Westerhoff, H. V., & Vasudevan, S. G. (2000). The Escherichia coli signal transducers PII (GlnB) and GlnK form heterotrimers in vivo: fine tuning the nitrogen signal cascade. *Proceedings of the National Academy of Sciences, 97*(8), 3942-3947.

Vázquez-Bermúdez, M. a. F., Paz-Yepes, J., Herrero, A., & Flores, E. (2002). The NtcA-activated amt1 gene encodes a permease required for uptake of low concentrations of ammonium in the cyanobacterium Synechococcus sp. PCC 7942. *Microbiology, 148*(3), 861-869.

Vlasova, V., Lapina, T., Statinov, V., & Ermilova, E. (2023). N-Acetyl-L-glutamate Kinase of Chlamydomonas reinhardtii: In Vivo Regulation by PII Protein and Beyond. *International Journal of Molecular Sciences, 24*(16), 12873.

Wallner, J., Lhota, G., Jeschek, D., Mader, A., & Vorauer-Uhl, K. (2013). Application of Bio-Layer Interferometry for the analysis of protein/liposome interactions. *Journal of pharmaceutical and biomedical analysis, 72*, 150-154.

Wang, J., Lin, W., Cao, E., Xu, X., Liang, W., & Zhang, X. (2017). Surface plasmon resonance sensors on Raman and fluorescence spectroscopy. *Sensors, 17*(12), 2719.

Wang, Y., & Wang, L. V. (2012). Förster resonance energy transfer photoacoustic microscopy. *Journal of Biomedical Optics, 17*(8), 086007-086007.

Wang, Y., & Wang, L. V. (2013). *Förster resonance energy transfer photoacoustic microscopy.* Paper presented at the Photons Plus Ultrasound: Imaging and Sensing 2013.

Watzer, B., Engelbrecht, A., Hauf, W., Stahl, M., Maldener, I., & Forchhammer, K. (2015). Metabolic pathway engineering using the central signal processor P II. *Microbial Cell Factories, 14*, 1-12.

Watzer, B., Spät, P., Neumann, N., Koch, M., Sobotka, R., Macek, B., . . . Forchhammer, K. (2019). The signal transduction protein PII controls ammonium, nitrate and urea uptake in cyanobacteria. *Frontiers in microbiology, 10*, 1428.

Weber, I. T., & Steitz, T. A. (1987). Structure of a complex of catabolite gene activator protein and cyclic AMP refined at 2.5 Å resolution. *Journal of molecular biology, 198*(2), 311-326.

Wei, X., Yin, M., Zhang, L., Lin, H., Wang, J., Xie, W., & Xu, D. (2022). Surface Plasmon Resonance (SPR) biosensor for detection of mycotoxins: A review. *Journal of Immunological Methods*, 113349.

Yang, C., Hua, Q., & Shimizu, K. (2002). Metabolic flux analysis in Synechocystis using isotope distribution from 13C-labeled glucose. *Metabolic engineering, 4*(3), 202-216.

Yano, H., Cai, N. S., Javitch, J. A., & Ferré, S. (2018). Luciferase complementation based-detection of G-protein-coupled receptor activity. *BioTechniques, 65*(1), 9-14.

Yuan, J., Doucette, C. D., Fowler, W. U., Feng, X. J., Piazza, M., Rabitz, H. A., . . . Rabinowitz, J. D. (2009). Metabolomics-driven quantitative analysis of ammonia assimilation in E. coli. *Molecular systems biology, 5*(1), 302.

Zeth, K., Fokina, O., & Forchhammer, K. (2012). An engineered PII protein variant that senses a novel ligand: atomic resolution structure of the complex with citrate. *Acta Crystallographica Section D: Biological Crystallography, 68*(8), 901-908.

Zeth, K., Fokina, O., & Forchhammer, K. (2014). Structural basis and target-specific modulation of ADP sensing by the Synechococcus elongatus PII signaling protein. *Journal of Biological Chemistry, 289*(13), 8960-8972.

Zhang, H., Liu, Y., Nie, X., Liu, L., Hua, Q., Zhao, G.-P., & Yang, C. (2018). The cyanobacterial ornithine–ammonia cycle involves an arginine dihydrolase. *Nature Chemical Biology, 14*(6), 575-581.

Zhao, M.-X., Jiang, Y.-L., Xu, B.-Y., Chen, Y., Zhang, C.-C., & Zhou, C.-Z. (2010). Crystal structure of the cyanobacterial signal transduction protein PII in complex with PipX. *Journal of molecular biology, 402*(3), 552-559.

Zheng, L., Kostrewa, D., Bernèche, S., Winkler, F. K., & Li, X.-D. (2004). The mechanism of ammonia transport based on the crystal structure of AmtB of Escherichia coli. *Proceedings of the National Academy of Sciences, 101*(49), 17090-17095.

VIII. ADDITIONAL RESEARCH

1. Investigating the interaction between PII and the PII-interacting protein PirA using NanoBiT technology analysis

1.1.Introduction

The goal of our sensor development was to examine the intricate nature of interactions between PII and target proteins in the presence of bound metabolites and inside the cells. PirA, a protein involved in the modulation of flux into the ornithine-ammonia cycle (OAC) (Zhang, et al., 2018), has been identified as an additional interaction partner of the PII protein. The PirA protein specifically engages in competition with NAGK for PII binding, resulting in the inhibition of NAGK activation. Consequently, this leads to a reduction in the biosynthesis of arginine. In our attempt to study the PII-PirA interaction using the NanoBiT technique, we employed the insights acquired through the construction of the PII-NAGK NanoBiT sensor (Figure 1A).

1.2.Result and discussion

To monitor the kinetics of PII-PirA complex formation in vitro by measuring luminescence, increasing concentrations of PirA-SmBiT were titrated to the fixed amounts of PII-LgBiT (10 pM trimer) in the presence of various PII effector molecules. The luminescence background from PII-LgBiT and PirA-SmBiT alone was subtracted from the luminescence signal of the PII-LgBiT-PirA-SmBiT complex formation. Then the luminescence was plotted against the PirA-SmBiT concentrations (Figure 1B). The data indicates that PII and PirA readily form complexes when ADP is present (K_D value: 2.4 ± 1.2 μM), In the presence of a mixture containing 1 mM ATP and 1 mM ADP, the formation of complexes occurred, but with reduced affinity (K_D value: 8.3 ± 3.4 μM). With ATP present, the affinity of the complex decreased even more. While in the absence of effector molecules, a minimal increase in luminescence was observed (K_D value: 17.88 ± 1.1 μM in the presence of ATP and 36.3 ± 2.6 μM without metabolites) (Figure 1B and Table 1). In biolayer interferometry (BLI) experiments, complex formation was only detected in the presence of ADP, and no interaction was observed in the presence of ATP or in the absence of effector molecules (Figure 5B, Publication 2). This indicates the high sensitivity of the NanoBiT method.

To find out the effect of 2-OG on PII-PirA complex formation, a 10 pM PII-LgBiT trimer was incubated for 10 minutes with 300 nM PirA-SmBiT in the presence of 2 mM ATP and different concentrations of 2-OG. The result indicated that the luminescence signal gradually increased as the concentration of 2-OG went up (Figure 1C), but no binding was seen with the BLI method (Figure 5B, Publication 2). Therefore, 2-OG has a supportive effect on PII-LgBiT-PirA-SmBiT complex formation.

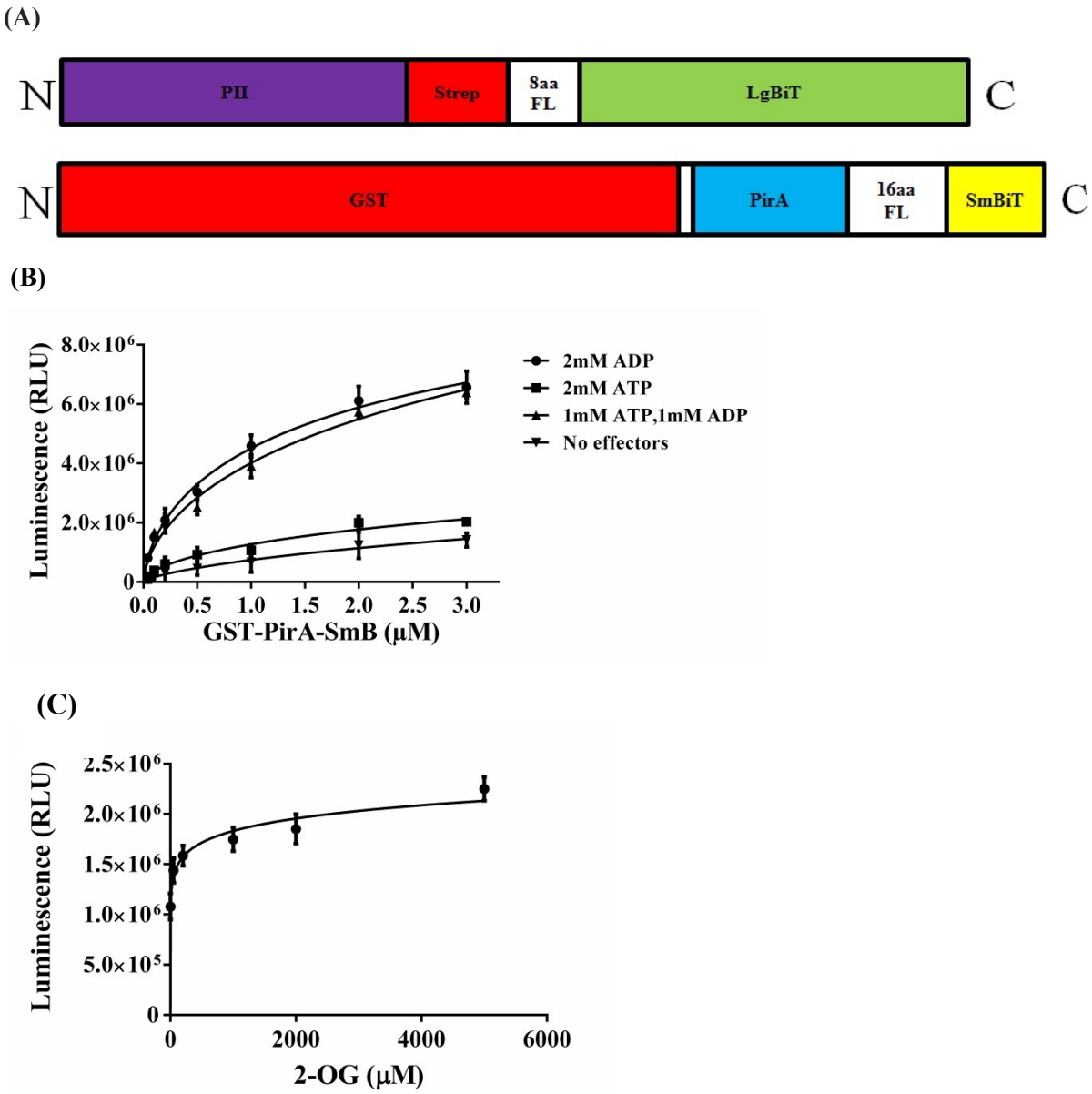

Figure 1. Fusion protein constructs and PII-LgBiT – PirA-SmBiT complex formation in the presence of effector molecules. (A) Schematic representation of PII-LgBiT and PirA-SmBiT fusion proteins. Flexible linkers in constructs fused to LgBiT and SmBiT. (B) Titration of PirA-SmBiT (0,0.04, 0.1, 0.2, 0.4, 1, 2, 3 µM) to PII-LgBiT (10 pM) in the presence of 2mM ATP, 2mM ADP, 1mM ATP/1mM ADP and without effector molecules. (C) Interaction of PII-LgBiT (10 pM trimer) and PirA-SmBiT (300 nM monomer) in the presence of: 0, 0.05, 0.2, 1, 2, 5 mM 2OG and 2mM ATP. Data are the means ± SD from triplicate measurements.

Next, we studied the effect of different ADP and ATP concentrations on PII-PirA complex formation. The time-course luminescence assay was followed by mixing 10 pM PII-LgBiT trimer and 1000 nM PirA-SmBiT monomer. First, PII-LgBiT and PirA-SmBiT were pre-incubated without adenyl nucleotides. After three minutes of measurement, different concentrations of ADP (0, 0.01, 0.05, 0.1, 0.25, 0.5, 1, 1.5, 2 mM) or ATP (0, 0.1, 1

mM) were added to allow complex formation. The rise of the luminescence signal indicated that the subsequent addition of ADP from 0.05 mM upwards immediately stimulated the interaction. In the presence of ADP, the increase was much steeper, and it reached a plateau after 3 min. The maximum interaction occurred at a concentration of 1 mM ADP (Figure 2, left panel). While at different ATP concentrations, the affinity of the PII-LgBiT-PirA-SmBiT complex was low and almost in the same ranges (Figure 2, right panel).

To find out the impact of the ATP-to-ADP ratio as an indicator of cellular energy state on PII-PirA complex formation by the NanoBiT sensor, the luminescence signal was recorded at diverse ATP/ADP ratios while the total concentrations of effectors were kept at 2 mM. Figure 2B demonstrated that ATP acted as an inhibitor of the ADP effect. The data in Figure 2A indicated that 1 mM ADP exhibited the strongest interaction between PII-LgBiT-PirA-SmBiT. However, in the presence of ATP, the addition of 1 mM ADP partially elevated the luminescence signal (Figure 2B). This implies that in the presence of ATP, the effect of ADP is simply mitigated. Consequently the interaction is not able to reach the maximum binding. The formation of the PII-PirA complex remains unaffected at low ADP concentrations, in contrast to the PII-PipX complex where even a small amount of ADP has a significant impact on complex formation. For PirA, a favorable increase is observed only when a 1:1 ratio between ATP and ADP is achieved, requiring an equal proportion of both nucleotides (Figure 2B). On the other hand, in the case of PipX, a 1:1 ratio between ATP and ADP results in luminescence close to the maximum, indicating that the addition of ATP has a less pronounced effect (Rozbeh & Forchhammer, 2021).

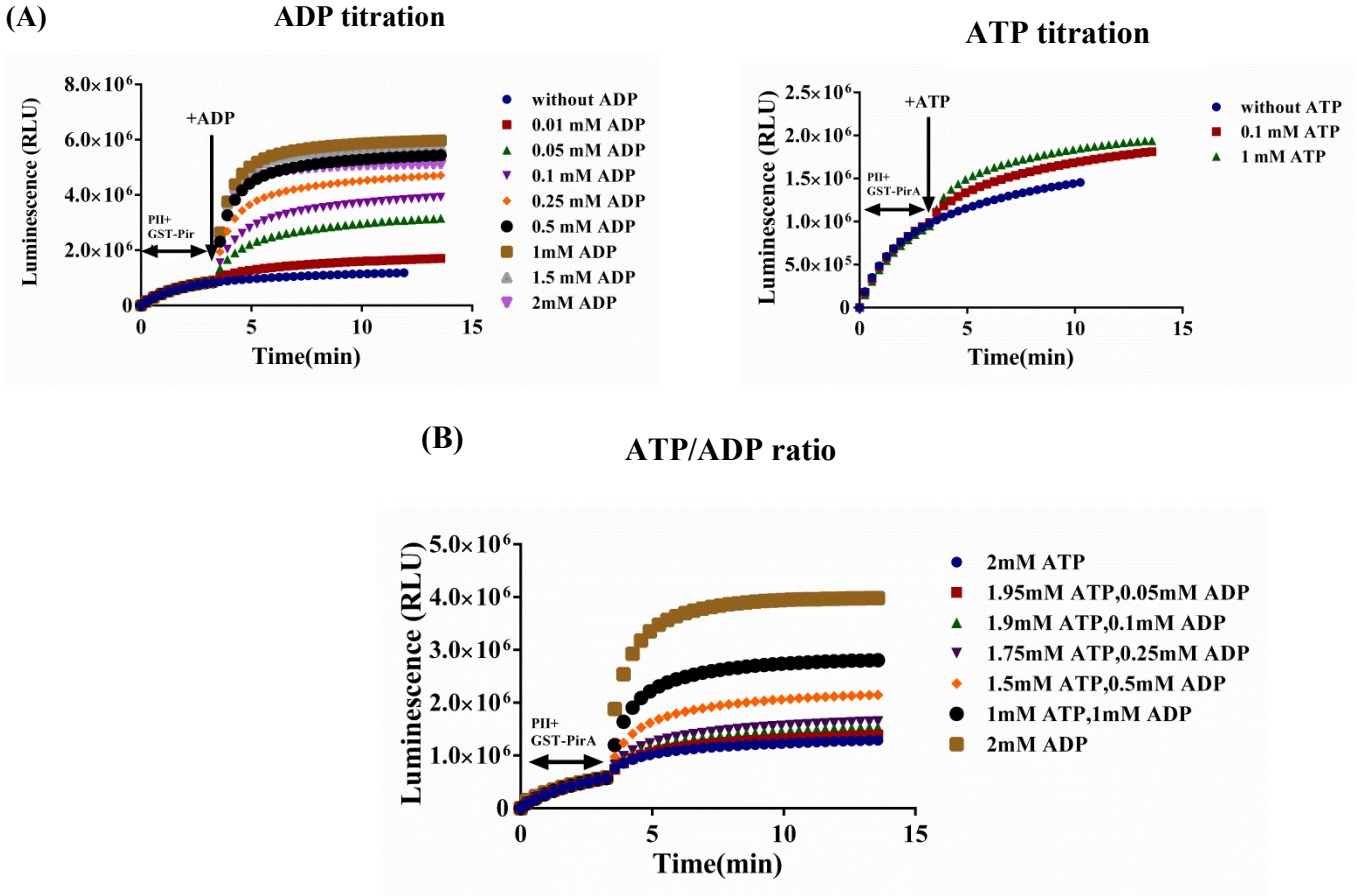

Figure 2. Effect of ATP or ADP concentrations and ATP/ADP ratio on PII-LgBiT - PirA-SmBiT complex formation. (A) Interaction of PII-LgBiT (10 pM trimer) and PirA-SmBiT (1000 nM monomer) in the presence of different concentrations of ADP (left panel) and different concentrations of ATP (right panel). (B) Interaction of PII-LgBiT (10 pM trimer) and PirA-SmBiT (1000 nM monomer) in ATP/ADP ratio.

To verify the association kinetics of PirA-SmBiT with two mutant PII-LgBiT variants, the purified PirA-SmBiT fusion protein was titrated to 10 pM PII (S49E)-LgBiT and PII (I86N)-LgBiT in the presence of 2 mM ATP or 2 mM ADP. As shown earlier through the BLI method, complex formation was observed in the presence of ADP, and PII (S49E) exhibited same complex formation as PII (WT). The NanoBiT sensor also supported this conclusion. The complex formation of PII (S49E)-LgBiT-PirA-SmBiT was much more detectable in the presence of ADP. The affinity of the complex for PII (S49E) revealed by the NanoBiT experiment (K_D value: 2.1 ± 1.5 µM) was approximately four times higher than the BLI result. (K_D value: 9 ± 3.1 µM) (Figure 3A and Table 1). In BLI experiments, interactions between PirA and PII variants were not detectable in the presence of ATP (Figure 5B, Publication 2); however, low affinities were observed in NanoBiT analysis (Figure 3B and Table 1).

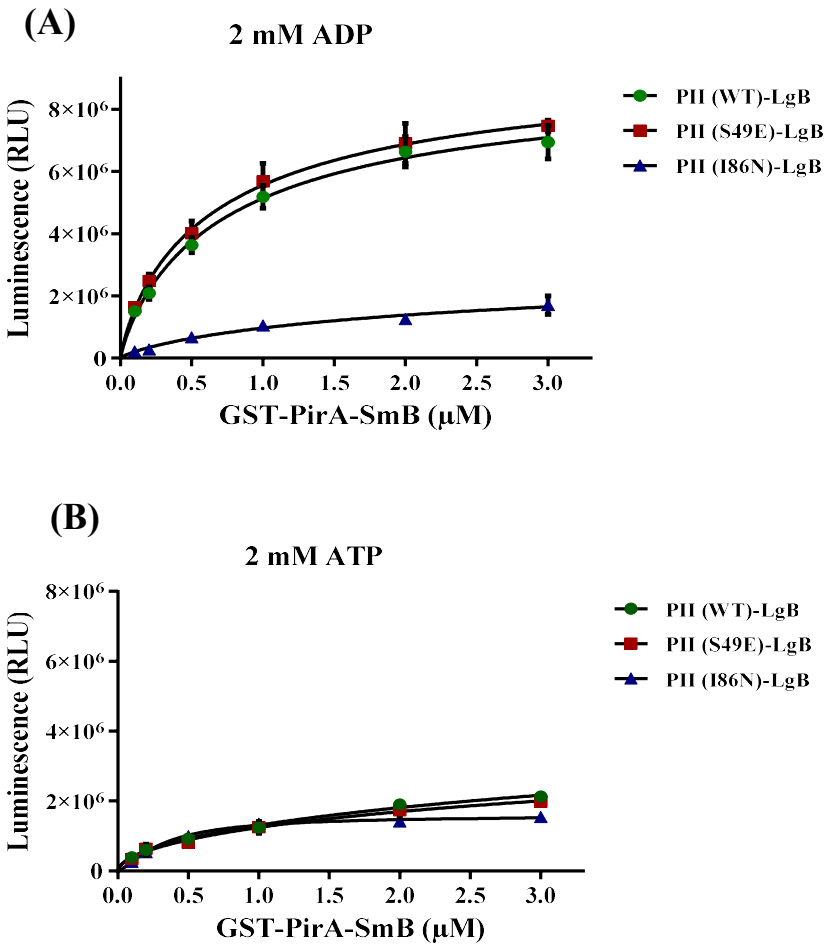

Figure 3. complex formation between PII-LgBit variants and PirA-SmBiT in the presence of ADP or ATP. (A). Titration of PirA-SmBiT (0, 0.04, 0.1, 0.2, 0.4, 1, 2, 3 µM) to 10 pM PII-LgBiT variants (WT, S49E, I86N) in the presence of 2mM ADP. (B) Titration of PirA-SmBiT (0, 0.04, 0.1, 0.2, 0.4, 1, 2, 3 µM) to 10 pM PII-LgBiT variants (WT, S49E, I86N) in the presence of 2mM ATP. Data are the means ± SD from triplicate measurements.

Protein complexes	Effector molecules condition and K_D (nM) of protein complex			
	2mM ADP	2mM ATP	1mMATP/1mM ADP	No effectors
PII(WT) - PirA	2.4 ± 1.2	17.88 ± 1.1	8.3 ± 3.4	36.3± 2.6
PII(S49E) - PirA	2.1 ± 1.5	16.7 ± 5.8	nm	nm
PII(I86N) - PirA	9 ± 3.1	41.2 ± 3.8	nm	nm

Table 1. Dissociation constants of PII fusion variants with PirA-SmBiT in the presence of different metabolites. Data are the means ± SD from triplicate measurements. The raw data was fitted using one site-specific binding with hill slope. nm: not measured

1.2.1. Competition assay

PirA plays a pivotal role in the arginine pathway by interfering with the PII - NAGK complex formation in the rate-limiting step of arginine synthesis (Figure 6B, Publication 2). To validate this concept, a competition assay was conducted using the NanoBiT sensor, employing NAGK-SmBiT and PirA with a GST tag to compete for binding with PII-LgBiT. The experiment involved 10 pM PII-LgBiT trimer, 120 nM NAGK-SmBiT monomer, and escalating concentrations of PirA in the presence of 1 mM ATP, 1 mM ADP, and 0.1 mM arginine. When NAGK-SmBiT was mixed together with PirA in the ratio of 1:20, the luminescence signal decreased to approximately 20%. Further addition of PirA resulted in a more significant decrease in the signal (Figure 4A). These findings suggest that PirA has the potential to disrupt the PII-NAGK interaction by binding to PII, thus affecting the signaling cascade.

As demonstrated previously, ADP increases the dissociation constant of the PII – NAGK interaction. The binding level of PII to NAGK decreases with increasing concentrations of ADP (Fokina, et al., 2010b). In competition assays for NAGK-SmBiT and PirA to PII-LgBiT binding with increasing concentrations of ADP, 10 pM PII trimers were utilized along with a fixed amount of NAGK (120 nM monomer) and PirA (2.4 µM monomer). Increasing concentrations of ADP could successfully affect the PirA-PII interaction and reduce the binding of PII to NAGK (Figure 4B and Table 2).

In the experiment, arginine was titrated to PirA-PII-LgBiT-NAGK-SmBiT complexes, and luminescence levels were recorded to investigate how arginine affects the binding ability of NAGK-SmBiT and PirA to PII-LgBiT. As expected, PirA could compete more effectively with NAGK for PII binding by increasing the arginine amount. This is in agreement with the reduced luminescence signal observed at Arg concentrations (Figure 4C and Table 3).

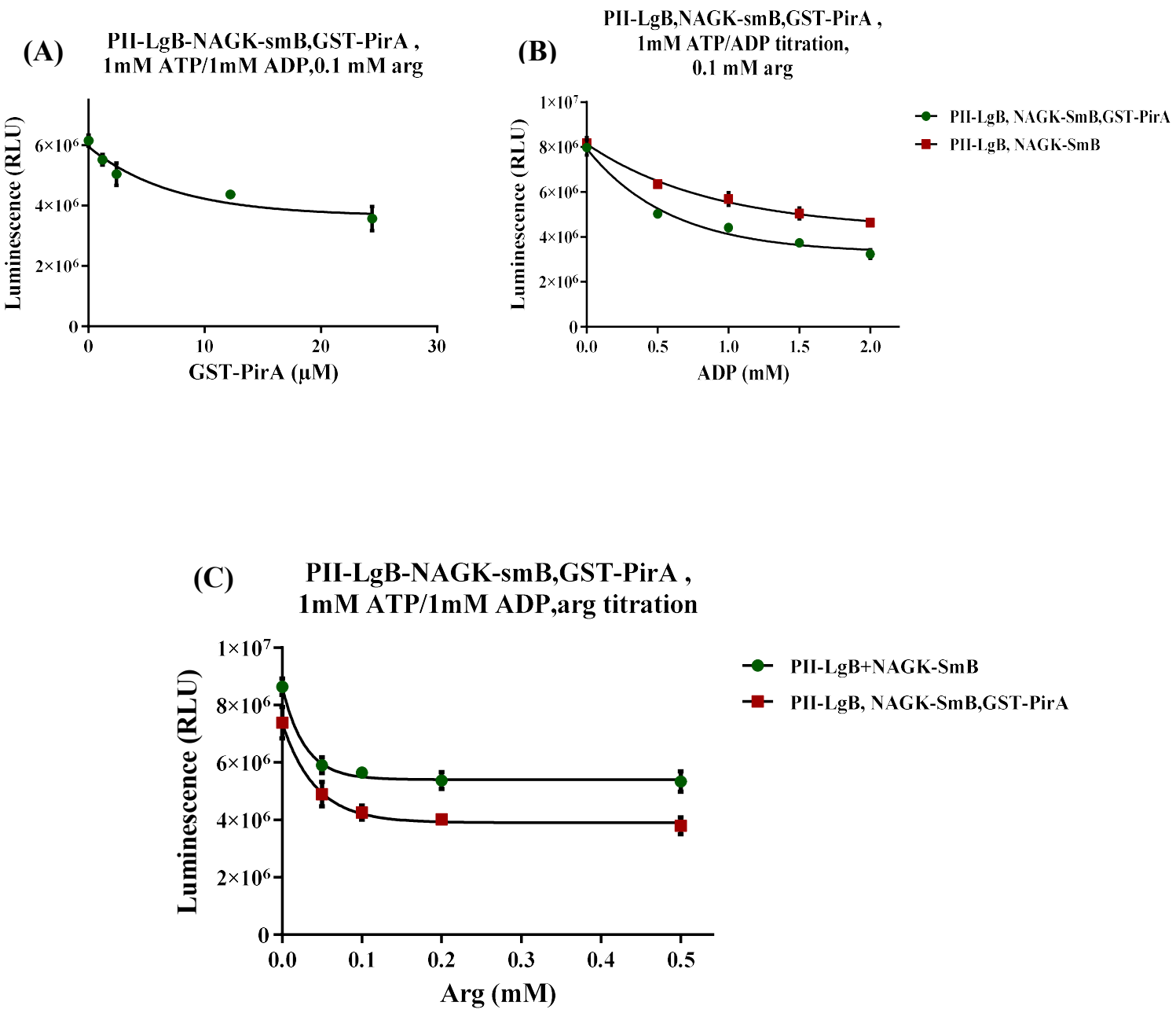

Figure 4. Competition between PII interaction partners to bind to PII in the presence of effector molecules. (A) competition between 120 nM NAGK-SmBiT and different concentrations of PirA (1.2, 2.4, 12.2 and 24.4 µM) to bind to 10 pM PII trimer in the presence of 1mM ATP, 1mM ADP and 0.1 mM arginine. (B) competition between 120 nM NAGK-SmBiT and 2.4 µM PirA to bind to 10 pM PII trimer in the presence of 1mM ATP, 0.1mM arginine and different concentrations of ADP (0.5, 1, 1.5 and 2 mM). (C) competition between 120 nM NAGK-SmBiT and 2.4 µM PirA to bind to 10 pM PII trimer in the presence of 1mM ATP, 1mM ADP and different concentrations of arginine (0, 0.05, 0.1, 0.2 and 0.5 mM). Data are the means ± SD from triplicate measurements.

ADP (mM)	0	0.5	1	1.5	2
ΔRLU	194.435	1.318050	1.273.409	1.308.070	1.397.013
% reduction	1.5	20.7	22.3	25.9	30.1

Table 2. The effect of ADP concentrations on competition of NAGK-SmBiT and PirA to bind to PII-LgBiT

Arginine (mM)	0	0.05	0.1	0.2	0.5
ΔRLU	1.253.861	1.006.439	1.387.940	1.349.433	1.543.857
% reduction	14.5	17	24.4	25.3	28.8

Table 3. The effect of arginine concentrations on competition of NAGK-SmBiT and PirA to bind to PII-LgBiT

1.2.2. Observing metabolic changes through PII-PirA sensor

The genetic construct depicted in Fig. 5 was employed to express the PII-PirA NanoBiT sensor in *E. coli*.

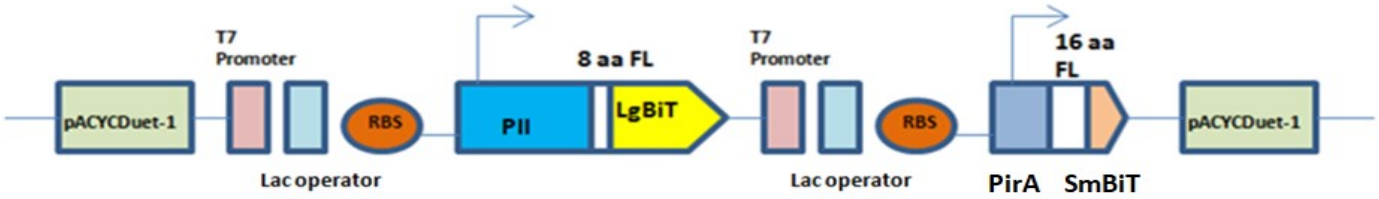

Figure 5. Expression vectors and fusion protein constructs. Schematic overview of PII-LgBiT – PirA-SmBiT sensor for in vivo experiment. Flexible linker with 8 amino acids (8aa) fused to LgBiT and flexible linker with 16 amino acids (16aa) fused to SmBiT in constructs.

The initial assay aimed to examine the response of the sensor to ammonium upshift treatment. Previous studies indicate that the PirA molecules strongly accumulated in response to 10 mM ammonium addition. This accumulation disrupts the complex formation between PII and NAGK as PirA binds to the PII protein (Bolay et al., 2021). In the present case, the addition of 4 mM ammonium resulted in a slight initial increase in RLU signal when compared to the untreated control with 1 mM ammonium. Whereas the noticeable increase in RLU signal was observed with 40 mM ammonium treatment. Subsequently the response of PII-PirA sensor to inhibition of nitrogen assimilation by MSX was examined. Addition of 0.1 or 1 mM MSX resulted in a slight increase in the formation of PII-PirA NanoBiT complex, evidenced by an increase in RLU signal. However this increase returned to the basal level after around 5 min. Finally, the sensor's response to nitrogen starvation was investigated. An immediate decrease in RLUs was noted, but this subsequently increased to nearly the initial RLU ratio. This demonstrates the PII-PirA NanoBiT sensor effectively read out the metabolic perturbation in a manner akin to the PII-PipX sensor, where both interactions are significantly influenced by the presence of ADP.

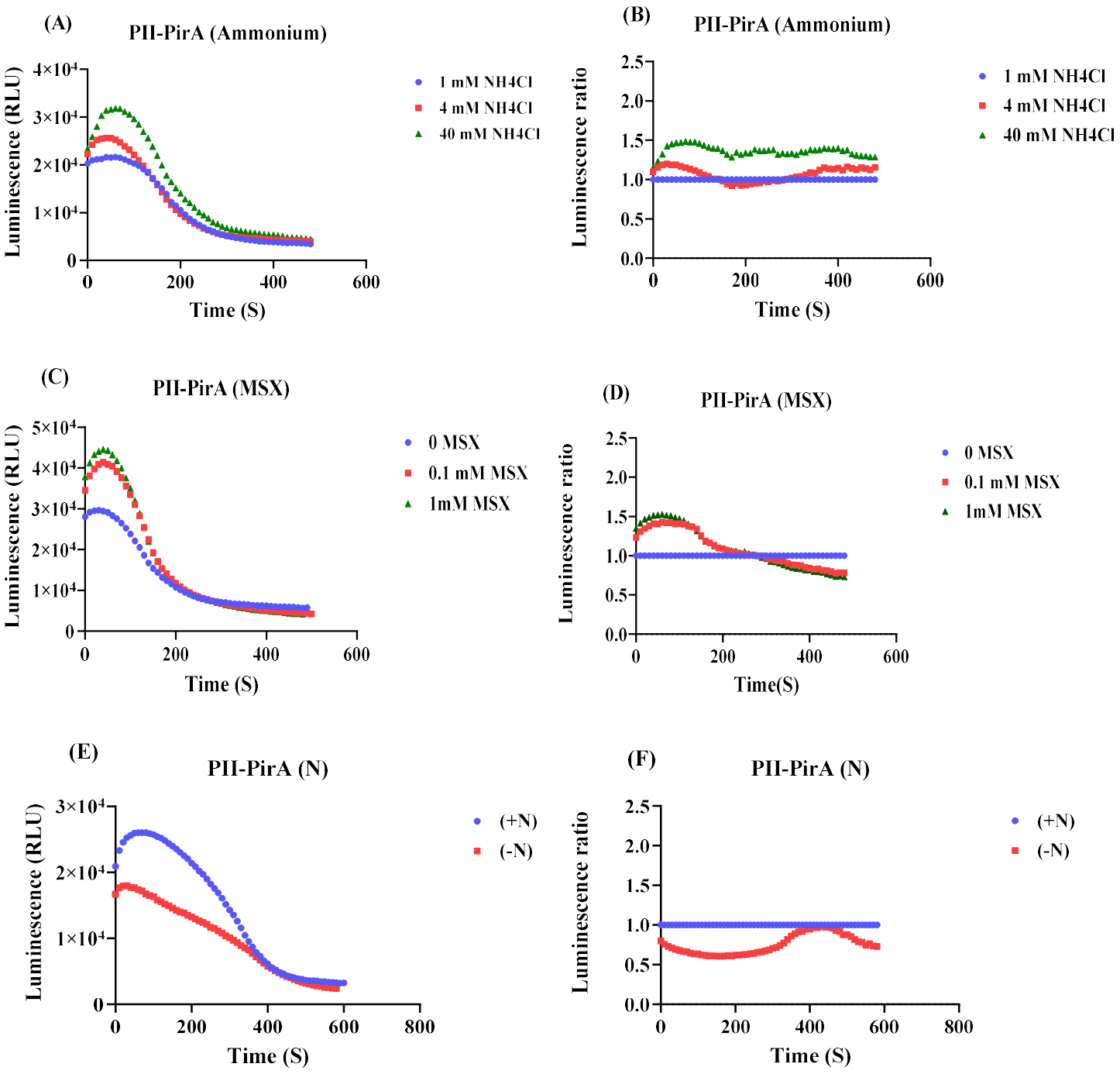

Figure 6. Luminescence response of the PII-PirA NanoBiT sensor towards ammonium upshift, MSX addition and nitrogen starvation treatments. A) Time course of the luminsescence signal (RLU) after addition of luminescence reagent in untreated sample (1mM NH_4Cl), and to samples, where the NH_4Cl concentration was increased to 4 mM or 40 mM. B) Normalization of the RLU response curve to the RLU response curve of the reference sample (untreated, 1 mM NH_4Cl). C) RLU time course of PII-PirA NanoBiT sensor in the absence and presence of 0.1 mM and 1 mM MSX. D) RLU response curves of (C) normalized to the reference sample. E) RLU time course of PII-PirA NanoBiT sensor following nitrogen depletion. F) RLU response curves of (E) normalized to the reference sample.

1.3.Materials and methods

1.3.1. Cloning and purification of fusion proteins

Generation, cloning, and purification of PII-LgBiT were performed as previously described (Publication 1). To make the PirA-SmBiT construct, synthetic genes with overlapping sequences for Gibson assembly were ordered from Integrated DNA Technologies (a biotechnology company in Leuven, Belgium). The *pirA-SmBiT* gene was cloned into the XhoI and EcoRI sites of the pGEX-4T3 vector (GE Healthcare Life Science, Freiburg, Germany) with an N-terminal-fused GST tag. The plasmid was overexpressed into electrocompetent *E. coli Lemo21* cells. The purification of PirA-SmBiT with a GST tag was followed as described in Harper et al. (2011).

1.3.2. Bioluminescence assay for protein-protein interactions

The time-point luminescence assay was performed with 10 pM PII-LgBiT tirmer and increasing concentrations of PirA-SmBiT (0–3 µM) in 500 µl of experimental buffer containing 50 mM Tris/HCl (pH 7.6), 100 mM KCl, 10% glycerol, 2 mM $MgCl_2$, 0.1% BSA, and respective concentrations of metabolites (ATP, ADP, and ATP/2-OG). After 10 minutes of incubation of the complex at 30˚ C, 0.5 µl of Nano-Glo® Luciferase substrate (Promega, Walldorf, Germany) was added to each reaction tube, and incubation was followed for another 5 minutes at room temperature. Then luminescence was measured in a luminometer (Sirus Luminometer, Berthold Detection System, Germany) for 10 s with a 10 s delay. The luminescence background from every single protein was subtracted from the recorded luminescence of complex formation.

The time course luminescence assay was done with 10 pM PII-LgBiT tirmer and 1000 nM of PirA-SmBiT monomer in 500 µl of the above experimental buffer without effector molecules. After 5 minutes of incubation of 0.5µl of Nano-Glo® Luciferase substrate with the protein mixture, luminescence was measured continuously via FB12 Sirius software with 20-s intervals in the Sirus luminometer for 4 minutes. Then the respective amounts of metabolites were added to each reaction tube, and measurement was continued for another 10 minutes to reach the plateau.

1.3.3. NanoBiT-based competition assays

10 pM PII-LgBiT trimer was incubated with different concentrations of PirA (1.2, 2.4, 12.2, and 24.4 µM) monomer for 10 minutes at 30˚ C in the presence of 1 mM ATP, 1 mM ADP, and 0.1 mM arginine. Next, a constant concentration of NAGK-SmBiT (120 nM) was added to each reaction tube, and incubation was followed for another 30 minutes at 30˚ C. By adding 0.5 µl of Nano-Glo® Luciferase substrate to each tube, incubation was continued for another 5 minutes at room temperature. Then luminescence was quantified in a luminometer for 10 s with a 10 s delay.

To investigate the effect of ADP and arginine concentrations on the competition of NAGK-SmBiT and PirA to bind to PII, 10 pM PII trimer, 120 nM NAGK-SmBiT monomer, and 2.4 µM PirA monomer were applied. The rest followed as described above.

1.3.4. Cloning of NanoBiT sensor for in vivo assay

To create the split NanoLuc sensor for in vivo study, pACYC-Duet vector with two multiple cloning sites (MCS) were applied. PII-LgBiT gene was cloned in the linearized vector with NcoI in the first cloning site. PirA-SmBiT was cloned into NdeI site in second cloning site for pACYC-Duet vector following the Gibson cloning protocol (Cloning, 2024). The amplification and extraction of plasmid were conducted in accordance to previously described methods (publication 3). Subsequently, the verified plasmids were incorporated into E. coli BL21 cells that are electrocompetent, paving the way for the expression of recombinant proteins.

1.3.5. Expression of proteins: The cells obtained from LB agar plates containing the relevant NanoBiT constructs were cultivated in LB broth supplemented with the chloramphenicol antibiotic at 37 °C with ongoing shaking over night to facilitate the production of recombinant proteins. The following morning, cells with an optimal density of 0.07 at 600 nm (OD600) were transferred to 10 ml of M9 media in a 100 ml flask. They were then allowed to grow until they reached an OD600 between 0.9 and 1 at 37 °C with shaking. Subsequently, cells with an OD600 of 0.1 were placed into 5 ml of M9 media, enriched with the chloramphenicol antibiotic, in a 50 ml flask. After incubating at 37 °C for several hours, the cells reached the exponential growth phase with an OD600 between 0.5 and 0.6. These cells were then utilized for luminescence testing.

1.3.6. Development of the bioluminescence measurement in live cells. In order to evaluate the effect of various substances and inhibitors on live E. coli cells through real-time bioluminescence measurement, a mixture was prepared by combining 20 µl of the selected concentration of the substances with 10 µl of Nano-Glo® Live Cell Reagent (formulated by combining 1 part of Nano-Glo® Live Cell Substrate with 19 parts of Nano-Glo® LCS Dilution Buffer) (Promega, Walldorf, Germany) in a luminescence reaction tube. Subsequently, 500 µl of the bacterial culture was added to this mixture. The resulting luminescence was then assessed for 5 sec. with 5 sec. delay using a Sirus Luminometer (from Berthold Detection System, Germany) operated through FB12 Sirius software. Measurement commenced promptly upon closing the luminometer's door.

IX. APPENDIX

1. Publication 1 (Accepted)

Research article

Rokhsareh Rozbeh & Karl Forchhammer

Split NanoLuc technology allows quantitation of interactions between PII protein and its receptors with unprecedented sensitivity and reveals transient interactions

2021. *Scientific Reports*. 11, 12535.

scientific reports

Check for updates

OPEN

Split NanoLuc technology allows quantitation of interactions between PII protein and its receptors with unprecedented sensitivity and reveals transient interactions

Rokhsareh Rozbeh & Karl Forchhammer✉

PII proteins constitute a widespread signal transduction superfamily in the prokaryotic world. The canonical PII signal proteins sense metabolic state of the cells by binding the metabolite molecules ATP, ADP and 2-oxoglutarate. Depending on bound effector molecule, PII proteins interact with and modulate the activity of multiple target proteins. To investigate the complexity of interactions of PII with target proteins, analytical methods that do not disrupt the native cellular context are required. To this purpose, split luciferase proteins have been used to develop a novel complementation reporter called NanoLuc Binary Technology (NanoBiT). The luciferase NanoLuc is divided in two subunits: a 18 kDa polypeptide termed "Large BiT" and a 1.3 kDa peptide termed "Small BiT", which only weakly associate. When fused to proteins of interest, they reconstitute an active luciferase when the proteins of interest interact. Therefore, we set out to develop a new NanoBiT sensor based on the interaction of PII protein from *Synechocystis* sp. PCC6803 with PII-interacting protein X (PipX) and N-acetyl-L-glutamate kinase (NAGK). The novel NanoBiT sensor showed unprecedented sensitivity, which made it possible to detect even weak and transient interactions between PII variants and their interacting partners, thereby shedding new light in PII signalling processes.

PII signalling proteins are ubiquitous in nature, in particular in Prokaryotes and plastids of Archaeplastida[1]. Their general task is to sense the metabolic state of the cells by binding in an interactive manner the metabolite status reporter molecules ATP and ADP as well as 2-oxoglutarate[2]. Effector molecule binding results in different conformational states of PII proteins, in particular, of their large flexible T-loops acting as versatile protein–protein interaction modules. Depending on the metabolite binding status, and thus, the PII-conformation, various PII receptors read out the metabolic information processed by PII. This is achieved through transient interactions with PII, which alter the activities of the PII-receptor proteins. Although initially thought to be confined to the regulation of nitrogen metabolism, research in the past years has unveiled a plethora of PII regulated proteins[2,3].

The focus of our work has been on the PII regulated processes in cyanobacteria. These are oxygenic photosynthetic, autotrophic bacteria playing important roles in global carbon- and nitrogen cycles. The first PII interaction partners, the N-acetyl-L-glutamate kinase (NAGK), a key enzyme of arginine synthesis, and PipX, a transcriptional co-activator of the global nitrogen control transcription factor NtcA, were identified by yeast-two hybrid screening[4,5]. Detailed mechanistic insight in the interaction of PII with these receptors has been obtained by solving the X-ray crystallographic structures of the proteins in complex[6,7], and characterizing the PII interactions mainly through Surface-Plasmon-Resonance analysis[8–11]. Even more details have been obtained by FRET-based quantitative analysis by fusing PII and NAGK or PipX to fluorescent proteins[12–14].

More recently, mainly through PII-co-purification approaches, novel interaction partners of PII proteins have been identified in cyanobacteria, such as the biotin carboxyl carrier protein (BCCP)-subunit of the Acetyl-CoA carboxylase[15], an ensemble of nitrogen uptake systems (the nitrate transport system NRT, urea-transport

Interfaculty Institute of Microbiology and Infection Medicine, University of Tübingen, Auf der Morgenstelle 28, 72076 Tübingen, Germany. ✉email: karl.forchhammer@uni-tuebingen.de

system URT and ammonium transport protein AMT1)[16], the Phosphoenolpyruvate carboxylase (PepC)[17] and two regulatory peptides, termed PirC and PirA, the former regulating carbon flow through interaction with the Phosphoglycerate mutase (PGAM), and the second, the arginine synthesis pathway[18,19]. However, for all the latter interaction partners, structural information is not yet available. Of the recently identified PII-receptors, in vitro protein interaction analysis has been performed for BCCP, PEPC, PirC and PirA. A striking feature of PII–PII-receptor interactions is in the ability of the same effector molecule to differentially affect the interaction of PII with different receptors. For example, PII binds NAGK in the absence of effector molecules. Binding of ADP to PII increases complex dissociation[10], and ATP in combination with 2-OG completely prevents complex formation[20]. By contrast, ADP enhances the stability of the PII–PipX complex, whereas ATP together with 2-OG again prevents complex formation. When small amounts of ADP were added to Mg-ATP/2-OG pre-loaded PII, PipX was again able to bind to PII, whereas small amounts of ADP did not affect PII-NAGK interactions in presence of ATP[10]. Structural analysis provided a mechanistic explanation: Formation of the PII-PipX complex stabilizes the conformation of PII that preferentially binds ADP. By contrast, PII in the NAGK complex adopts a conformation that preferentially binds ATP but is incompatible with 2-OG binding[11]. As a consequence, interaction between PII and PipX is highly sensitive to fluctuations in the ATP/ADP ratio whereas PII -NAGK complex responds mainly to changes to the 2-oxoglutarate levels, as long as sufficient ATP is present. This allows PipX to sense the energy status via PII interaction whereas at the same time, NAGK can read out the level of 2-oxoglutarate (a status reporter of the carbon/nitrogen balance), provided that PII is present in excess over the receptors, which appears to be the case[21].

A limitation of the interaction analyses using Surface-Plasmon-Resonance (SPR) or Biolayer interferometry (BLI) comes from the fact that one interaction partner has to be immobilized on a sensor-surface, restricting access and mobility of the proteins. Indeed, fixing PII via a C-terminal Strep-tag to the surface of a Biacore sensor disturbed the response of the PII-PipX complex to ATP and 2-oxoglutarate[10]. Likewise, the use of FRET based analytics requires the fusion of large fluorescence proteins to both interaction partners and is highly sensitive to background fluorescence[22]. An alternative is the use of protein fragment complementation assays (PCA). PCA is a powerful approach to determine protein–protein interactions and has been applied in various variants[23]. A very attractive PCA version that was recently developed to determine PII protein interactions in solution is the split NanoLuc system. NanoLuc is an engineered luciferase enzyme from the deep ocean shrimp with exceptionally bright bioluminescence[24]. A variant of the enzyme was further engineered as protein fragment complementation reporter[25], now commercially available as NanoLuc Binary Technology (NanoBiT)[26]. The small 11 amino acids fragment (termed Small BiT, SmBiT) was constructed in a way that it has low intrinsic affinity (190 µM) towards the large complementation fragment (Large BiT, LgBiT). When LgBiT and SmBiT fragments are fused to candidate interacting proteins, luminescence is only restored when the candidate proteins interact with each other.

Recently, the NanoBiT technology was used to quantitatively analyse several protein–protein interactions in mammalian cells. It was used to verify the interaction between SME1 β-lactamase and a set of inhibitor binding proteins in vivo with the optimal performance when LgBiT was attached to the C-terminus of SME1 and SmBiT was attached to the C-terminus of inhibitor binding proteins[25]. The system was also used to accurately characterize the interaction between bacterial transcription factors NusB and NusE, was well as the interaction between RNA polymerase and σA from *Bacillus subtilis*[27]. Here, we employed NanoBiT technology to analyse the interactions of PII with PipX and NAGK, and show that this method provides superior quantitative results with exceptionally high sensitivity in comparison to SRP or BLI. These analyses also provide additional insights into the sophisticated network of PII interactions.

Results

Development of the NanoBiT sensor. Initially we constructed hybrid PII fusion proteins that contained LgBiT fragment at the C-terminus and SmBiT fragments were fused to the tip of the T-loop with three different linkers (24aa linker, 16aa linker and 8aa linker) in a similar manner than previously reported for hybrid PII-FRET constructs[22]. Of these constructs, only the 16 aa linker construct showed a response to the addition of PII effector molecules, however with only a response of 30% signal difference (data not shown). Therefore, we decided to separate the NanoBiT fragments in two distinct polypeptites: on PII and a PII-receptor protein, using the 16 aa linker to fuse the SmBiT fragment, which appeared most suitable from the initial experiments. The LgBiT fragment was fused at the C-terminally located Strep-tag purification linker of PII, which was already successfully used as linker for PII-VENUS FRET constructs[12]. The SmBiT fragment was fused at the C-terminus of PipX, with a 16 amino acids flexible linker in between (Fig. 1a). The gene for the PipX-SmBiT construct was cloned into expression vector pTEV5, containing an N-terminal His_6 affinity tag. When expressed in *E.coli* the recombinant proteins formed inclusion bodies. These were dissolved in 8 M urea for His-tag affinity purification, and the purified proteins were subsequently re-folded. Purified, refolded PipX-SmBiT and PII-LgBiT alone showed low levels of background luminescence ~ 1×10^{-5} RLU (relative light unit). This background was subtracted from the luminescence signals of the subsequent assays. In initial trials, PipX-SmBiT was used at a concentration of 10 nM and PII-LgBiT was titrated at increasing concentrations starting with 0.33 pM in a buffer containing 2 mM ADP, which are the conditions that were previously shown to be optimal for PII-PipX interaction[10]. After 15 min of incubation at 30 °C, the luminescence signal was recorded and plotted against the respective PII-LgBiT concentration. As shown in Fig. 1b, at low PII-LgBiT concentrations, a linear increase of luminesce up to 1×10^7 RLU was detected (corresponding to 10 pM PII) whereas the curved flattened at higher concentration of PII-LgBiT. This indicates that the higher concentrations of NanoLuc are beyond the linear detection range of the assay. Therefore, in all subsequent assays the concentration of PII-LgBiT was limited to 10 pM.

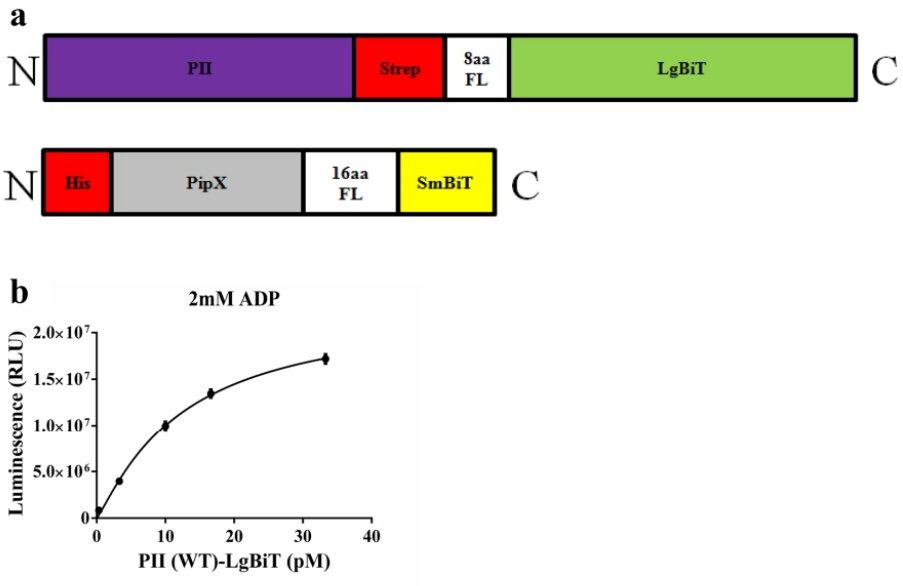

Figure 1. Fusion protein constructs and NanoBiT responce. (**a**) Schematic representation of PII-LgBiT and PipX-SmBiT fusion proteins. Flexible linker with 16 amino acids (16aa) in construct fused to SmBiT. (**b**) Titration of PII-LgBiT (0.33–33 pM) with constant amount of PipX-SmBiT (10 nM) in the presence of 2 mM ADP. Graph represents mean ± SD of three independent experiments.

PII-PipX binding kinetics and influence of effector molecules. The next step was to monitor the kinetics of PII-PipX complex formation in real-time by continuously measuring the luminescence in the presence of various PII effector molecules. Therefore, PII-LgBiT (concentration of 10 pM trimer) was first mixed with the indicated amounts of PipX-SmBiT and luminescence was measured for five minutes without effector molecules. As shown in Fig. 2a,b, this resulted only in a very low increase in luminescence. Subsequent addition of adenyl-nucleotides immediately stimulated the interaction as shown by the rise of luminescence signal (Fig. 2a,b). With 2 mM ATP, complex formation reached a plateau after about 10 min, indicating equilibrium between complex association and dissociation. In presence of ADP, the increase was much steeper, and 10 min after ADP addition, equilibrium was not yet reached, with a maximal signal for the ADP-promoted complex 2,5 times higher than that of the ATP-promoted complex.

To quantitatively determine the dissociation constant of PII-PipX interaction in presence of 2 mM ATP or ADP, increasing concentrations of PipX were titrated to a fixed concentration of PII-LgBiT (10 pM trimer). Then, the RLUs were plotted against the PipX-SmBiT concentrations (Fig. 2c). From these curves, K_D values were calculated assuming that in equilibrium the dissociation constant follows the Eq. (1):

$$K_D = [\mathrm{PII} - \mathrm{LgBiT}] \times [\mathrm{PipX} - \mathrm{SmBiT}] / [\mathrm{PII} - \mathrm{LgBiT} * \mathrm{PipX} - \mathrm{SmBiT}].$$

At the concentration of PipX-SmBiT at which half maximal luminescence is observed, 50% of PII should be in the PipX complex. This concentration should therefore correspond to the K_D of the complex (provided that PipX is in large excess over PII so that the free PipX concentrations approximately equal the total PipX concentration). We estimated the half-maximal RLU value by hyperbolic fitting, resulting in a K_D of 5.7 ± 0.78 nM for the PII-PipX complex in presence of ADP and of 52.4 ± 0.92 nM in presence of ATP (Table 1).

The ATP to ADP ratio is an indicator of the cellular energy state. To determine its impact on PII-PipX interaction as revealed by NanoBiT analysis, the real-time luminescence increase was recorded at various ATP/ADP ratios, keeping the total ADP + ATP concentration constant at 2 mM. As shown in Fig. 2d, ADP is the dominant effector over ATP. Already 0.5 mM ADP in presence of 1.5 mM ATP (ATP/ADP ratio 3) is sufficient to increase luminescence signal up to 80%. The result reported in this study matches a previous similar experiment performed by SPR, which also showed that the interaction between PII and PipX is highly sensitive to fluctuations in the ATP/ADP ratios[11]. Strongly fluctuating ATP to ADP levels in Synechocystis cells have been reported in particular in response to light – dark shifts or different nutritional conditons[28–30], Therefore, the response of PII-PipX interaction to differing ATP-ADP ratios seems physiologically relevant and matches the observations reported by Espinosa et al[29].

Next, we studied the effect of different 2-OG concentrations on PII-PipX complex formation (10 pM PII and 10 nM PipX) in the presence of 2 mM ATP. First, the mixtures of PII-LgBiT and PipX-SmBiT were incubated with the various 2-OG concentrations in the absence of ATP. After 5 min, 2 mM ATP was added and complexes

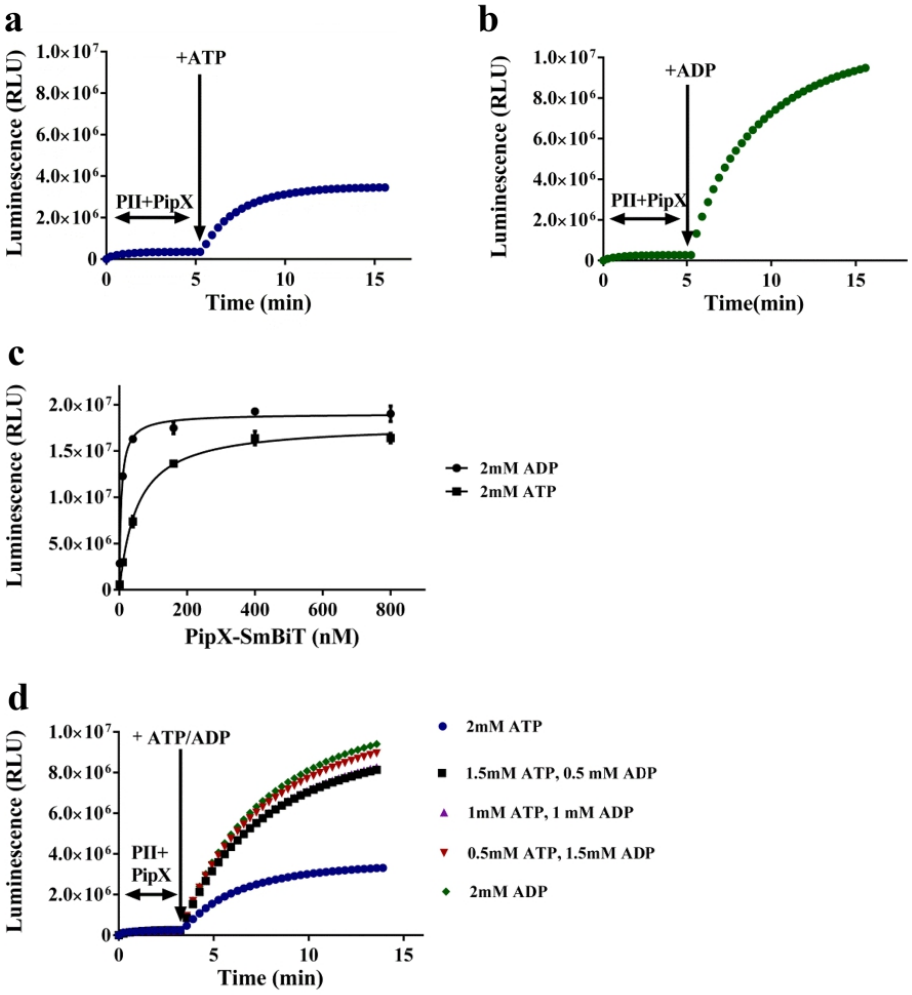

Figure 2. Effect of ATP or ADP on PII-LgBiT-PipX-SmBiT complex formation. (**a** and **b**) Time course of complex formation after adding 2 mM ATP (**a**) or 2 mM ADP (**b**). (**c**) Titration of PipX-SmBiT (0, 1, 10, 40, 160, 400, 800 nM) to PII-LgBiT (10 pM) in the presence of 2 mM ATP or 2 mM ADP. (**d**) Time course of complex formation PII-LgBiT (10 pM) and PipX-SmBiT (10 nM) in the presence of different ATP/ADP mixtures at a total ADP + ATP concentration of 2 mM. Graphs represent mean ± SD of three independent experiments.

Protein complex	Effector molecules condition and K_D (nM) of protein complex									
	2 mM ATP	2 mM ADP	No effector	2 mM ATP/ 2 mM Arg	2mMATP/ 2mMNAG	2 mM ATP/ 50 mM NAG	2 mM ATP/ 2 mM Arg/ 2 mM NAG	2mM ATP/2 mM Arg/50 mM NAG	2 mM ADP/ 2 mM NAG	2 mM ADP/ 50 mM NAG
PII (WT)-NAGK	8.8 ± 0.72	30.8 ± 0.12	12.9 ± 0.65	17.8 ± 0.72	4.7 ± 0.35	0.74 ± 0.081	16.5 ± 1.08	9.5 ± 0.20	14.9 ± 1.13	1.2 ± 0.053
PII(S49E)-NAGK	155 ± 0.37	95.3 ± 1.05	133 ± 0.62	432 ± 1.34	10.7 ± 0.91	3.39 ± 0.73	nm	nm	nm	nm
PII (I86N)-NAGK	7 ± 0.20	11.7 ± 0.14	12.9 ± 0.20	1.56 ± 0.48	4.1 ± 0.33	0.68 ± 0.031	nm	nm	nm	nm
PII (WT)-PipX	52 ± 0.92	5.7 ± 0.78	nd	nm	nm	nm	nm	nm	nm	nm

Table 1. Dissociation constants (nM) of PII-LgBiT fusion variants with NAGK-SmBiT and PipX-SmBiT in presence of different metabolites. Data are the mean ± SD of triplicate measurements. The raw data was fitted using one site-specific binding with hill slope. *nd* not detectable; *nm*: not measured

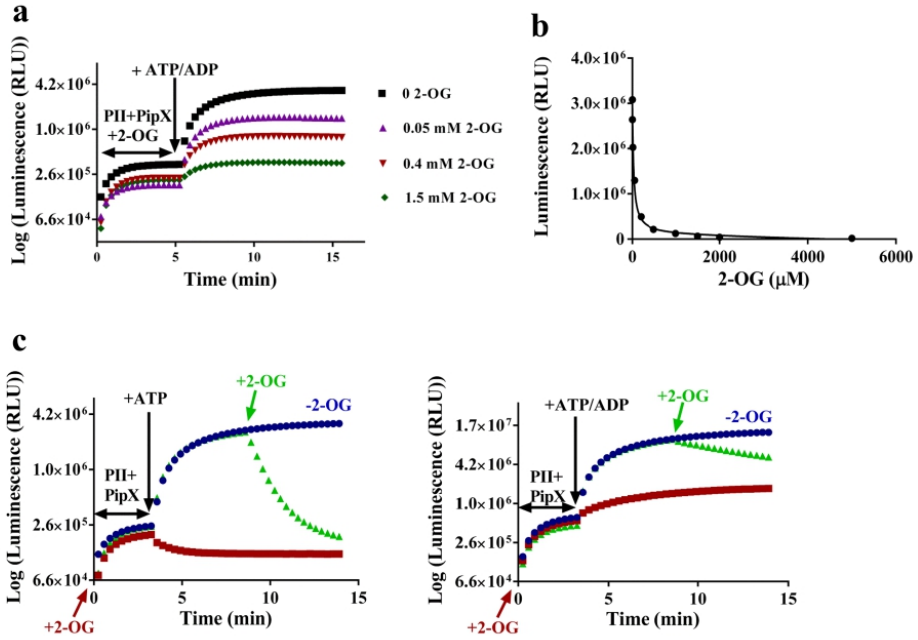

Figure 3. Effect of 2-OG on PII-LgBiT (10 pM) and PipX-SmBiT (10 nM) complex formation. (**a**) Interaction of PII-LgBiT and PipX-SmBiT in the presence of: none, 0, 0.05 mM, 0.4 mM and 1.5 mM 2-OG. (**b**) Quantitative analysis of 2-OG dependent inhibition of complex formation. (**c**) Time course of complex dissociation after addition of 2 mM 2-OG at indicated time point (green symbols). Control without 2-OG addition (blue symbols). First, PII-LgBiT and PipX-SmBiT were incubated without effectors (blue and green) or with only 2-OG (red symbols). After 4 min, either ATP (left) or 1 mM ATP and 1 mM ADP (right) were added, followed by the addition of 2-OG.

formed until reaching saturation after 15 min (Fig. 3a). To quantify the effect, the maximal RLU values were plotted against the respective 2-OG concentrations (0, 0.002, 0.01, 0.05, 0.2, 0.5, 1, 1.5, 2, 5 mM) in the assay (Fig. 3b). In a similar way as reported by SPR, increasing 2-OG concentrations gradually prevented complex formation. Curve fitting resulted in an IC_{50} of 25 µM (corresponding to a 50% signal drop) for the inhibition by 2-OG (Fig. 3b). This value is in a similar range, albeit 40% lower than the average K_D of 2-OG binding to PII-Mg-ATP (39 µM)[10], whereas the K_D of 2-OG binding to the first (highest affinity) binding site in trimeric PII is approx. 5 µM. This result indicates that trimeric PII with the highest affinity site occupied by 2-OG can still bind PipX via its free subunits, and only when fully occupied by 2-OG, PII is impaired in PipX binding.

To study the kinetics of 2-OG promoted PII-PipX complex dissociation with the NanoBiT technology, the luminescence signal dynamics was recorded in time-course experiments in which effector molecules were added successively (Fig. 3c). First, PII-LgBiT and PipX-SmBiT were pre-incubated without adenyl-nucleotides (green and blue symbols) or in a control experiment, in the presence of 2 mM 2-OG (red symbols). After four minutes, 2 mM ATP (left panel) or 1 mM ATP + 1 mM ADP (right panel) were added to allow complex formation. Five minutes later, 2 mM 2-OG was added to one sample each (green symbols) and the luminescence signal was recorded for further five minutes. In the presence of ATP alone, 2-OG completely dissociated the complex within two minutes to basal levels. After 45 s, about half of the complex was dissociated. A different response was observed in the presence of 1 mM ATP + 1 mM ADP, where dissociation was strongly mitigated. It required approximately 340 s to dissociate half of the complexes to basal level, 7–8-times longer than in the absence of ADP. The K_D of 2-OG binding to PII in presence of 1 mM ATP + 1 mM ADP was previously determined to be 180 µM, compared to about 39 µM in presence of 2 mM ATP [10]. Therefore, the slower dissociation of the PII-PipX complex is in accord with the decreased affinity of PII for 2-OG in presence of 1 mM ATP/ADP.

PII-NAGK binding kinetics and influence of effector molecules. To find out whether NanoBiT can also be applied to directly study PII interaction with other receptor N-acetyl-L-glutamate kinase (NAGK), the second well-characterized cyanobacterial PII-receptor, a PII-LgBiT-NAGK-SmBiT pair was developed. Therefore, the SmBiT fragment together with the 16 amino acids flexible linker was fused to the C-terminus of NAGK (Fig. 4a). As a first experiment, the purified NAGK-SmBiT fusion protein was titrated to 10 pM PII-LgBiT in the presence of 2 mM ATP, 2 mM ADP or in the absence of effector molecules (Fig. 4b). Efficient complex formation

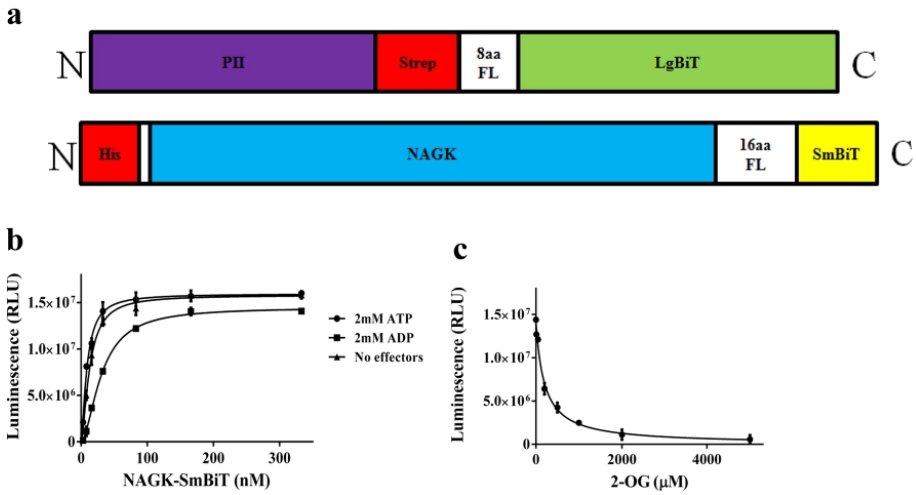

Figure 4. NanoBiT pair consisting of PII-LgBiT-NAGK-SmBiT. (**a**). Schematic representation of NanoBiT-sensor construct as indicated (**b**) Titration of NAGK-SmBiT in the range of 3–333 nM with 10 pM PII-LgBiT in the presence of 2 mM ATP or 2 mM ADP or in the absence of effector molecules. (**c**) Inhibitory effect of 2-OG (0, 0.01, 0.05, 0.2, 0.5, 1, 2, 5 mM) on PII-LgBiT (10 pM) and NAGK-SmBiT (27 nM) complex formation in the presence of 2 mM ATP. Graphs represent mean ± SD of three independent experiments.

was detected between PII-LgBiT and NAGK-SmBiT in the absence of effector molecules and in presence of ATP. Complex formation also occurred in the presence of ADP, albeit with lower affinity (Fig. 4b). Hyperbolic fitting resulted in apparent K_D values of 12.9 ± 0.65 nM in the absence of effectors, 8.8 ± 0.72 nM in the presence of ATP and 30.8 ± 0.12 nM in the presence of ADP. In SPR experiments, only weak and transient PII-NAGK complexes could be detected in presence of ADP, which prevented quantitative determination[10]. This result demonstrates superior sensitivity of the NanoBiT over SPR for the detection and quantification of weak interactions.

To monitor the effect of 2-OG on PII-NAGK complex formation, 10 pM PII-LgBiT trimer was incubated with 160 nM NAGK-SmBiT (26.6 nM hexameric NAGK) in the presence of 2 mM ATP and different concentrations of 2-OG. Preliminary experiments showed that to achieve equilibrium, at least 30 min incubation time was necessary. Therefore, for quantification of 2-OG effects, the luminescence reagent was added 40 min after the start of PII-LgBiT-NAGK-SmBiT complex formation. Then, luminescence was recorded and plotted against the 2-OG concentrations (Fig. 4c). Similar to what observed for the PII–PipX complex, the inhibitory effect of 2-OG was clearly revealed by the NanoBiT assay. The IC_{50} for 2-OG, which led to 50% drop in luminescence, was determined to be 0.15 mM. This value correlated well with previous data obtained through different experimental approaches. Determination of PII-NAGK interaction by FRET assay revealed an IC_{50} for 2-OG of 0.1 mM[12], and SPR and enzyme assays yielded an IC_{50} of 0.12mM[20].

Competition between PipX and NAGK for binding to PII. Another possible application of the NanoBiT system was to reveal competition between PipX and NAGK for PII binding. In a first experiment, PipX was titrated to a constant concentration of PII-LgBiT and NAGK-SmBiT (10 pM trimer and 180 nM monomer, respectively) in the presence of 2 mM ADP. As expected from higher affinity of PII to PipX than to NAGK in presence of ADP (compare Tab.1), the addition of PipX completely abolished luminescence of the PII-LgBiT-NAGK-SmBiT complex (Fig. 5a left panel). Vice versa, addition of increasing NAGK amounts to a constant concentration of PII-LgBiT and PipX-SmBiT in presence of ADP showed no effect on the luminescence signal, clearly indicating that in presence of ADP, PII exclusively binds to PipX, when both partners are present (Fig. 5a, right panel). A more complicated situation was observed when the same set of experiments was performed in presence of ATP. Titrating PipX to the PII-LgBiT and NAGK-SmBiT sensor pair resulted in a gradual decrease in luminescence. Although the affinity of PII to PipX is lower than towards NAGK in presence of ATP, the addition of a 1:1 stoichiometric amount of PipX to NAGK reduced the luminescence signal to about 50% and higher amounts of PipX decreased the signal further (Fig. 5b, left panel). Conversely, the PII-LgBiT and PipX-SmBiT sensor pair was quite resistant towards the addition of NAGK. Even a large excess of NAGK over PipX reduced the signal from the PII-LgBiT and PipX-SmBiT sensor pair only partially, although at these high NAGK concentrations, PII is expected to preferentially interact with NAGK (Fig. 5b, right panel). A possible explanation could be a weak interaction of PipX-SmBiT protein to PII-LgBiT-NAGK complexes, resulting in luminescence signals, due to the high sensitivity of the reporter system.

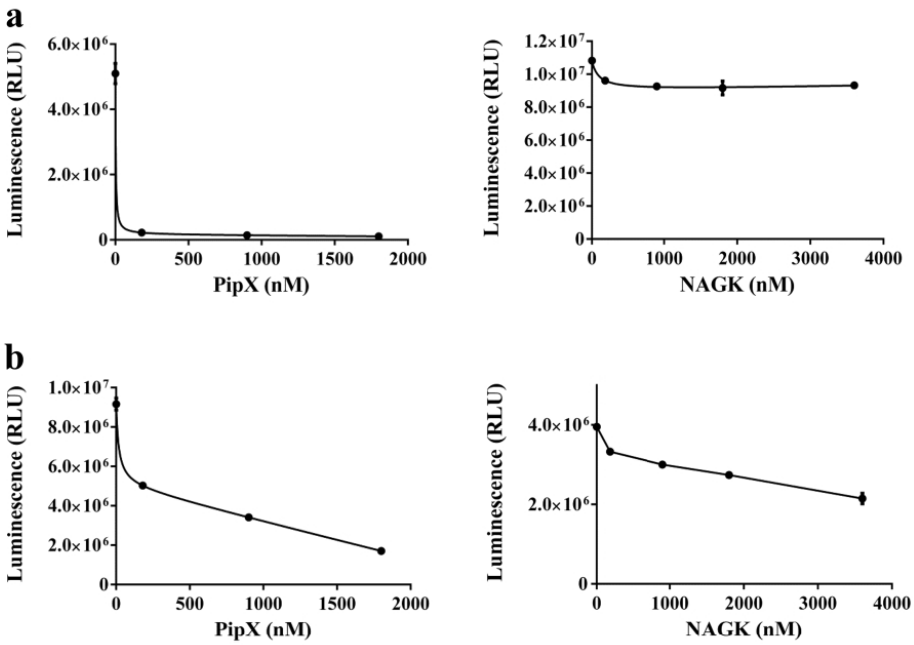

Figure 5. Competition between PII interaction partners to bind to PII in the presence of 2 mM effector molecules: (**a**, left panel) Competition between NAGK-SmBiT and PipX for PII-LgBiT binding in the presence of 2 mM ADP: The interaction between 10 pM PII-LgBiT (trimer) and 180 nM NAGK-SmBiT (monomer) was competed with increasing concentrations of PipX (180, 900 and 1800 nM) monomer. (a, right panel) Competition between NAGK and PipX-SmBiT for PII-LgBiT binding in the presence of 2 mM ADP: The interaction between 10 pM PII-LgBiT trimer and 10 nM PipX–SmBiT monomer was competed with the addition of increasing concentrations of NAGK (180, 900, 1800 and 3600 nM) monomer. (**b**, left panel) Competition between NAGK-SmBiT and PipX for PII-LgBiT binding in the presence of 2 mM ATP: The interaction between 10 pM PII-LgBiT (trimer) and 180 nM NAGK-SmBiT (monomer) was competed with increasing concentrations of PipX (180, 900 and 1800 nM) monomer. (**b**, right panel) Competition between NAGK and PipX-SmBiT for PII-LgBiT binding in the presence of 2 mM ATP: The interaction between 10 pM PII-LgBiT trimer and 50 nM PipX–SmBiT monomer was competed with the addition of increasing concentrations of NAGK (180, 900, 1800 and 3600 nM) monomer. Graphs represent mean ± SD of two independent experiments.

Affinity of NAGK to PII variants in the presence of effector molecules. The association kinetics of NAGK-SmBiT was analysed with two mutant PII-LgBiT variants: The T-loop variant PII-S49E was shown previously to be strongly impaired in NAGK interaction[6,12], whereas by contrast, the PII-I86N variant was identified as a hyperactive NAGK binder[20]. As shown in Fig. 6a-c, the NanoBiT assay was able to reveal low residual binding of the phosphomimetic variant PII-S49E to NAGK in the presence of ATP, ADP or without effector molecules. Under any of these conditions, complex formation could be detected, but the affinity of the phosphomimetic variant to NAGK was about 10–20 fold lower than that of wild-type PII. By SPR, NAGK interaction with the PII-S49E was undetectable and could so-far only be observed by FRET analysis[12]. The respective dissociation constants are shown in Table 1. The PII-I86N-LgBiT has a single amino acid replacement, IIe86 to Asp86, which leads to constitutive high activation of NAGK. In agreement, the NanoBiT analysis revealed high affinity to NAGK, and importantly, the affinity remained high in the presence of ADP.

Inhibitory effect of arginine on PII-NAGK interaction. Another effector molecule that interferes with the PII-NAGK complex is arginine. Arginine binds to allosteric sites in NAGK, one site per each subunit, which are occupied in an anti-cooperative manner, thereby inhibiting its activity[21,31]. In complex with PII, NAGK feedback-inhibition by arginine is strongly relieved, presumably because the PII complex lowers the affinity of Arg to the allosteric binding sites. To find out how arginine, conversely, affects NAGK-SmBiT-PII-LgBiT complex formation, arginine was titrated to PII-LgBiT-NAGK-SmBiT complexes and luminescence was recorded. As shown in Fig. S1, very low concentrations of arginine slightly enhanced complex formation, but with increasing concentrations of Arg (when 2 mM ATP or 1 mM ATP/1 mM ADP were present), the luminescence signal decreased gradually to a new steady state level of approx. 60% of the initial value. The same experiment in presence of 2 mM ADP revealed a slightly increasing luminescence signal at low Arg levels, which returned back to

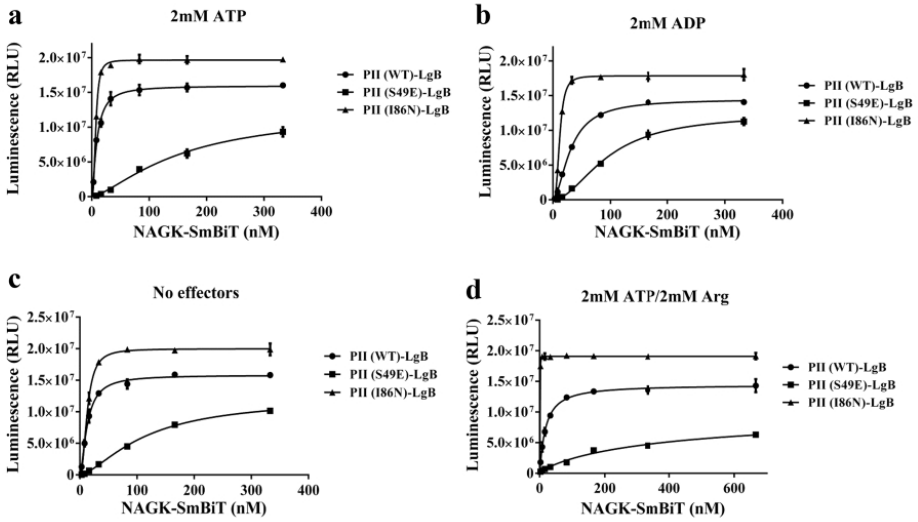

Figure 6. Determination of complex formation between PII-LgBiT variants (WT, S49E, I86N) and NAGK-SmBiT measured by NanoBiT-sensor. (**a**) NAGK-SmBiT titration in the range of 3–333 nM with 10 pM PII-LgBiT variants (WT, S49E, I86N) in the presence of 2 mM ATP. (**b**) NAGK-SmBiT titration in the range of 3–333 nM with 10 pM PII-LgBiT variants (WT, S49E, I86N) in the presence of 2 mM ADP. (**c**) NAGK-SmBiT titration in the range of 3–333 nM with 10 pM PII-LgBiT variants (WT, S49E, I86N) without effector molecules. (**d**) NAGK-SmBiT titration in the range of 3–666 nM with 10 pM PII-LgBiT variants (WT, S49E, I86N) in the presence of 2 mM ATP and 2 mM Arginine. Graphs represent mean ± SD of three independent experiments.

initial value at higher concentrations of Arg. In the absence of adenylnucleotides, low concentration of Arg were unable to increase complex formation and the luminescence signal (Fig. S1). These results indicate that the completely arginine-occupied NAGK has a reduced affinity for PII, whereas binding of Arg to the first allosteric site transiently increases the affinity. At a concentration of 2 mM arginine, arginine completely inhibits the activity of free NAGK and inhibits the activity of NAGK in PII-complex to about 90%. To determine the binding affinity of NAGK to PII under these assay conditions, increasing concentrations of NAGK were titrated to 10 pM of the respective PII-LgBiT variants (Fig. 6d, Quantitative data are shown in Table 1. The affinity of PII was approx twofold lower in presence of 2 mM Arg, in agreement with the reduced luminescence signal observed in the titration experiment with increasing Arg concentrations (Fig. S1). Obviously, the inhibition of enzyme activity is not caused by complex dissociation. Rather, it seems that PII can still bind to completely Arg-saturated NAGK, but the complex likely adopts a different conformation, which obstructs the catalytic activation of NAGK by PII.

Interestingly, Arg had a strong, differential effect on the affinity of NAGK towards different PII variants: Whereas on wild-type PII, it moderately reduced the affinity, an even stronger reduction was observed for the PII-S49E variant. Strikingly, the affinity towards PII-I86N variant was highly increased (Fig. 6d). This explains the strong stimulation of arginine synthesis in a *Synechocystis* strain, in which the PII wild-type protein was replaced by the PII-I86N variant, causing constitutive arginine overproduction and accumulation of cyanophycin[32].

Feed-forward regulation of N-acetylglutamate (NAG) on PII-NAGK complex formation. Next, we investigated how the substrate of NAGK, N-acetylglutamate (NAG), affects its interaction with PII. The influence of the substrate on the interaction of NAGK with PII was so-far never investigated, but must be taken into consideration for understanding the in vivo situation. NAG was titrated into a binding assay, whereby NAGK was used at a concentration equivalent to half Km, to enable the sensitive detection of changing affinity. As shown in Fig. 7a, increasing NAG concentrations caused a dramatic increase in PII-NAGK interaction. The binding constants were determined for a low (2 mM) and a high (50 mM) NAG concentration. 50 mM NAG is the concentration of NAG, routinely used in enzyme assays. The results are displayed in Fig. 7b,C and Table 1. NAG stimulates PII-NAGK interaction under any conditions. In the presence of ATP the affinity doubles with 2 mM NAG and increases more than tenfold with 50 mM NAG (as compared to the absence of NAG). The stimulating effect of NAG on PII-NAGK interaction is so strong that efficiently stabilizes the complex in presence of ADP (see Fig. 7d) (20-fold increase with 50 mM NAG, Table 1). The presence of Arg mitigated the strong stimulating effect of NAG on PII-NAGK affinity. In presence of 2 mM Arg, only a moderate increase by NAG on PII-NAGK interaction was detected (Fig. S2 and Table 1).

Interestingly, the S49E PII variant strongly bound to NAGK in the presence of 50 mM NAG and ATP, although this variant is unable to relieve NAGK from arginine inhibition (Fig. 7c). These results clearly demonstrate binding of PII to NAGK is not sufficient to cause a relief from Arg inhibition. The sophisticated hydrogen-bonding network organized by the –OH group of Ser49, which propagates into the catalytic centre of NAGK[6] is required

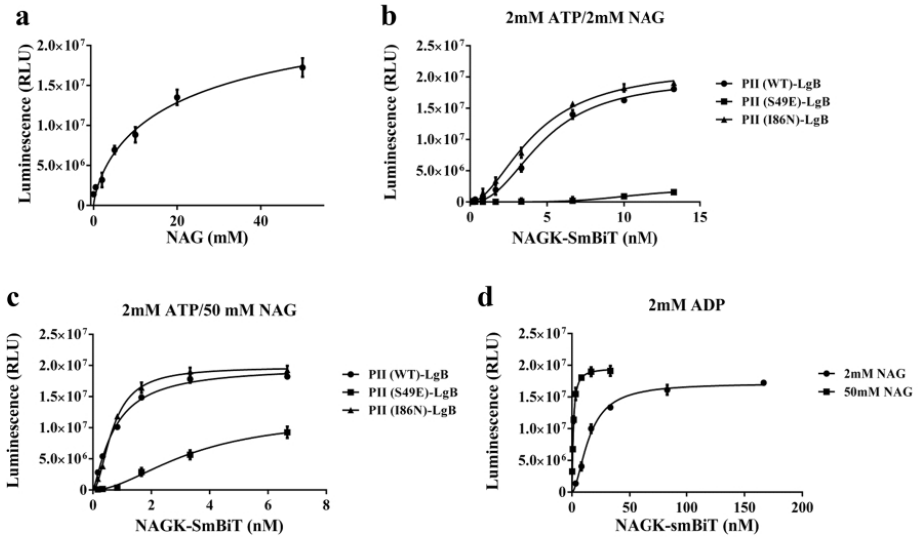

Figure 7. Effect of NAG on PII-NAGK interaction. (**a**): NAG titration (0–50 mM) for 10 pM PII-LgBiT and 5 nM NAGK-SmBiT in the presence of 2 mM ATP. (**b**): NAGK-SmBiT titration to 10 pM PII-LgBiT variants in the presence of 2 mM ATP/ 2 mM NAG. (**c**): NAGK-SmBiT titration to 10 pM PII-LgBiT variants in the presence of 2 mM ATP/ 50 mM NAG. (**d**): NAGK-SmBiT titration to 10 pM PII-LgBiT in the presence of 2 mM ADP with either 2 mM NAG or 50 mM NAG. Graphs represent mean ± SD of three independent experiments.

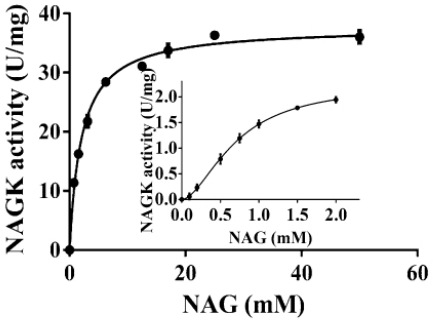

Figure 8. Activation of catalytic activity of NAGK by NAG in standarad NAGK assay and coupled NAGK assay. Standarad NAGK assay with NAG titration (0–50 mM) PII (1.2 µg) in the form of complex with NAGK (2 µg) in the presence of 10 mM ATP. Coupled NAGK assay with NAG titration (0–2 mM) for PII (2.4 µg) in the form of complex with NAGK (6 µg) in the presence of 1 mM ATP/1 mM ADP and 0.1 mM Arginine. Graphs represent mean ± SD of three independent experiments.

to tune the enzyme. Therefore, the weak interaction of the S49E PII variant with NAGK does not affect enzyme activity. Under in vivo conditions, the concentration of NAG is probably in the low millimolar range (as deduced from the low abundance in metabolome data, e.g.[17]. Hence, the dependence of PII-NAGK complex formation on NAG should have physiological consequences.

With increasing substrate concentrations, the affinity of NAGK for PII binding increases, leading to enhanced kinetic activation. Therefore, we tested whether NAGK activity in the PII complex at low NAG concentration and with 1 mM ATP/1 mM ADP and 0.1 mM Arg follows a sigmoidal curve, and in comparison, performed the standard assay in presence of 10 mM ATP (Fig. 8). The inset in Fig. 8 shows the result of the complex metabolite mixture. In fact, substrate-dependent activity follows a sigmoidal curve that could be fitted to a Hill slope of 1.76 ± 0.032. The increasing affinity of PII-NAGK with increasing concentrations of NAG results in a unique feed-forward like activation of the PII-NAGK complex by the enzyme substrate.

Conclusions

The present analysis has established that NanoBiT is a reliable approach for the analysis of PII – receptor interactions. For the first time, we were able to accurately determine the affinity constants of PII with its target PipX and NAGK under identical experimental conditions.

The assay is robust and requires only minute amounts of protein. In contrast to surface plasmon resonance or Bio-layer interferometry analysis, the interaction occurs with proteins in solution. The only unnatural feature is the fusion of LgBiT and SmBiT fragments to the proteins of interest. Of note, the intrinsic affinity for LgBiT and SmBiT is extremely low through optimization of NanoBiT system, achieving a K_D value as high as 190 μM[25]. Therefore the weak association between two parts of sensor should not influence the affinity of interacting proteins which is by several orders of magnitude higher (PII-PipX and PII-NAGK complexes in our study with K_D values in the range of nM). The specificity of association through PII interactions is also clearly indicated by the observation of fast dissociation of the PII-PipX complex upon addition of 2-OG. (See Fig. 3c): If the LgBiT-SmBiT fragments would affect the affinity, no such rapid dissociation would be visible. The intrinsic affinity is therefore so low that it doesn't affect the experimentally measured affinities between PII and its partner proteins. In accord, we observed almost negligible background under our experimental conditions, probably due to the low concentration of proteins used, far below the intrinsic affinities to Lg-BiT and Sm-BiT. Therefore, the emergence of luminescence can safely be interpreted as indication of complex formation.

In previous experiments on cyanobacterial PII protein interactions by Surface-Plasmon-Resonance (SPR), the K_D values for the PII-NAGK and PII-PipX interactions were never reported (the assays were carried out with the aim to determine the relative influence of effector molecules on PII interactions). The only K_D value for the PII-NAGK complex was determined previously by ultrafiltration experiments in presence of very high NAGK concentrations, so that complex formation equilibrium was almost completely on the side of the complex. From the small amount of free PII a K_D of approximately 73 nM was reported[6]. The K_D value that we here obtained by NanoBiT system (K_D = 12.9 nM) is almost six times lower although still in the same magnitude of order. In principle, the difference could be caused by different buffers used in these experiments. Very recently, we applied Biolayer interferometry, to measure PII interactions, whereby the interaction of PII with NAGK was tested as a proof of principle for the method (Supplementary material in Scholl et al.)[17]. Therefore, we now re-calculated the binding curves using curve fitting from association and dissociation kinetics according to Octet data analysis HT software (ForteBio) and this results in an apparent K_D of 11.7 ± 0.005 nM which is perfect agreement with the NanoBiT sensor data with the $K_{D=}$ 12.9 ± 0.65 nM. This gives additional credibility to the results from the NanoBit sensor.

Due to the high sensitivity of the interaction assay, it was even possible to detect residual low-affinity interactions, such as those between the PII variant PII-S49E with NAGK, which had never been detected before with SPR or BLI analysis. From the crystal structure of the PII-NAGK complex it is known that the seryl-residue at the tip of the T-loop stabilizes the tight PII-NAGK complex and causes the enzymatic activation of NAGK by PII. A weak interaction of the PII S49 variant (PII-S49G) could, however, be detected by FRET analysis[12,13] and was interpreted as indication of the transient encounter complex that is formed between PII and NAGK. This encounter complex was already predicted from the analysis of PII and NAGK mutants[20]. The NanoBiT study now for the first time resolved the affinity of the encounter complex, and revealed that this complex is not favoured by the state of adenyl-nucleotide binding to PII, as can be deduced from the dissociation constants of PII-S49E-NAGK in presence of different effectors. The PII-S49E variant represents a phosphomimetic variant of PII: wild-type PII is phosphorylated at S49 under nitrogen-poor conditions. The phopshomimetic variant is not able to catalytically activate NAGK, and it is reasonable to assume that likewise, also phospho-PII will not activate PII. However, the result of the NanoBiT analysis shows that the complex doesn't dissociate completely, suggesting that upon phosphorylation of PII at the tip of the T-loop, the proteins remain loosely associated. Dephosphorylation of PII under appropriate condition would then enable an immediate re-formation of the PII-NAGK complex.

A further application of the PII-based NanoBiT toolbox is the quantification of competitive binding of different PII receptors to PII. Here, we have demonstrated adenyl-nucleotide-dependent competition between PipX and NAGK for PII binding. PII has the highest affinity for PipX in the presence of ADP (5.7 nM), whereas under these conditions, affinity for NAGK is low (30.8 nM). Therefore, not surprisingly, NAGK was not able to compete with PipX: binding of PipX-SmBiT was unaffected by the addition of NAGK. By contrast, in presence of ATP, affinity of PII to PipX is diminished (52.4 nM) concomitantly with an increased affinity for NAGK (8.8 nM). Under these conditions, addition of NAGK lowered PII-LgBiT-PipX-SmBiT interaction, reflecting successful competition. Surprisingly, however, even a large excess of NAGK was unable to abolish the signal of the PII-LgBi-PipX-SmBiT sensor pair, although PII should have been almost completely saturated with NAGK in these conditions. The remaining luminescence signal could indicate vicinity between PipX-SmBiT and PII-LgBiT bound to NAGK, but the type of interaction remains to be clarified.

Altogether, this study has demonstrated the usefulness of the NanoBiT technology to study the interactions between PII and its receptors, and in a general sense, to investigate weak and transient protein–protein interactions. Future studies will transfer the method to the analysis of the recently identified PII receptors to gain quantitative insights in PII interactions with the ultimate goal to be able to model the network of PII interactions, for which quantitative data are required.

Methods

Cloning and DNA purification. To generate the split NanoLuc sensor, PII-LgBiT, PipX-SmBiT and NAGK-SmBiT synthetic genes, which already contained overlapping sequences for Gibson assembly, were ordered from Integrated DNA Technologies (Biotechnology company, Leuven, Belgium) (Table S1). PII- LgBiT was cloned in pASK-IBA3 vector linearized by EcoR1 and HindIII. Two other constructs, PipX-SmBiT and NAGK-SmBiT

were cloned into NdeI and BamHI sites of pTEV5 vector with N-terminal-fused His_6-tag via Gibson cloning as described previously[33]. Plasmid DNA was amplified by transformation into *E. coli DH10β*, which was grown at 37 °C overnight on agar media containing the appropriate antibiotic for selection. Positive colonies were identified by colony PCR and then transferred to Lysogeny broth (LB) supplemented with the appropriate antibiotic and grown at 37° C overnight. Plasmid DNA was purified from cells using the Monarch Plasmid Miniprep Kit (New England Biolabs, Frankfurt a.M., Germany) according to the manufacturer's instructions. All sequences were verified using the GATC LIGHTRUN service (Eurofins Genomics, Ebersberg, Germany). Afterwards, the resulting plasmids were transformed into electrocompetent *E. coli Lemo21* cells for subsequent expression of recombinant proteins.

Overexpression and Purification of recombinant proteins. The expression of recombinant proteins was performed by growing the cells at 37 °C under continuous shaking at 120 rpm to an OD600 of about 0.6–0.8. Depending on the plasmid the appropriated amount of the antibiotic was added to the culture. Overexpression was induced by the addition of 0.5 mM isopropyl-β-D-thiogalactopyranoside for His-tagged proteins and 0.2 µg/ml of anhydrotetracycline for Strep-tagged proteins. Induction was performed at 20 °C/120 rpm overnight. Then, the cells were harvested on the next morning by centrifugation (3.500 rpm for 15 min at 4 °C) and pellets were stored at -20° C until use.

The recombinant protein (PII) containing the $strep_{10}$-tag was purified via 5 ml Strep-tactin® superflow columns. The cells were lysed in 50 ml lysis buffer containing 50 mM Tris/HCl (pH 7.4), 50 mM KCl, 5 mM $MgCl_2$, 2 mM EDTA, 2 mM DTT and 0.5 mM PMSF. Ultrasonication was applied to disrupt the cells and lysate was centrifuged for 45 min at 55,000 × g at 4 °C. The supernatant was loaded on a 5 ml of Strep-Tactin Superflow column (IBA, Göttingen, Germany) that was equilibrated with the appropriate lysis buffer before use. Next, the column was washed with 100 ml of Strep washing buffer containing 100 mM Tris/HCl (pH 8.0), 150 mM NaCl, 1 mM EDTA and then it was eluted with Strep elution buffer containing 100 mM Tris/HCl (pH 8.0), 150 mM NaCl, 1 mM EDTA, 2.5 mM D-desthiobiotine. Roti-Quant (Roth, Karlsruhe, Germany) was applied to estimate the concentration of the eluted proteins in the elution fractions by following the manufacturer's instructions. The eluted protein was loaded on SDS-PAGE to check the purity and size of protein. The recombinant PII protein was dialyzed against PII dialysis buffer containing 20 mM Tris/HCl (pH 7.8), 150 mM KCl, 50% glycerol, 1 mM DTT and stored at -20° C until use.

The recombinant proteins (PipX and NAGK) containing His_6-tags were purified via 1 ml Ni–NTA HisTrap columns. The purification steps were similar to those of strep tag-proteins, while the buffers and columns were different. The lysis buffer contained 50 mM Tris/HCl (pH 7.4), 50 mM KCl, 5 mM $MgCl_2$, 10 mM Imidazole, 2 mM DTT and 0.2 mM PMSF. HisTrap columns were washed with 100 ml of His washing buffer 1 including 50 mM NaH_2PO_4 (pH 8.0), 300 mM NaCl, 20 mM Imidazole, followed by 50 ml of His washing buffer 2 with 50 mM NaH_2PO_4 (pH 8.0), 300 mM NaCl, 40 mM Imidazole. Elution of the bound proteins from the column with Ni–NTA was performed with an elution buffer containing 50 mM NaH_2PO_4 (pH 8.0), 300 mM NaCl, 250 mM Imidazole. The fractions consisting of recombinant protein were dialyzed in the respective dialysis buffer containing 50 mM Tris/HCl (pH 7.8), 100 mM KCl, 5 mM $MgCl_2$, 0.5 mM EDTA, 1 mM DTT and 50% glycerol. The proteins were stored at -20° C for further use.

Establishment of the bioluminescence assay. The luminescence assay for both types of measurement-time point and time course-was performed in a buffer containing 50 mM Tris/HCl (pH 7.6), 100 mM KCl, 10% glycerol, 2 mM $MgCl_2$ and 0.1% BSA. Next, the sensor proteins were added to the final concentration of 10 pM (trimer) for PII-LgBiT and a range of concentrations (0–800 nM) for PipX-SmBiT. The respective concentrations of effector metabolites (ATP, ADP, and ATP/2-OG) were included to the final volume (500 µl) in the test tubes. The mixture was incubated for 15 min at 30° C. Afterwards, 0.5 µl of Nano-Glo® Luciferase substrate (Promega, Walldorf, Germany) per 500 µl of total volume was added to each reaction tube. The solution was incubated for 5 min at room temperature to allow the reagent and proteins to adapt to the buffer. Subsequently the luminescence was quantified in a luminometer (Sirus Luminometer, Berthold Detection System, Germany) for 10 s with 10 s delay. The recorded luminescence is reported as relative light units (RLU). For background value, every protein was measured separately. Then, the recorded signal was subtracted from the luminescence of the forming complex.

To investigate the subsequent effect of metabolites in time-course experiments for PII-LgBiT and PipX-SmBiT, 10 pM PII was added to 10 nM PipX-SmBiT in the above mentioned buffer. Then, 0.5 µl of Nano-Glo® Luciferase substrate was added to the reaction tube. After 5 min incubation, the luminescence was measured via FB12 Sirius software with 20 s intervals in the Sirus luminometer for some minutes. To monitor the effect of metabolites on complex formation, the appropriate amounts were added to the reaction tube and the measurement was continued for several minutes until a maximum binding was reached.

In the case of luminescence measurement (time point) for PII-LgBiT variants and NAGK-SmBiT, the respective concentration of proteins and metabolites were incubated for 40 min at 30° C. The rest of the procedure was the same as the one described above.

Competition assay based on NanoBiT sensor. Competition assay between PipX and NAGK-SmBiT to bind to PII-LgBiT in the presence of 2 mM effector molecules, was performed with incubation of 10 pM PII-LgBiT trimer and different concentration of PipX (180, 900 and 1800 nM) monomer for 15 min at 30° C. Then a constant concentration of NAGK-SmBiT (180 nM) monomer was added to the mixure and incubation was continued for other 30 min at 30° C. Later, 0.5 µl of Nano-Glo® Luciferase substrate (Promega, Walldorf, Ger-

many) per 500 µl of total volume was added to each reaction tube. After 5 min of incubation, luminescence was quantified in a luminometer (Sirus Luminometer, Berthold Detection System, Germany) for 10 s with 10 s delay.

Competition assay between NAGK and PipX-SmBiT to bind to PII-LgBiT was performed with incubation of 10 pM PII-LgBiT trimer and different concentration of NAGK (180, 900, 1800 and 3600 nM) monomer for 30 min at 30° C. Then a constant concentration of PipX-SmBiT (10 nM) monomer was added to the mixture and incubation was continued for other 15 min at 30° C. The final steps were performed as described above.

AGPR coupled NAGK activity assay. To study the effect of NAG on the activity of the P_{II}-NAGK complex, the specific activity of NAGK from *Synechocystis sp.* PCC 6803 was assayed by coupling NAGK-dependent NAG phosphorylation to an auxiliary enzyme (AGPR) from *E. coli*. AGPR reduced the NAG-phosphate by using NADPH as reductant and the change was recorded at 340 nm as described[34,35]. The reaction buffer consisted of 50 mM imidazole (pH 7.5), 50 mM KCl, 20 mM $MgCl_2$, 0.2 mM NADPH, 0.5 mM DTT, 1 mM ATP, 1 mM ADP and 0.1 mM arginine. Each reaction contained 10 µg AGPR, 2.4 µg PII and 6 µg NAGK with different concentration of NAG (0–2 mM). The reaction was started by the addition of NAGK. Thereby, oxidation of one molecule of NADPH was recorded over a period of 10 min with a spectrophotometer (SPECORD 200, Analytik Jena). The reaction velocity was calculated with molar absorption of NADPH of $\Sigma_{340} = 6178$ L mol^{-1} cm^{-1} from the slope of the change of absorbance per time.

Standard NAGK activity assay. To assess the activity of NAGK, the ADP production was coupled to the NADH oxidation using the auxiliary enzymes pyruvate kinase and lactate dehydrogenase according to previously described[35,36]. The activity of NAGK was expressed in µmol/min/mg.

Statistical analysis. The results were performed three times to confirm reproducibility. They were expressed as the mean ± SEM of the indicated experiment. The FB12 Sirius software was used to record the luminescence in time-course experiments. Then, statistical analysis was performed by applying GraphPad Prism 6 with fitting curve "one site-specific bind with Hill slope".

Received: 23 March 2021; Accepted: 24 May 2021
Published online: 15 June 2021

References

1. Selim, K. A., Ermilova, E. & Forchhammer, K. From cyanobacteria to Archaeplastida: new evolutionary insights into PII signalling in the plant kingdom. *New Phytol.* **227**, 722–731 (2020).
2. Forchhammer, K. & Selim, K. A. Carbon/nitrogen homeostasis control in cyanobacteria. *FEMS Microbiol. Rev.* **44**, 33–53 (2020).
3. Gerhardt, E. C. *et al.* The protein-protein interaction network reveals a novel role of the signal transduction protein PII in the control of c-di-GMP homeostasis in *Azospirillum* brasilense. *Msystems* **5**, 10 (2020).
4. Burillo, S., Luque, I., Fuentes, I. & Contreras, A. Interactions between the nitrogen signal transduction protein PII and N-acetyl glutamate kinase in organisms that perform oxygenic photosynthesis. *J. Bacteriol.* **186**, 3346–3354 (2004).
5. Heinrich, B. *Bumblebee Economics* (Harvard University Press, 2004).
6. Llácer, J. L. *et al.* The crystal structure of the complex of PII and acetylglutamate kinase reveals how PII controls the storage of nitrogen as arginine. *Proc. Natl. Acad. Sci.* **104**, 17644–17649 (2007).
7. Llácer, J. L. *et al.* Structural basis for the regulation of NtcA-dependent transcription by proteins PipX and PII. *Proc. Natl. Acad. Sci.* **107**, 15397–15402 (2010).
8. Espinosa, J., Forchhammer, K., Burillo, S. & Contreras, A. Interaction network in cyanobacterial nitrogen regulation: PipX, a protein that interacts in a 2-oxoglutarate dependent manner with PII and NtcA. *Mol. Microbiol.* **61**, 457–469 (2006).
9. Fokina, O., Chellamuthu, V.-R., Zeth, K. & Forchhammer, K. A novel signal transduction protein PII variant from Synechococcus elongatus PCC 7942 indicates a two-step process for NAGK–PII complex formation. *J. Mol. Biol.* **399**, 410–421 (2010).
10. Fokina, O., Herrmann, C. & Forchhammer, K. Signal-transduction protein PII from Synechococcus elongatus PCC 7942 senses low adenylate energy charge in vitro. *Biochem. J.* **440**, 147–156 (2011).
11. Zeth, K., Fokina, O. & Forchhammer, K. Structural basis and target-specific modulation of ADP sensing by the Synechococcus elongatus PII signaling protein. *J. Biol. Chem.* **289**, 8960–8972 (2014).
12. Lüddecke, J. & Forchhammer, K. From P II signaling to metabolite sensing: a novel 2-oxoglutarate sensor that details P II-NAGK complex formation. *PLoS One* **8**, e83181 (2013).
13. Lüddecke, J. & Forchhammer, K. Energy sensing versus 2-oxoglutarate dependent ATPase switch in the control of Synechococcus P II interaction with its targets NAGK and PipX. *PLoS One* **10**, e0137114 (2015).
14. Chen, H. L., Bernard, C. S., Hubert, P., My, L. & Zhang, C. C. Fluorescence resonance energy transfer based on interaction of PII and PipX proteins provides a robust and specific biosensor for 2-oxoglutarate, a central metabolite and a signalling molecule. *FEBS J.* **281**, 1241–1255 (2014).
15. Hauf, W., Watzer, B., Roos, N., Klotz, A. & Forchhammer, K. Photoautotrophic polyhydroxybutyrate granule formation is regulated by cyanobacterial phasin PhaP in Synechocystis sp. strain PCC 6803. *Appl. Environ. Microbiol.* **81**, 4411–4422 (2015).
16. Watzer, B. & Forchhammer, K. Cyanophycin synthesis optimizes nitrogen utilization in the unicellular cyanobacterium Synechocystis sp. strain PCC 6803. *Appl. Environ. Microbiol.* **84**, 25 (2018).
17. Scholl, J., Dengler, L., Bader, L. & Forchhammer, K. Phosphoenolpyruvate carboxylase from the cyanobacterium Synechocystis sp. PCC 6803 is under global metabolic control by PII signaling. *Mol. Microbiol.* **114**, 292–307 (2020).
18. Orthwein, T. *et al.* The novel PII-interacting regulator PirC identifies phosphoglycerate mutase as a key control point of carbon storage metabolism in cyanobacteria. *Proc. Natl. Acad. Sci.* **118** (6) e2019988118 (2021).
19. Bolay, P. *et al.* The novel PII-interacting protein PirA controls flux into the cyanobacterial ornithine-ammonia cycle. *MBio* **12** (2): e00229–21 (2021).
20. Fokina, O., Chellamuthu, V.-R., Forchhammer, K. & Zeth, K. Mechanism of 2-oxoglutarate signaling by the Synechococcus elongatus PII signal transduction protein. *Proc. Natl. Acad. Sci.* **107**, 19760–19765 (2010).
21. Rubio, V., Marco-Marín, C. & Llácer, J. L. Nitrogen storage regulation by PII protein: lessons learned from taxonomic outliers. *FEBS J.* **287**, 439–442 (2020).

22. Lüddecke, J. *et al.* P II protein-derived FRET Sensors For Quantification And Live-Cell Imaging Of 2-Oxoglutarate. *Sci. Rep.* **7**, 1–13 (2017).
23. Remy, I. & Michnick, S. W. A highly sensitive protein-protein interaction assay based on Gaussia luciferase. *Nat. Methods* **3**, 977–979 (2006).
24. Hall, M. P. *et al.* Engineered luciferase reporter from a deep sea shrimp utilizing a novel imidazopyrazinone substrate. *ACS Chem. Biol.* **7**, 1848–1857 (2012).
25. Dixon, A. S. *et al.* NanoLuc complementation reporter optimized for accurate measurement of protein interactions in cells. *ACS Chem. Biol.* **11**, 400–408 (2016).
26. Promega. *NanoBiT® Protein:Protein Interaction System Technical Manual*, https://www.promega.de/resources/protocols/technical-manuals/101/nanobit-protein-protein-interaction-system-protocol/.
27. Tsang, T. F. *et al.* Simple method for studying in vitro protein–protein interactions based on protein complementation and its application in drug screening targeting bacterial transcription. *ACS Infect. Dis.* **5**, 521–527 (2019).
28. Doello, S., Burkhardt, M. & Forchhammer, K. The essential role of sodium bioenergetics and ATP homeostasis in the developmental transitions of a cyanobacterium. *Curr. Biol.* **31,** 1606–1615 (2021).
29. Espinosa, J., Labella, J. I., Cantos, R. & Contreras, A. Energy drives the dynamic localization of cyanobacterial nitrogen regulators during diurnal cycles. *Environ. Microbiol.* **20**, 1240–1252 (2018).
30. Díaz-Troya, S., Roldán, M., Mallén-Ponce, M. J., Ortega-Martínez, P. & Florencio, F. J. Lethality caused by ADP-glucose accumulation is suppressed by salt-induced carbon flux redirection in cyanobacteria. *J. Exp. Bot.* **71**, 2005–2017 (2020).
31. Beez, S., Fokina, O., Herrmann, C. & Forchhammer, K. N-acetyl-L-glutamate kinase (NAGK) from oxygenic phototrophs: PII signal transduction across domains of life reveals novel insights in NAGK control. *J. Mol. Biol.* **389**, 748–758 (2009).
32. Watzer, B. *et al.* The signal transduction protein PII controls ammonium, nitrate and urea uptake in cyanobacteria. *Front. Microbiol.* **10**, 1428 (2019).
33. Gibson, D. G. *et al.* Enzymatic assembly of DNA molecules up to several hundred kilobases. *Nat. Methods* **6**, 343–345 (2009).
34. Takahara, K., Akashi, K. & Yokota, A. Continuous spectrophotometric assays for three regulatory enzymes of the arginine biosynthetic pathway. *Anal. Biochem.* **368**, 138–147 (2007).
35. Lapina, T., Selim, K. A., Forchhammer, K. & Ermilova, E. The PII signaling protein from red algae represents an evolutionary link between cyanobacterial and Chloroplastida PII proteins. *Sci. Rep.* **8**, 1–14 (2018).
36. Selim, K. A., Lapina, T., Forchhammer, K. & Ermilova, E. Interaction of N-acetyl-l-glutamate kinase with the PII signal transducer in the non-photosynthetic alga Polytomella parva: Co-evolution towards a hetero-oligomeric enzyme. *FEBS J.* **287**, 465–482 (2020).

Acknowledgements
We appreciate Dr. Libera Lo Presti for her helpful comments and proof-reading this manuscript.

Author contributions
R.R. developed the NanoBiT sensor and performed in vitro assays in bacteria. K.F. designed and supervised the experiments. R.R. and K.F. Analyzed the data and prepared the manuscript.

Funding
This project was supported by DFG Grant Fo195/21-1 and infrastructural support from DFG-funded EXC 2124 "Controlling Microbes to Fight Infections. Further, we acknowledge support by Open Access Publishing Fund of University of Tübingen. Open Access funding enabled and organized by Projekt DEAL.

Competing interests
The authors declare no competing interests.

Additional information
Supplementary Information The online version contains supplementary material available at https://doi.org/10.1038/s41598-021-91856-2.

Correspondence and requests for materials should be addressed to K.F.

Reprints and permissions information is available at www.nature.com/reprints.

Publisher's note Springer Nature remains neutral with regard to jurisdictional claims in published maps and institutional affiliations.

2. Publication 2 (Accepted)

Research article

Bolay, P., Rozbeh, R., Muro-Pastor, M. I., Timm, S., Hagemann, M., Florencio, F. J., . . . Klähn, S. The Novel PII-Interacting Protein PirA Controls Flux into the Cyanobacterial Ornithine-Ammonia Cycle 2021. *Mbio.* 12, 10.1128/mbio. 00229-00221

AMERICAN SOCIETY FOR MICROBIOLOGY | mBio®

RESEARCH ARTICLE

The Novel P_{II}-Interacting Protein PirA Controls Flux into the Cyanobacterial Ornithine-Ammonia Cycle

Paul Bolay,[a] Rokhsareh Rozbeh,[b] M. Isabel Muro-Pastor,[c] Stefan Timm,[d] Martin Hagemann,[d] Francisco J. Florencio,[c] Karl Forchhammer,[b] Stephan Klähn[a]

[a]Helmholtz Centre for Environmental Research, Department of Solar Materials, Leipzig, Germany
[b]Interfaculty Institute for Microbiology and Infection Medicine, Organismic Interactions Department, Tübingen University, Tübingen, Germany
[c]Instituto de Bioquímica Vegetal y Fotosíntesis, CSIC-Universidad de Sevilla, Sevilla, Spain
[d]Department of Plant Physiology, University of Rostock, Rostock, Germany

Paul Bolay, Rokhsareh Rozbeh, and M. Isabel Muro-Pastor contributed equally. The order was determined by mutual agreement.

ABSTRACT Among prokaryotes, cyanobacteria have an exclusive position as they perform oxygenic photosynthesis. Cyanobacteria substantially differ from other bacteria in further aspects, e.g., they evolved a plethora of unique regulatory mechanisms to control primary metabolism. This is exemplified by the regulation of glutamine synthetase (GS) via small proteins termed inactivating factors (IFs). Here, we reveal another small protein, encoded by the *ssr0692* gene in the model strain *Synechocystis* sp. PCC 6803, that regulates flux into the ornithine-ammonia cycle (OAC), the key hub of cyanobacterial nitrogen stockpiling and remobilization. This regulation is achieved by the interaction with the central carbon/nitrogen control protein P_{II}, which commonly controls entry into the OAC by activating the key enzyme of arginine synthesis, *N*-acetyl-L-glutamate kinase (NAGK). In particular, the Ssr0692 protein competes with NAGK for P_{II} binding and thereby prevents NAGK activation, which in turn lowers arginine synthesis. Accordingly, we termed it P_{II}-interacting regulator of arginine synthesis (PirA). Similar to the GS IFs, PirA accumulates in response to ammonium upshift due to relief from repression by the global nitrogen control transcription factor NtcA. Consistent with this, the deletion of *pirA* affects the balance of metabolite pools of the OAC in response to ammonium shocks. Moreover, the PirA-P_{II} interaction requires ADP and is prevented by P_{II} mutations affecting the T-loop conformation, the major protein interaction surface of this signal processing protein. Thus, we propose that PirA is an integrator determining flux into N storage compounds not only depending on the N availability but also the energy state of the cell.

IMPORTANCE Cyanobacteria contribute a significant portion to the annual oxygen yield and play important roles in biogeochemical cycles, e.g., as major primary producers. Due to their photosynthetic lifestyle, cyanobacteria also arouse interest as hosts for the sustainable production of fuel components and high-value chemicals. However, their broad application as microbial cell factories is hampered by limited knowledge about the regulation of metabolic fluxes in these organisms. Our research identified a novel regulatory protein that controls nitrogen flux, in particular arginine synthesis. Besides its role as a proteinogenic amino acid, arginine is a precursor for the cyanobacterial storage compound cyanophycin, which is of potential interest to biotechnology. Therefore, the obtained results will not only enhance our understanding of flux control in these organisms but also help to provide a scientific basis for targeted metabolic engineering and, hence, the design of photosynthesis-driven biotechnological applications.

KEYWORDS nitrogen metabolism, cyanobacteria, small inhibitory proteins, P_{II} protein

Citation Bolay P, Rozbeh R, Muro-Pastor MI, Timm S, Hagemann M, Florencio FJ, Forchhammer K, Klähn S. 2021. The novel P_{II}-interacting protein PirA controls flux into the cyanobacterial ornithine-ammonia cycle. mBio 12:e00229-21. https://doi.org/10.1128/mBio.00229-21.

Invited Editor Ray Dixon, John Innes Centre

Editor Eduardo A. Groisman, Yale School of Medicine

Address correspondence to Stephan Klähn, stephan.klaehn@ufz.de.

Received 28 January 2021
Accepted 16 February 2021
Published 23 March 2021

Nitrogen (N) is one of the key elements of life and needs to be incorporated into biomolecules via assimilatory pathways. Despite being an ever-present resource in the atmosphere, only a few bacteria can fix dinitrogen (N_2), and the majority rely on the uptake and assimilation of combined N sources from their environment (1–3). To respond to fluctuations in the availability of combined N sources, bacteria possess complex regulatory networks to control N uptake as well as the activity of assimilatory enzymes (for reviews, see references 4–7). As a prime example, glutamine synthetase (GS), a key enzyme of bacterial ammonium assimilation, is tightly regulated in a variety of ways. In *Escherichia coli* and other proteobacteria, the expression of the GS-encoding *glnA* gene is controlled at the transcriptional level by the widespread NtrC/NtrB two-component system (7). Moreover, GS is controlled at the activity level via cumulative feedback inhibition from numerous metabolites related to N and energy metabolism as well as by covalent modification, i.e., adenylylation of the GS subunits. This modification system is operated by a bicyclic modification cascade involving the ubiquitous P_{II} signal transducer protein as a regulatory element (reviewed in reference 8). However, striking differences compared to widely accepted paradigms of N assimilation have been revealed in other bacteria, e.g., cyanobacteria.

Cyanobacteria are the only prokaryotes performing oxygenic photosynthesis and play a major role in global biogeochemical cycles (9–14). Presently they are receiving growing interest as biocatalysts in photobiotechnological applications, e.g., for the sustainable production of valued chemicals and fuels (15–19). To rationally engineer cyanobacteria, i.e., channeling metabolic fluxes to obtain the maximum yield of a desired chemical product, it is of paramount importance to fully comprehend underlying regulatory processes targeting primary metabolism. Although our overall understanding of cyanobacterial systems is still fragmentary compared to other well-established bacterial models, a few systems have been extensively investigated and include distinctive features. For instance, GS activity is controlled via the interaction with small, inhibitory proteins unique to cyanobacteria (20, 21). These GS-inactivating factors (IFs) exclusively control GS activity linearly with their abundance. Moreover, with the global nitrogen control protein NtcA, cyanobacteria use another type of transcription factor to control the expression of genes in response to N fluctuation (22). NtcA belongs to the CRP transcriptional regulator family and commonly works as an activator of N assimilatory genes (23–26). During N limitation, increasing levels of 2-oxoglutarate and the coactivator protein PipX stimulate DNA binding of NtcA (27–29). The interaction between NtcA and PipX is antagonized by the P_{II} protein, which acts as a global multitasking sensor and regulator, adjusting the carbon-nitrogen homeostasis through versatile protein-protein interactions (30, 31). This, for instance, includes the key enzyme for arginine synthesis, N-acetyl glutamate kinase (NAGK), which is activated by complex formation with P_{II} (32).

In addition to the activation of N assimilatory genes, NtcA can also act as a repressor of genes under N limitation. The physiological consequences of simultaneous positive and negative transcriptional regulation are again exemplified by the well-investigated GS regulatory system. Under N-limiting conditions, NtcA activates the transcription of the *glnA* gene, thereby increasing GS abundance and the rate of ammonium assimilation. Simultaneously, enhanced DNA binding of NtcA represses the transcription of the genes *gifA* and *gifB*, encoding the two known IFs, IF7 and IF17 (33). GS activity thereby is tuned in a trade-off between cellular N demands and relief from the metabolic burden imposed by the glutamate- and ATP-consuming GS-catalyzed reaction (for a review, see reference 88). Besides *gifA* and *gifB*, only a few other genes appear to be negatively regulated by NtcA. In an attempt to define the entire regulon of NtcA in the unicellular model strain *Synechocystis* sp. strain PCC 6803 (here called *Synechocystis*), Giner-Lamia et al. identified the gene *ssr0692* as another NtcA-repressed candidate (23). It encodes a small protein consisting of 51 amino acids with a high portion of N-rich, positively charged residues that were shown to be indispensable for protein-protein interaction in the case of the GS IFs

(21). These distinguishing traits point toward a vital function related to N control similar to the known GS IFs, e.g., as a regulator of a metabolic pathway.

Here, we report on the functional analysis of the small protein Ssr0692 in *Synechocystis*. It accumulates in response to ammonium supply and fulfills crucial regulatory roles in cyanobacterial metabolism via interaction with the P_{II} signaling protein. We show that it directly interferes with the P_{II}-dependent activation of NAGK. Consistent with this, under fluctuating N regimes, *ssr0692* mutant strains are impaired in balancing the synthesis of arginine and other amino acids associated with the cyanobacterial ornithine ammonia cycle identified recently (34). Therefore, we named Ssr0692 the P_{II}-interacting regulator of arginine synthesis (PirA).

RESULTS

Homologs of the *pirA* gene of *Synechocystis* are frequently present in cyanobacterial genomes and show a high degree of sequence conservation at the amino acid level (Fig. 1A and B). With only a few exceptions, sequences similar to that of PirA are absent from genomes of other bacterial phyla (as of July 2020, exceptions are "*Candidatus* Gracilibacteria bacterium," *Chloroflexaceae bacterium*, *Flavobacterium* sp. strain CLA17, and *Methylacidiphilales bacterium*). At first glance, this observation suggests a function associated with oxygenic photosynthesis. However, *pirA* has previously been identified as part of the NtcA regulon in *Synechocystis* (23), consistent with two putative NtcA binding motifs located upstream of the transcriptional start site (TSS) (Fig. 1C). In promoters that are activated by NtcA, the respective binding motifs are centered close to position −41.5 with regard to the TSS (+1), bringing NtcA into a favorable position to promote the binding of RNA polymerase (35). However, the location of both motifs present in the *pirA* promoter is compatible with a repressive role of NtcA in the transcription of this gene. The proximal site, which is centered at −33.5 bp upstream of the TSS, is in a position very similar to the binding sites described for the well-characterized NtcA-repressed *gifA-B* genes (23, 33). NtcA binding in close proximity to the TSS would mediate repression by steric hindrance of the RNA polymerase interaction. This assumption is consistent with *pirA* downregulation under N limitation, similar to the *gifA-B* genes and in contrast to NtcA-activated genes such as *glnA* or *nrtA*, encoding GS and a nitrate transporter component, respectively (Fig. 1D). Interestingly, the distal site, centered at −48.5 bp, could also interfere with the polymerase binding, specifically by preventing the correct interaction of the carboxy-terminal domain of its alpha subunit with the promoter (36). The presence of two NtcA binding motifs probably contributes to a tighter control of *pirA* expression as a function of N conditions.

PirA accumulates under N excess and is linked to a function in cyanobacterial N metabolism. Genes that are repressed by NtcA, such as the *gifA-B* genes, show low or even nondetectable transcription under N limitation but are highly expressed in response to excess N supply. To test whether this is also true for *pirA*, we precultivated *Synechocystis* cells in the presence of nitrate and analyzed transcript levels after induction of N excess by adding 10 mM ammonium. As expected, the *pirA* mRNA strongly accumulated under these conditions (Fig. 1E). To investigate whether this regulatory pattern is conveyed to the protein level, we obtained an antibody specific to the PirA protein. Consistent with the observed transcriptional regulation, the PirA protein also accumulated in response to ammonium upshifts (Fig. 1F). Moreover, the protein appeared to have a high turnover because it eluded detection shortly after N was depleted (see Fig. S1 in the supplemental material). These observations clearly link PirA and its function to cyanobacterial N metabolism.

To investigate the biological function of PirA, knockout and overexpression strains for the *pirA* gene were established in *Synechocystis*. The Δ*pirA* knockout mutant was generated by replacing the entire *pirA* open reading frame with a kanamycin resistance cassette via homologous recombination. In the case of the *pirA*$^+$ overexpression strain, a pVZ322 plasmid derivative harboring a transcriptional fusion of *pirA* with the Cu^{2+}-inducible *petE* promoter (P*petE*) was transferred into the *Synechocystis* wild type (WT) (Fig. 2A). Full segregation of the mutant allele in the Δ*pirA* mutant as well as the

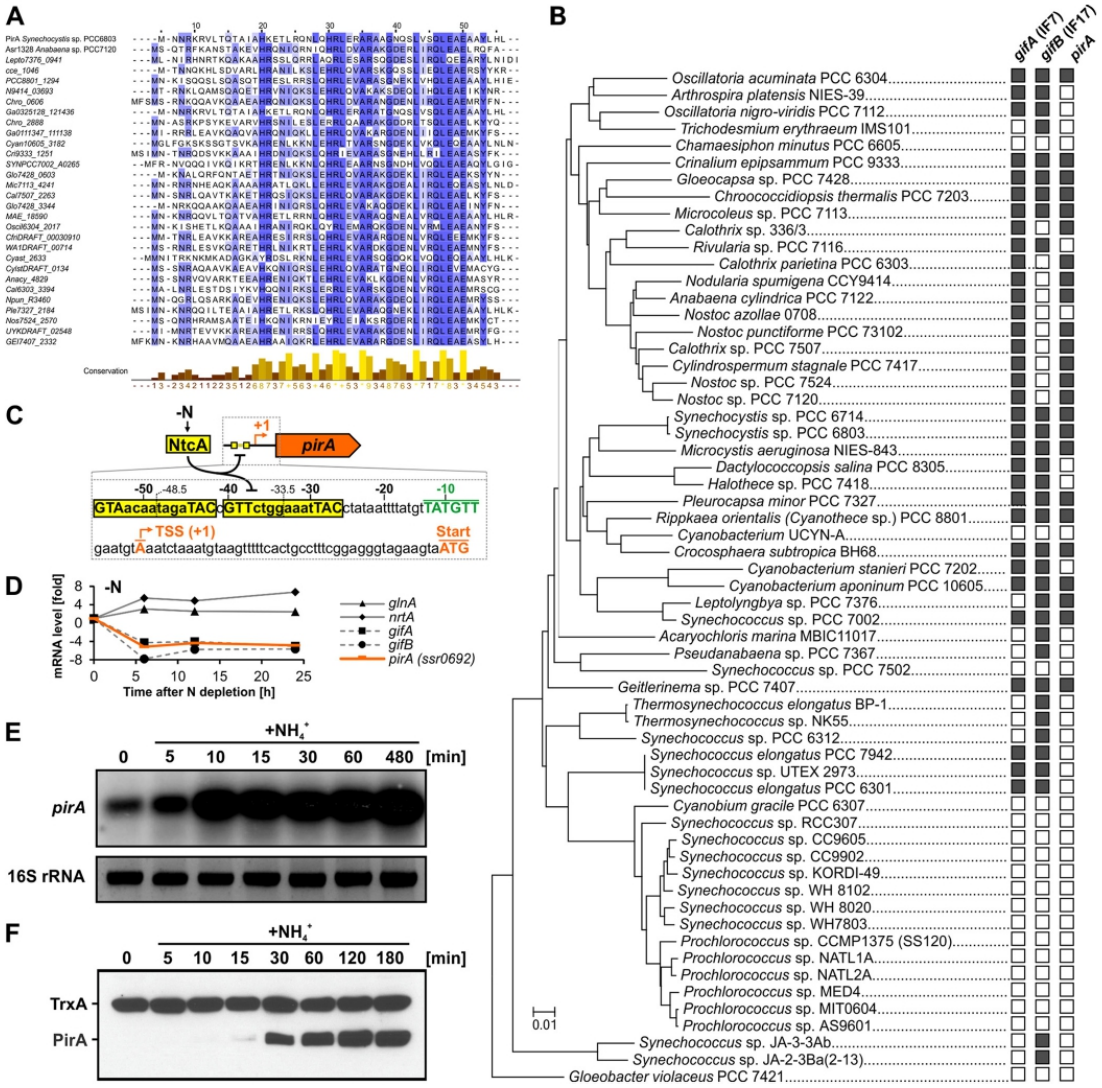

FIG 1 N-regulated gene *pirA* and its occurrence among cyanobacteria. (A) Amino acid alignment of randomly selected cyanobacterial PirA homologs. The alignment was made using ClustalW and visualized by using Jalview. (B) Phylogenetic tree of selected cyanobacteria based on 16S rRNA gene sequences. The tree was generated with the MEGA7 (83) software package and the neighbor-joining method. Note that we reused a calculated tree from our previous publication (38) and assigned the presence of genes in the corresponding genomes manually. Gene presence (illustrated by filled rectangles) was investigated using the BLASTP algorithm (84). As a reference, the amino acid sequences of PirA, IF7 (GifA, Ssl1911), and IF17 (GifB, Sll1515) from *Synechocystis* were used. (C) Overview of the promoter region upstream of the *pirA* gene in *Synechocystis*. Two putative NtcA binding sites are highlighted. The transcriptional start site (TSS; +1) and the location of the −10 element were extracted from differential transcriptome sequencing data (85). (D) Changes of mRNA levels for several *Synechocystis* genes in response to N limitation. Data were extracted and plotted from previously published microarray data (86). (E) Northern blot showing transcript accumulation of *pirA* in nitrate-grown *Synechocystis* cells upon addition of 10 mM ammonium chloride. 16S rRNA was used as a loading control. (F) Western blot showing changes in PirA protein levels in response to ammonium upshifts. For this, a specific, customized antibody against PirA was raised in rabbit. An antibody against thioredoxin (TrxA) was used to verify equal loading.

presence of the recombinant plasmid in the *pirA*$^+$ strain were verified by PCR (Fig. 2B). Subsequent Northern blot analyses with RNA isolated from cells grown in the presence of 1 μM $CuSO_4$ confirmed the generated mutants: the overexpression strain showed increased *pirA* mRNA levels compared to the WT, while in the knockout strain the *pirA*

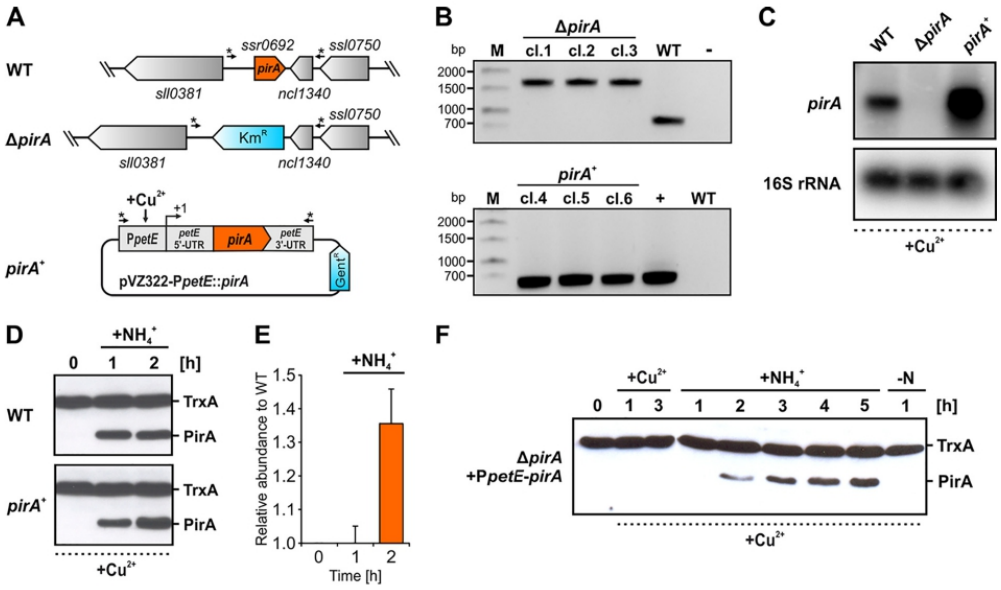

FIG 2 Properties and expression profiles in Δ*pirA* and *pirA*$^+$ recombinant strains. (A) Schematic view of the *pirA* locus in the WT and in the Δ*pirA* knockout strain as well as of a pVZ322 plasmid derivative harboring a *pirA* gene copy under the control of the Cu^{2+}-inducible promoter P*petE* that is present in the *pirA*$^+$ overexpression strain. In the Δ*pirA* knockout strain, *pirA* was replaced by a kanamycin resistance cassette (Km^r) via homologous recombination. The plasmid enabling ectopic *pirA* expression was introduced into *Synechocystis* WT. The arrows labeled with asterisks indicate the binding sites for primers used to verify the mutants. (B) PCR verification of the genotype of independently obtained mutant strains. In each case three clones were tested using primer combinations Ssr0692_KO-seg_fw/Ssr0692_KO-seg_rev (in case of Δ*pirA* strain) or P*petE*_fw(XhoI) and Toop_rev(AseI) (in case of *pirA*$^+$ strain). M, marker; bp, base pairs; cl., clone; −, negative control (water as the template); +, positive control (purified plasmid as the template). (C) Relative abundance of the *pirA* mRNA, measured via Northern blotting using sequence-specific ^{32}P-labeled ssRNA probes. In all cases, RNA was isolated from cells grown in the presence of 1 μM $CuSO_4$. (D) Western blot showing PirA protein levels in cells of the WT and *pirA*$^+$ strains, treated with 1 μM Cu^{2+} for 3 h and afterwards with 10 mM ammonium. Thioredoxin (TrxA) levels verify equal loading. (E) PirA levels relative to WT. Data were obtained by densitometric evaluation of respective bands using the ImageJ software (87). Data are mean ± standard deviation (SD) values obtained from two independent Western blots, i.e., two biological replicates (independent clones). (F) PirA accumulation in a Δ*pirA* strain that was complemented with a *pirA* gene fused to the *petE* promoter. Note that the data shown here were obtained using a mutant in which the P*petE-pirA* construct was integrated into the chromosome, i.e., this strain does not harbor the plasmid derivative shown in panel A.

transcript was absent (Fig. 2C). Interestingly, even though the mRNA was present and its abundance significantly increased in the *pirA*$^+$ strain due to the ectopic expression triggered by Cu^{2+}, the PirA protein could not be detected in nitrate-grown cells. However, after adding ammonium, which triggers the expression of the native *pirA* gene from the chromosome, increased PirA levels were detectable in the *pirA*$^+$ strain compared to the WT (Fig. 2D). This, in addition to the verified increase at the mRNA level, clearly confirmed that the overexpression construct is operative. Obviously, PirA abundance is not exclusively controlled at the transcriptional level. This observation was further supported by experiments using a *pirA* knockout mutant in which a P*petE*-fused gene copy was introduced. As observed before, the PirA protein could not be detected after adding Cu^{2+} to nitrate-grown cells (Fig. 2E). Remarkably, its presence was still N dependent, similar to the WT, i.e., it was detectable only after adding ammonium (Fig. 2E), even though *pirA* transcription was controlled by P*petE* and, hence, exclusively triggered by Cu^{2+}. Consequently, these data indicate an additional, posttranscriptional control mechanism, which obviously prevents stable PirA accumulation unless N availability suddenly increases. This again resembles the GS IFs encoded by the *gifA-B* genes, which are tightly regulated at the transcriptional as well as posttranscriptional level (37–39).

PirA plays a critical role upon changes in the C/N balance. Under standard conditions, i.e., with nitrate as the sole N source and under ambient CO_2, at which PirA is not

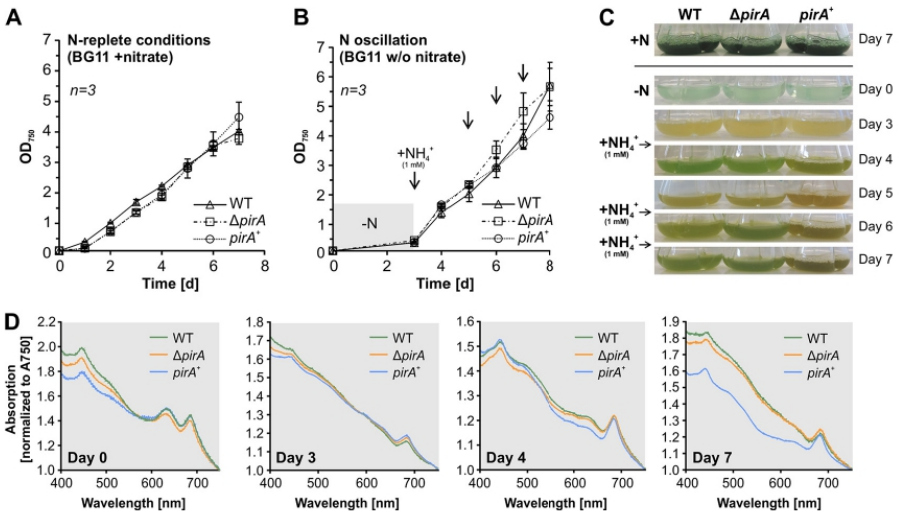

FIG 3 Growth and pigmentation of the WT and the Δ*pirA* and *pirA*$^+$ mutant strains when N is oscillating. (A and B) Growth under standard conditions and when ammonium is consecutively added to N-starved cultures. Arrows indicate time points at which 1 mM NH_4Cl was added. Data are the means ± SD from three independent cultures (including three independent clones of each mutant). (C) Representative photographs of cultures used in the experiment. Ammonium was added after day 3 and again after days 5 and 6. (D) Whole-cell absorption spectra. Values were normalized to A_{750} values.

detectable in the WT, the *pirA*-manipulated recombinant strains grew similarly to the WT, as expected (Fig. 3A and C). Given that PirA rapidly accumulated in response to increasing N availability, which suggests a function related to these conditions, it was tempting to speculate whether both recombinant strains show a phenotype, e.g., an affected pigment synthesis/degradation, when the N concentration is altered. To test this, we cultivated the WT, Δ*pirA*, and *pirA*$^+$ strains under N oscillating conditions. We inoculated cultures in nitrate-free BG11 and cultivated for 3 days, which was accompanied by pigment degradation (Fig. 3B and C), causing nitrogen starvation-induced chlorosis (40). Cultures of both recombinant strains showed the same behavior as the WT and did not show a nonbleaching (*nbl*) phenotype, as is known for *nbl* mutants that are affected in phycobilisome degradation (41). Consistent with this, the phycocyanin content was strongly reduced in all cells, measured by the diminished absorption at 630 nm (Fig. 3D, day 3). The similar bleaching kinetics of all strains is consistent with the fact that PirA is not detectable under N limitation. Afterward, the fully chlorotic cells were exposed to consecutive pulses of limited amounts of ammonium (1 mM) to simulate conditions under which PirA is rapidly accumulating and likely important. The regreening process was monitored by measuring growth as well as whole-cell absorption spectra at wavelengths in a range between 400 and 750 nm. While growth recovery was rather similar in all three strains, a clearly altered pigmentation was observed in the *pirA*$^+$ strain after iterated ammonium pulses (Fig. 3C and D). Consistent with the visible difference, a lower absorption at 630 nm was detected, resulting from reduced phycocyanin content. These data indicate that the cells are impeded in coping with fluctuating N concentrations and struggle to recover from chlorosis when PirA accumulation is not correctly balanced. This supports the assumption that this small protein plays a crucial role and participates in regulatory processes that control N metabolism.

Altered PirA abundance affects metabolites of N metabolism. To further examine a potentially regulatory function of PirA, time-resolved quantification of selected metabolites was performed for nitrate-grown cells of the WT and both mutants after addition of 10 mM ammonium. Interestingly, perturbation of PirA levels had a distinct

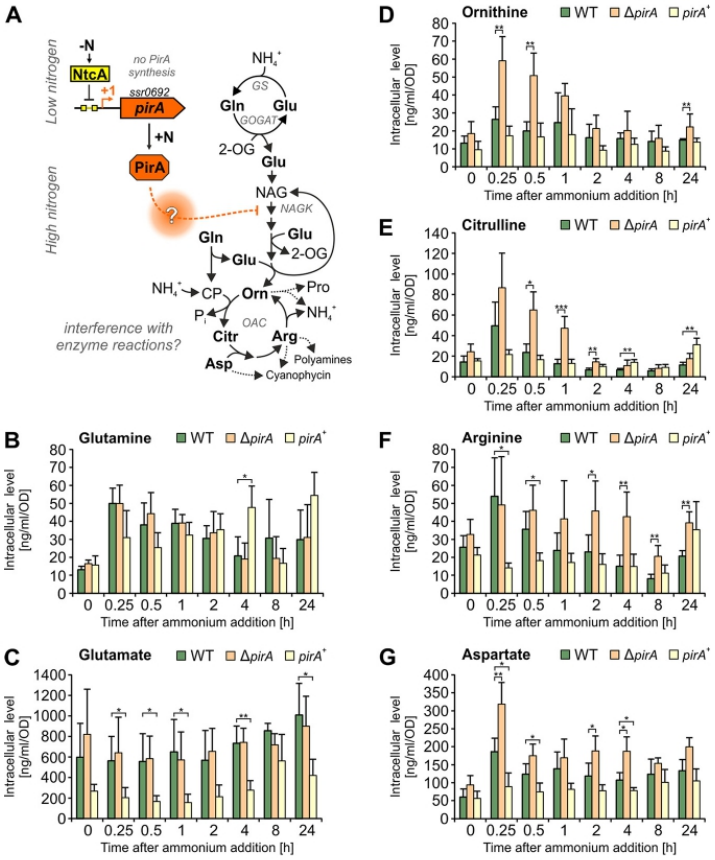

FIG 4 Kinetics of metabolites linked to the OAC cycle in response to ammonium addition. (A) Simplified overview of metabolic pathways associated with ammonium assimilation and a possible regulatory impact of PirA on certain enzymatic reactions. 2-OG, 2-oxoglutarate; CP, carbamoyl phosphate; GS, glutamine synthetase; GOGAT, glutamine oxoglutarate aminotransferase; NAG, N-acetyl-glutamate; NAGK, N-acetyl glutamate kinase; OAC, ornithine-ammonia cycle. (B to G) Kinetics of selected metabolites after adding 10 mM ammonium to nitrate-grown cells in the exponential phase. Metabolites were determined by ultrahigh-performance liquid chromatography-tandem mass spectrometry after ethanol extraction from cells of the WT, Δ*pirA*, and *pirA*$^+$ strains. Data are the means ± SD from two independent experiments, each conducted with three biological replicates (independent clones). Significant differences in the mutant strains compared to WT at each time point are labeled and were revealed by one-way analysis of variance (ANOVA; *, $P < 0.05$; **, $P < 0.01$; ***, $P < 0.001$).

impact on the accumulation of several key metabolites in *Synechocystis*. Most intriguingly, the kinetics of metabolites that are part of or are associated with the recently discovered ornithine-ammonia cycle (34) were strongly affected in Δ*pirA* and *pirA*$^+$ strains compared to the WT (Fig. 4; an extended data set is shown in Fig. S2). In general, N upshift triggered a transient accumulation of citrulline, ornithine, arginine, and aspartate in WT cells, similar to previous reports (34). Interestingly, the absence of PirA intensified and prolonged the accumulation of these metabolites, while the overexpression of *pirA* prevented or delayed their accumulation to a significant extent (Fig. 4). Moreover, kinetics of glutamine and glutamate, both key amino acids in N metabolism, showed striking differences between the tested strains. For instance, glutamate, which represents the main amine donor in a plethora of pathways, was significantly decreased in the *pirA*$^+$ strain throughout the experiment.

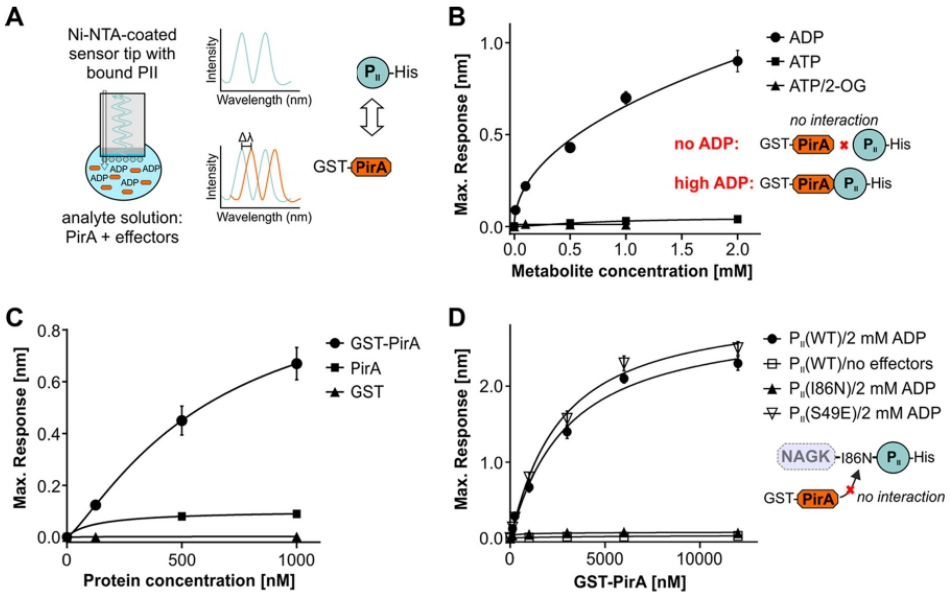

FIG 5 Determination of complex formation between PirA and the P_{II} protein, measured by biolayer interferometry (BLI). (A) Schematic view of the measuring principle. (B) Representation of the maximum binding response of P_{II}(WT)-His and GST-PirA interaction in the presence of different concentrations of ADP, ATP, or ATP/2-OG. (C) The maximum binding response at different protein concentrations of GST-PirA, tag-free PirA, or free GST in the presence of 2 mM ADP. As the binding response is a function of the mass of bound interactor, the response with GST-tagged PirA is correspondingly higher than that with isolated PirA peptide. (D) Representation of the maximum binding response at increasing concentrations of GST-PirA in the absence of effector molecules or in the presence of 2 mM ADP with three different T-loop variants of P_{II}. Data are the means ± SD from triplicate measurements.

The data clearly indicate that PirA plays a pivotal role in balancing fluxes through or into key amino acids, such as arginine. In cyanobacteria, the rate-limiting step of arginine synthesis is controlled by a well-investigated regulatory mechanism through complex formation of the key enzyme NAGK with the P_{II} protein (31, 32, 42). Moreover, a P_{II} variant with highly increased affinity toward NAGK (P_{II}-I86N) causes constitutive NAGK activation and, hence, arginine accumulation (43), which was at least transiently observed in cells of the Δ*pirA* strain. Thus, it was tempting to speculate that PirA interferes at this regulatory node.

PirA interacts with the signaling protein P_{II} in an ADP-dependent manner. Recently, PirA was found enriched in pulldown experiments of the signaling protein P_{II} (44). This indicated that PirA directly interacts with the P_{II} protein and thereby exercises a regulatory function similar to other small P_{II} interacting proteins, such as PipX (27) or CfrA/PirC, which has recently been discovered by two independent laboratories (45, 46). To verify the interaction between PirA and P_{II} from *Synechocystis*, *in vitro* binding experiments were performed using biolayer interferometry (BLI). To this end, recombinant protein variants were expressed in and purified from *E. coli*. His_8-tagged P_{II} protein was immobilized on a nickel-nitrilotriacetic acid (Ni-NTA)-coated sensor tip, and a glutathione *S*-transferase (GST)-tagged PirA variant was used as the analyte in the presence or absence of various effector molecules (Fig. 5A). Indeed, complex formation was detected in the presence of ADP in a clear concentration-dependent manner (Fig. 5B). In contrast, no interaction was observed in the presence of ATP, mixtures of ATP and 2-oxoglutarate (2-OG), or when no effector molecule was present. These data unambiguously revealed ADP-dependent interaction between P_{II} and GST-tagged PirA. To test the specificity of the interaction, we performed similar measurements using

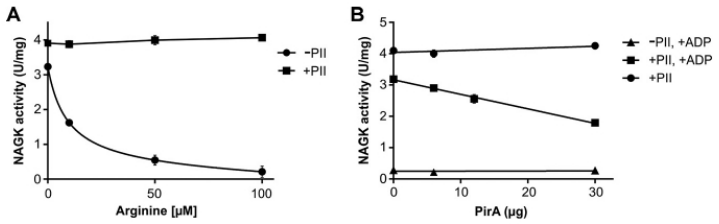

FIG 6 Impact of PirA on P_{II}-dependent NAGK activity *in vitro*. (A) Inhibition of NAGK by arginine in the presence or absence of 2.4 μg P_{II}. (B) NAGK activity as a function of increasing PirA concentration in the presence or absence of P_{II} and 1 mM ADP. The assay otherwise contained 0.1 mM arginine and 1 mM ATP. Data are the means ± SD from triplicate measurements.

PirA variants, where the GST tag was removed by proteolytic cleavage. The small PirA peptide yielded a binding signal that was about 6-fold lower than the signal observed for the GST fusion protein (Fig. 5C). This agrees well with the expected signal, since the BLI response depends on the mass changes at the sensor tip (GST-PirA versus PirA; 31.8 kDa/5.8 kDa = 5.5). Furthermore, BLI experiments with only the GST tag (26 kDa) did not result in any detectable signal (Fig. 5C), which clearly confirms that P_{II} specifically interacts with PirA in these binding studies. Since the GST fusion protein is easier to handle accurately and the signal is superior to that of the isolated PirA peptide, further experiments were performed with GST-tagged PirA.

To further study the P_{II}-PirA interaction, different P_{II} variants were examined. In most cases, interaction of proteins with P_{II} involves the highly flexible T-loop structure that can adopt a multitude of conformations (30, 47). Accordingly, a P_{II} variant lacking the T-loop ($P_{II}(\Delta T)$-His_8) was also tested. As expected, no response was observed, confirming interaction with PirA via the T-loop (not shown). Moreover, we tested the variant P_{II}(I86N), where a single amino acid replacement, Ile86 to Asn86, locks the T-loop in a conformation that promotes constitutive NAGK binding (48, 49). Strikingly, this variant was not able to bind PirA, even in the presence of 2 mM ADP, which otherwise promotes binding to the native P_{II} (Fig. 5D). In contrast, the phosphomimetic variant P_{II}(S49E), which does not interact with NAGK (50), shows unaffected complex formation with PirA (Fig. 5D). The affinity of P_{II}(S49E) to PirA was even slightly higher than that observed for the native variant [K_D values, 2.9 ± 0.34 μM for P_{II}(WT) and 2.5 ± 0.27 μM for P_{II}(S49E)]. Obviously, a conformation of the T-loop that mediates a high P_{II} affinity to NAGK prevents its interaction with PirA. Together with the metabolite profiles showing dysregulated arginine synthesis in the Δ*pirA* mutant, the present data implicate the interference of PirA with NAGK regulation through interaction with P_{II}.

PirA antagonizes P_{II}-dependent activation of arginine-inhibited NAGK. To further demonstrate that PirA interferes with the P_{II}-NAGK complex, an enzyme assay with purified components was conducted. Using the standard NAGK assay, where ADP formation is coupled to pyruvate-kinase and lactate-dehydrogenase activity (48), thereby keeping ADP concentrations at zero, no effect of PirA on P_{II}-promoted activation of NAGK could be observed (not shown). Therefore, an assay was employed where NAG phosphorylation was coupled to subsequent NADPH-dependent N-acetyl-γ-glutamyl-5-phosphate reduction (51), allowing the addition of ADP. In this assay, the presence of P_{II} protects NAGK from arginine inhibition, with 100 μM arginine fully discriminating free NAGK from P_{II}-complexed NAGK (Fig. 6A). When the assay was performed in the presence of 0.1 mM arginine and 1 mM ATP, again no effect of adding increasing PirA concentrations could be detected. When, however, the same assay was performed in the presence of 1 mM ATP and 1 mM ADP, a concentration-dependent inhibition of NAGK activity of up to 50% could be detected, in accord with the ADP requirement for P_{II}-PirA interaction (Fig. 6B). Altogether, the data point to a PirA-mediated disaggregation of the P_{II}-NAGK complex that subsequently leads to NAGK inhibition by arginine.

DISCUSSION

Arginine serves as a proteinogenic amino acid and precursor for the synthesis of polyamines and other N storage compounds, such as the cyanobacterial cyanophycin. In bacteria, arginine can be synthesized either by a linear pathway, e.g., present in *Enterobacteriaceae*, or by an energetically more favorable cyclic pathway. In the latter, N-acetyl-ornithine reacts with glutamate to yield ornithine and N-acetyl-glutamate, the starting metabolite of the pathway, which is widely distributed in nature and also present in cyanobacteria (52, 53). Nevertheless, arginine synthesis requires vast amounts of energy and N (42) and, thus, is tightly regulated in bacteria. This is mainly achieved by feedback inhibition of the corresponding key enzymes by the end product arginine. In *E. coli*, this addresses N-acetylglutamate synthase (NAGS), which catalyzes the first step of linear arginine synthesis from glutamate (52). In contrast, in those bacteria harboring the cyclic pathway, the second enzyme, NAGK, is feedback inhibited by arginine (53).

PirA, a novel player in the distinctive regulation of arginine synthesis in cyanobacteria. In cyanobacteria, NAGK is the target of a molecular regulatory mechanism that involves complex formation with the signal transduction protein P_{II} (32, 50). This interaction diminishes feedback inhibition of NAGK by arginine and, hence, boosts the metabolic flux toward the end product (32). Its importance for the control of cyanobacterial metabolism is supported by the fact that this mechanism is widely present in oxygenic phototrophs such as plants (54, 55) and microalgae (56) but appears to be absent from other bacteria (for an overview, see reference 57). Regarding arginine metabolism, the uniqueness of cyanobacteria within prokaryotes is also exemplified by the recent discovery of active cycling between ornithine and arginine via an ornithine-ammonia cycle (OAC), similar to the known ornithine-urea cycle (OUC) that is present in terrestrial animals but typically absent from bacteria (34).

Here, we introduce the small cyanobacterial protein PirA as a novel key regulator in the cyanobacterial arginine synthesis pathway and, hence, the OAC. Our data confirm PirA accumulation under N excess, particularly when ammonium is added. This accumulation is obviously required to adjust a certain pool of metabolites that are part of the OAC, including arginine. Mechanistically, we propose a model where PirA competes with NAGK for the P_{II} protein (Fig. 7). In response to ammonium addition, the accumulating PirA molecules interfere with the complex formation between P_{II} and NAGK, thereby mitigating NAGK activation and preventing an overaccumulation of arginine.

Surprisingly, detectable PirA accumulation only occurred under ammonium shock, even when *pirA* mRNA was transcribed independently from N and energy status of the cell. A similar situation can be encountered with the GS IFs, which were shown to be degraded by metalloproteases when not bound to GS (37). Thus, it is tempting to speculate that PirA accumulation can only occur when bound to P_{II}. However, to reveal the mechanism of PirA turnover, detailed research beyond the scope of this study is required.

PirA integrates N and energy sensing. Remarkably, PirA forms a complex with P_{II} only in the presence of ADP. Accordingly, the pivotal stimulus for the suggested regulatory mechanism is not only the N status, which is mainly sensed by 2-OG in cyanobacteria, similar to other prokaryotes (58, 59). The 2-OG level determines the affinity of NtcA to its binding motif (24, 29), which therefore also determines PirA accumulation. Moreover, PirA was found to transiently but strongly accumulate during low C supply (60). This is consistent with the derepression of the *pirA* gene by the dissociation of NtcA from its binding motif upstream, since low C supply, i.e., a low C/N ratio, leads to a decreased 2-OG pool (61). The interaction between PirA and P_{II} strongly responds to ADP as another signal and, hence, depends on the cellular energy status. These observations resemble another small P_{II}-interacting protein, PipX, whose interaction with P_{II} is enhanced by ADP as well (51, 62). PipX functions as a coactivator of the transcription factor NtcA and is required for the 2-OG-dependent DNA binding and transcriptional activation of genes (27). In the presence of high ADP levels, PipX preferably interacts

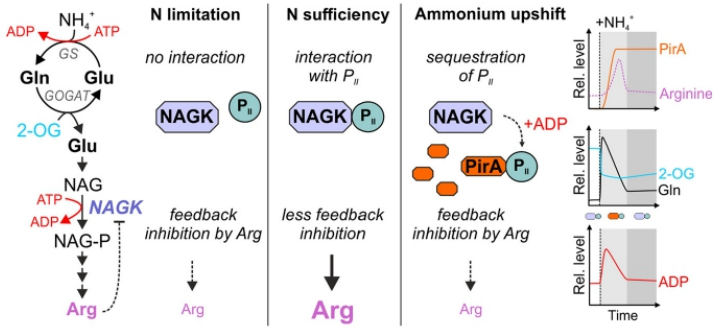

FIG 7 Anticipated model of PirA function. Metabolite kinetics have been approximated based on available literature data (34, 38). Upon shifts in the ammonium concentration, PirA accumulates via 2-OG-dependent derepression of the *pirA* gene. The gene product is presumably required to slow down ATP-consuming synthesis of arginine. This could be achieved by ADP-dependent sequestration of P_{II} protein bound to NAGK, which is required to diminish feedback inhibition of the enzyme and, in turn, activate arginine synthesis. The sequestration of P_{II} results in stronger arginine feedback inhibition of NAGK, diminishing energy consumption and flux into arginine. After metabolic reorganization (e.g., by inactivating glutamine synthetase activity and decreasing ATP consumption), ADP levels may fall below a critical level, preventing interaction between PirA and P_{II}. Accordingly, a higher fraction of the P_{II} pool will again interact with and activate NAGK, which in turn results in elevated arginine synthesis.

with P_{II}, which attenuates NtcA activity and in turn leads to derepression and upregulation of the *pirA* gene, similar to the *gif* genes encoding the GS IFs (33).

Interestingly, *in vitro* data showed that the NAGK-P_{II} interaction is also ADP sensitive. While ADP does not entirely prevent complex formation, it increases dissociation of NAGK from ADP-bound P_{II} (48). However, detailed analysis revealed that increasing ADP levels have only a minor effect on the NAGK-P_{II} complex as long as ATP is present, whereas this interaction is mainly tuned by changing the 2-OG levels (51, 63). It should be kept in mind that the sensing properties of P_{II} are influenced by the binding partner in such a way that, for certain targets, small fluctuations in the ADP/ATP ratios are sensed (e.g., P_{II}-PipX complex formation), whereas in other cases fluctuations in the 2-OG levels are perceived (e.g., P_{II}-NAGK interaction). In light of these data, PirA appears to amplify the energy-dependent signal in P_{II}-mediated activation of NAGK. By sequestering P_{II} under conditions of low 2-OG and high ADP levels, PirA may shift the equilibrium of the P_{II}-NAGK complex toward noncomplexed NAGK, i.e., in case the cell transiently experiences energy limitation. Given that bacteria employ GS-GOGAT only during sufficient energy supply (64), it can be assumed that the high ATP consumption by GS in consequence of ammonium addition to nitrate-grown cells could create such an energy limitation. This, in turn, might require the limiting of ATP-dependent flux via NAGK into arginine and to couple such a regulatory mechanism to the intracellular ADP levels, which are a direct result of high ATP turnover.

Depending on the detailed structure of the complexes, P_{II} phosphorylation either abrogates interaction with its targets, as demonstrated for NAGK (32), or has no effect on them, as in the case of P_{II}-PipX interaction (35). The phosphomimetic variant P_{II}(S49E) showed slightly enhanced interaction with PirA compared to P_{II}(WT). In a similar way, P_{II} interacts with PipX irrespective of Ser49 modification; nevertheless, the interaction is T-loop dependent (27). The major interaction surface is at the proximal part of the T-loop, whereas the tip region with the critical Ser49 residue does not participate in complex formation. From the Ser49-independent mode of PirA-P_{II} interaction, we conclude that the PirA-P_{II} interaction also takes place with phosphorylated P_{II} that does not bind to NAGK. In any case, the interaction of P_{II} with NAGK or PirA appears to be mutually exclusive, since both P_{II} interaction partners require the T-loop in different conformations for interaction. This

explains the effect of PirA on the *in vitro* activity of the P_{II}-NAGK complex in the presence of a concentration of arginine that is inhibitory for free NAGK but permissive for the P_{II}-NAGK complex. By competing for P_{II} binding, PirA releases free NAGK, which is strongly subject to arginine feedback inhibition. The efficiency of competition between NAGK and PirA depends on the cellular ATP/ADP ratio.

The competition between NAGK and PirA for P_{II} is further illustrated by the inability of PirA to bind P_{II}(I86N). This variant adopts a constitutive NAGK-bound-like structure of the T-loop (48, 49). Accordingly, the lack of PirA interaction with P_{II}(I86N) also agrees with the strong *in vivo* activation of NAGK by this variant (43). However, for a more detailed understanding of the mechanism, by which PirA affects P_{II} signaling, further functional biochemical studies and structural analyses are required.

Homologs of *pirA* are widespread in cyanobacterial genomes, which generally supports its crucial regulatory role. For instance, the *pirA* homolog *asr1328* of the filamentous, diazotrophic cyanobacterium *Anabaena* sp. strain PCC 7120 was shown to be negatively regulated by NtcA as well (65). Similar to the GS IFs, gene annotations in a few strains, such as *Thermosynechococcus elongatus* or *Synechococcus* sp. strain JA-3-3Ab, suggest that alternative versions of PirA with an extended N terminus also exist (see Fig. S3 in the supplemental material). Nevertheless, the existence of those proteins has not been experimentally investigated yet; hence, false annotations cannot be excluded. This assumption is supported by the fact that only a few of those elongated sequences could be found in protein databases and show only partial similarity. Therefore, the function of these PirA-like proteins with N-terminal extensions remains elusive. In addition, it is worth noting that PirA is, similar to the GS IFs, completely absent from marine picocyanobacteria (Fig. 1). In accordance with this, this clade lacks several salient features of N-sensing and utilization that are widespread among cyanobacteria. For instance, P_{II} is not subject to phosphorylation in *Prochlorococcus* (66, 67), and both *Prochlorococcus* and *Synechococcus* genera are incapable of cyanophycin synthesis and lack several OAC cycle genes (68). These genome-streamlined strains occur in oligotrophic realms of the ocean with hardly any fluctuation in nutrient supply (69). Thus, it is compelling to speculate that PirA-mediated short-term adjustment of arginine synthesis to the N and energy status of the cell is not required in such habitats.

MATERIALS AND METHODS

Strains and growth conditions. *Synechocystis* sp. strain PCC 6803, originally obtained from N. Murata (Japan), was used as the wild type. Cells were grown in BG11 medium (70) depleted of Cu^{2+} ions and supplemented with 10 mM TES buffered at pH 8.0. The sole N source in that medium is nitrate at a concentration of 17.64 mM (termed nitrate grown). Cultivation was performed in baffled Erlenmeyer flasks in the presence of ambient CO_2 under constant illumination (white light, 50 μmol photons m^{-2} s^{-1}) at 30°C, 75% humidity and 150 rpm. Each recombinant strain was isolated on BG11 agar plates and maintained in medium containing either kanamycin or gentamicin at a concentration of 50 μg/ml and 2 μg/ml, respectively. Prior to the experiments investigating the impact of altered PirA abundance, the cultures were supplemented with 1 μM $CuSO_4$.

Mutant strain generation. To knock out the *ssr0692* (*pirA*) gene, the upstream and downstream regions of *pirA* were amplified from *Synechocystis* genomic DNA (gDNA) using primer combinations Ssr0692upst_fw/Ssr0692upst_rev and Ssr0692downst_fw/Ssr0692downst_rev (all primers are listed in Table S1 in the supplemental material). The kanamycin resistance cassette was amplified from a customized construct obtained by gene synthesis using primers KmR_fw and KmR_rev. The synthesized construct harbored the *aphII* gene and its promoter, which were originally obtained from pUC4K (Amersham). In addition, an *oop* terminator was introduced downstream of *aphII*. All amplicons had short fragments of sequence complementarity and were fused via polymerase cycling assembly (PCA) using primers Ssr0692upst_fw/Ssr0692downst_rev. The resulting construct was introduced into pJET1.2 (Thermo Scientific) and used to transform chemically competent *E. coli* DH5α. After isolation of the pJET_ssr0692_KmR_KO plasmid from *E. coli*, the knockout construct was introduced into *Synechocystis* WT by natural transformation and homologous recombination into the chromosome. To enable the overexpression of *pirA*, the 5′ untranslated region (UTR) and 3′UTR of the *petE* gene were amplified from *Synechocystis* gDNA using primers P*petE*_fw (XhoI)/5′*petE*_ssr0692_rev and 3′*petE*_ssr0692_fw/Toop_rev(AseI). The *pirA* coding sequence was amplified from *Synechocystis* gDNA using primers ssr0692_fw/rev. All amplicons had short fragments of sequence complementarity and were fused via polymerase cycling assembly (PCA) using primers P*petE*_fw(XhoI)/Toop_rev (AseI) and introduced into the broad-host-range plasmid pVZ322 via restriction digestion and ligation into XhoI/AseI sites. The recombinant plasmid pVZ322-P*petE*:*pirA*, obtained after transformation of and

purification from *E. coli* DH5α, was introduced into *Synechocystis* WT via electroporation. All strains and constructs were verified by PCR and Sanger sequencing.

To generate the alternative Δ*pirA*/P_{petE}-*pirA* strain (chromosomal integration), a DNA fragment containing the *pirA* open reading frame and the coding sequence for six histidine residues at the carboxyl-terminal end was amplified by PCR using *Synechocystis* genomic DNA and primers ssr0692.KpnI and ssr0692.HisBamHI. This fragment was cloned into KpnI-BamHI-digested pPLAT plasmid (37), a pGEM-T derivative containing a 2-kb region of the nonessential *nrsBACD* operon, which includes targets for these restriction enzymes (71). This cloning generated pPLAT-*pirA*. In a second step, the *Synechocystis petE* promoter was amplified by PCR using genomic DNA and primers P*petE*.KpnI.1 and P*petE*.KpnI.2 and cloned into the KpnI site of pPLAT-*pirA*. Finally, a Km^r CK1 cassette from pRL161 (72) was cloned in the BamHI site of pPLAT-*pirA*, generating pPLAT-P*petE-pirA*. For the amplification of the plasmids, chemically competent *E. coli* DH5α cells were used in all cases. pPLAT-P*petE-pirA* plasmid was used to transform a *Synechocystis* Δ*pirA* strain. All generated strains and their properties are given in Table S2.

N oscillation experiment. WT and mutant strains were inoculated in triplicates at an optical density at 750 nm (OD_{750}) of 0.1 in 3-baffled 100-ml flasks in 20 ml N-depleted BG11 supplemented with 1 μM $CuSO_4$. For comparison, the same strains were also cultivated in standard BG11 medium containing 17.64 mM nitrate. After 3 days, the N-starved cells were supplemented with 1 mM NH_4Cl, a step that was repeated after 5 and 6 days. Whole-cell spectra of cell suspensions were conducted with a Cary 300 UV-visible spectrophotometer (Agilent).

RNA extraction and Northern blots. Cells for Northern blot analysis were harvested by rapid filtration on polyether sulfone filters (pore size 0.8 μm; Pall). Filters were immediately resolved in 1 ml PGTX solution (73) and frozen in liquid N_2. RNA extraction was conducted as previously described (74). For Northern blots, 3 μg of RNA was separated on 1.5% agarose gels supplemented with 6% formaldehyde. The gels were run in MEN buffer containing 20 mM MOPS, 5 mM NaOAc, 1 mM EDTA, pH 7.0. Prior to loading, the RNA samples were incubated at 65°C for 10 min in loading buffer containing a final concentration of 62.5% (vol/vol) deionized formamide (Sigma-Aldrich). Afterward, RNA was transferred via capillary blotting to an Amersham Hybond N^+ nylon membrane (GE Healthcare) and cross-linked at 1,250 μJ in a UVP cross-linker (Analytik Jena). To specifically detect the *pirA* transcript, the RNA-mounted nylon membrane was hybridized with a complementary α-^{32}P-labeled single-stranded RNA (ssRNA) probe that was generated by *in vitro* transcription using the MAXIscript T7 transcription kit (Thermo Fisher Scientific). As a transcription template, a DNA fragment obtained by PCR with primers Ssr0692_T7_fw and Ssr0692_rev was used. Subsequently, Fuji BAS-IIIS imaging plates were exposed to the membranes and read out by an Amersham Typhoon laser scanner (GE Healthcare). As a loading control, the same membranes were hybridized with ssRNA probes complementary to the 5S rRNA, which were generated in the same way using primers 5sRNA_fw/rev (Table S1).

Anti-PirA antibody production. A DNA fragment encompassing the *pirA* open reading frame (ORF) was amplified by PCR from *Synechocystis* genomic DNA, using the oligonucleotides Ssr0692ORF-fw and Ssr0692ORF-rv. This fragment was cloned into NdeI-XhoI-digested pET24a(+) plasmid (Novagen) to generate pET24-Ssr0692 plasmid. Exponentially growing *E. coli* BL21 cells transformed with pET24-Ssr0692 were treated with 1 mM isopropyl ß-D-1-thiogalactopyranoside for 4 h. For purification of PirA-His_6 protein, cells were collected, resuspended in buffer A (20 mM sodium phosphate, pH 7.5, 150 mM NaCl, 5 mM imidazole) with 1 mM phenylmethylsulfonyl fluoride (PMSF), and disrupted by sonication. The lysate was centrifuged at 18,000 × *g* for 20 min. PirA-His_6 from the supernatant was purified by Ni-affinity chromatography using a HisTrapHP column (GE Healthcare) and following the manufacturer's instructions. Elution was performed with a linear gradient (5 to 500 mM imidazole) in buffer A. Fractions with PirA-His_6 were pooled, concentrated using centrifugal filter units (Amicon Ultra-15 3 kDa) (Millipore), and subjected to gel filtration chromatography using a Hiload 16/60 Superdex 75 gel filtration column (GE Healthcare) running on an AKTA fast protein liquid chromatography (FPLC) system and using buffer A without imidazole. Fractions containing purified PirA-His_6 protein were pooled, concentrated, and quantified in a NanoDrop 1000 spectrophotometer (Thermo Scientific) using the extinction coefficient of PirA-His_6 calculated with the ExPASy-ProtParam tool. Anti-PirA antiserum was obtained according to standard immunization protocols. A female specific-pathogen-free rabbit was used. Before immunization, preimmune serum was obtained to carry out the pertinent controls. Three immunizations were carried out with the antigen, PirA protein, separated by a period of 2 weeks. For the first immunization, 1.5 mg of PirA was used, and for the next two immunizations, 1 mg of antigen was used. In all cases, 0.5 ml of antigen was emulsified with 0.5 ml of Freund's incomplete adjuvant, and 3 to 5 subcutaneous injections were made. Ten days after the last immunization, the animal was exsanguinated and the serum obtained was stored at −80°C.

Preparation of crude extracts and Western blot analysis. For the analysis of protein abundance, cells of 2 ml culture were harvested and resuspended in 80 μl of 50 mM HEPES-NaOH buffer (pH 7.0), 50 mM KCl, 1 mM PMSF. Crude extracts were prepared using glass beads as previously described (75). For Western blot analysis, proteins were fractionated on 15% SDS-PAGE (76) and transferred to nitrocellulose membranes (Bio-Rad). Blots were blocked with 5% (wt/vol) nonfat dry milk (AppliChem) in phosphate-buffered saline (PBS)-Tween 20 for 1 h. Antisera were used at the following dilutions: anti-PirA (1:5,000) and anti-TrxA (1:10,000) (77). In all cases, the incubation of the membranes with the primary antibody was carried out overnight at 4°C. After four washes (15 min for each one) with PBS-Tween 20, the nitrocellulose membranes were incubated with a secondary antibody against rabbit IgG (1:25,000) (Sigma-Aldrich) for 1 h at room temperature. After washing again four times with PBS-Tween 20, the ECL Prime Western blotting detection reagent (GE Healthcare) was used to detect the different antigens by following the manufacturer's instructions.

Metabolite analysis. For metabolite analysis, cells were grown in BG11 containing the standard nitrate amount until reaching an OD_{750} of ~0.8. Cells were harvested shortly before and after the addition of 10 mM ammonium chloride by centrifugation of 2 ml culture at 17,000 × *g* for 1 min. Supernatant was discarded and pellets were snap-frozen in liquid N. Metabolite extraction was performed by resuspending cell pellets in 1 ml of 80% (vol/vol) ethanol supplemented with 1 μg/ml L-carnitine hydrochloride as an internal standard and heating for 2 h at 60°C. After centrifugation at 17,000 × *g* for 5 min, the supernatant was transferred to a fresh vial and the pellet was again resuspended in 1 ml of 80% (vol/vol) ethanol and heated at 60°C for 2 h. After centrifugation at 17,000 × *g* for 5 min, supernatants were combined and dried in a centrifugal evaporator (Concentrator plus; Eppendorf, Germany).

The dried extracts next were dissolved in 1,000 μl liquid chromatography-mass spectrometry (LC-MS)-grade water and filtered through 0.2-μm filters (Omnifix-F; Braun, Germany). A volume of 1 μl of the cleared supernatants was analyzed using the high-performance liquid chromatograph mass spectrometer LCMS-8050 system (Shimadzu) and the incorporated LC-MS/MS method package for primary metabolites (version 2; Shimadzu) as described previously (78). Briefly, quantification of metabolites was done via multiple reaction monitoring (MRM; positive ion mode) based on the specific mass/charge ratio (*m/z*) values of the analyzed compounds defined in the method package: alanine, 89.90→44.10; arginine, 175.10→70.10 and 60.10; asparagine, 133.10→87.15 and 28.05; aspartate, 134.11→88.10 and 74.05; carnitine, 162.10→103.05 and 60.10; citrate, 191.20→111.10 and 87.05; citrulline, 176.10→159.00 and 70.05; glutamate, 147.90→84.10 and 56.10; glutamine, 147.14→130.10 and 84.15; histidine, 155.90→110.10 and 56.10; isoleucine, 132.10→86.20 and 69.15; leucine, 132.10→86.05 and 30.05; ornithine, 133.10→116.00 and 70.10; phenylalanine, 166.10→120.10 and 103.10; proline, 116.10→70.15 and 28.00; serine, 105.90→60.10; succinate, 117.30→73.00 and 99.05; threonine, 120.10→74.15 and 56.05; tryptophan, 205.10→188.10 and 146.10; tyrosine, 182.10→130.10 and 146.10; valine, 118.10→72.15 and 91.00; 3PGA, 185.10→97.10 and 79.10. Authentic standard substances (Merck) of each compound at various concentrations were used for verification and quantification. Peak areas were normalized to signals of the internal standard (carnitine).

BLI. Protein interaction studies via BLI were performed on an Octet K2 instrument (Fortébio Molecular Devices [UK] Limited, Wokingham, United Kingdom), which allows simultaneous binding experiments on two channels, one of which is used as a negative control. All experiments were done in buffer containing 50 mM Tris-HCl, pH 7.4, 150 mM KCl, 2 mM $MgCl_2$, 0.02% lauryldimethylamine oxide, and 0.2 mg/ml bovine serum albumin. Effector molecules were used at the following concentrations: 2 mM ATP, 2 mM 2-OG, and 0.1, 0.25, 0.5, 1, and 2 mM ADP. Interaction experiments were performed as reported previously (46). Briefly, His_8-tagged variants of P_{II}, namely, P_{II}(WT), P_{II}(S49E), P_{II}(I86N), and P_{II}(ΔT)-His_8, were used as ligands bound to Ni-NTA-coated sensor tips. Various concentrations of GST-PirA, from 125 to 12,000 nM, were used as analytes to display association reactions at 30°C. As preliminary experiments showed GST-PirA binds unspecifically to the Ni-NTA sensor tips, the noninteracting P_{II}(ΔT) variant was used to saturate the tips and thereby remove unspecific binding. The binding of P_{II} ligands was performed by first loading 10 μg/ml P_{II} on the Ni-NTA sensor tip, followed by dipping the tip into buffer for 60 s (to remove unbound P_{II}) and recording the first baseline. To block unoccupied sites on the sensor surface that cause disturbing unspecific binding, 72 μg/ml P_{II}(ΔT) was loaded onto the tip. Afterward, a second baseline was recorded for 60 s. Association and dissociation of the analyte were carried out by dipping the tip first into GST-PirA solution for 180s and then transferring it into buffer solution for a further 120s. In every single experiment, one sensor loaded with P_{II}(ΔT) was used as a negative control. To investigate the binding of GST tag alone and PirA without the GST-tag to P_{II} protein, parallel experiments were performed in the presence of 2 mM ADP. The interaction curves were achieved by subtracting the control curve and adjusting them to the average of baseline and dissociation steps. In every set of experiments, K_D values were calculated by plotting concentration versus maximum response.

His_8-tagged variants of P_{II} were prepared as previously described (79). For the preparation of recombinant PirA protein for BLI analysis, the *pirA* gene was cloned into XhoI and EcoRI sites of pGEX-4T-3 vector (GE Healthcare Life Sciences, Freiburg, Germany), encoding recombinant PirA with N-terminally fused GST tag. In addition, *pirA* was cloned into the SapI site of pBXC3GH vector (Addgene, Toddington, UK), encoding PirA with a C-terminally fused GFP-His_{10} tag. The plasmids were overexpressed in *E. coli* strain BL21(DE3). Purification of PirA with GST or GFP-His_{10} tags was performed as previously described (80, 81). To remove the GFP-His_{10} tag from PirA, 2.4 mg of recombinant PirA in 750 μl of PirA buffer (50 mM Tris-HCl, 100 mM KCl, 100 mM NaCl, 5 mM $MgCl_2$, 0.5 mM EDTA, 1 mM dithiothreitol, pH 7.8) was treated with 50 μl 3C protease (0.1 mg) at 4°C overnight. Afterward, 200 μl Ni-NTA agarose beads (Qiagen GmbH, Hilden, Germany) were added to the mixture and gently shaken at room temperature for 60 min. The beads were removed by filtration, and the tag-free PirA protein was dialyzed against PirA buffer containing 50% (vol/vol) glycerol and stored at −20°C until use.

NAGK activity measurements. To study the effect of PirA on the activity of the P_{II}-NAGK complex, the activity of a recombinant NAGK from *Synechocystis* was assayed in the presence of PirA by coupling NAGK-dependent NAG phosphorylation to an auxiliary enzyme, the N-acetyl-γ-glutamyl-5-phosphate reductase (AGPR) from *E. coli*, which catalyzes the reduction of NAG-phosphate using NADPH as the reductant. The change in NADPH absorbance was recorded at 340 nm as described previously (51, 82). The reaction buffer contained 50 mM imidazole (pH 7.5), 50 mM KCl, 20 mM $MgCl_2$, 0.2 mM NADPH, 0.5 mM DTT, 1 mM ATP, 1 mM ADP, and 0.1 mM arginine. Each reaction consisted of 10 μg of AGPR, 6 μg NAGK, and 2.4 μg P_{II}. A constant concentration of 3 mM NAG and different concentrations of PirA from 0 to 30 μg were applied. The reaction was started by the addition of NAGK, and the absorbance was recorded over a period of 10 min with a spectrophotometer (SPECORD 200; Analytik Jena). The velocity

of the reaction was calculated with a molar absorption of 1 NADPH of Σ_{340}= 6,178 liters mol^{-1} cm^{-1} from the slope of the change of absorbance per time.

SUPPLEMENTAL MATERIAL

Supplemental material is available online only.

FIG S1, TIF file, 0.1 MB.

FIG S2, TIF file, 1.9 MB.

FIG S3, TIF file, 0.9 MB.

TABLE S1, DOCX file, 0.01 MB.

TABLE S2, DOCX file, 0.01 MB.

ACKNOWLEDGMENTS

The project was funded by grants from the German Research Foundation (DFG) to S.K. (KL 3114/2-1), K.F. (Fo195/17-1), and M.H. (HA2002/22-2 and HA 2002/23-1), grants BIO2016-75634-P and PID2019-104513GB-100/AEI/10.13039/501100011033 from Agencia Estatal de Investigación (AEI) to F.J.F. and M.I.M.P., and BIO-0284 Group from Junta de Andalucía to F.J.F., all cofinanced by FEDER (European regional development fund). The LC-MS/MS equipment at the University of Rostock was financed through the HBFG program (GZ INST 264/125-1 FUGG to M.H.). We also acknowledge the use of the facilities of the Centre for Biocatalysis (MiKat) at the Helmholtz Centre for Environmental Research (UFZ). The UFZ is supported by the European Regional Development Funds (EFRE, Europe funds Saxony) and the Helmholtz Association.

REFERENCES

1. Herrero A, Flores E, Imperial J. 2019. Nitrogen assimilation in bacteria, p 280–300. *In* Schmidt TM (ed), Encyclopedia of microbiology, 4th ed. Academic Press, Oxford, United Kingdom.
2. Zehr JP, Capone DG. 2020. Changing perspectives in marine nitrogen fixation. Science 368:eaay9514. https://doi.org/10.1126/science.aay9514.
3. Smercina DN, Evans SE, Friesen ML, Tiemann LK. 2019. To fix or not to fix: controls on free-living nitrogen fixation in the rhizosphere. Appl Environ Microbiol 85:e02546-18. https://doi.org/10.1128/AEM.02103-19.
4. Magasanik B. 1982. Genetic control of nitrogen assimilation in bacteria. Annu Rev Genet 16:135–168. https://doi.org/10.1146/annurev.ge.16.120182.001031.
5. Reitzer L. 2003. Nitrogen assimilation and global regulation in *Escherichia coli*. Annu Rev Microbiol 57:155–176. https://doi.org/10.1146/annurev.micro.57.030502.090820.
6. van Heeswijk WC, Westerhoff HV, Boogerd FC. 2013. Nitrogen assimilation in *Escherichia coli*: putting molecular data into a systems perspective. Microbiol Mol Biol Rev 77:628–695. https://doi.org/10.1128/MMBR.00025-13.
7. Merrick MJ, Edwards RA. 1995. Nitrogen control in bacteria. Microbiol Rev 59:604–622. https://doi.org/10.1128/MR.59.4.604-622.1995.
8. Stadtman ER. 2004. Regulation of glutamine synthetase activity. EcoSal Plus 2004 https://doi.org/10.1128/ecosalplus.3.6.1.6.
9. Flombaum P, Gallegos JL, Gordillo RA, Rincón J, Zabala LL, Jiao N, Karl DM, Li WKW, Lomas MW, Veneziano D, Vera CS, Vrugt JA, Martiny AC. 2013. Present and future global distributions of the marine cyanobacteria *Prochlorococcus* and *Synechococcus*. Proc Natl Acad Sci U S A 110:9824–9829. https://doi.org/10.1073/pnas.1307701110.
10. Montoya JP, Holl CM, Zehr JP, Hansen A, Villareal TA, Capone DG. 2004. High rates of N2 fixation by unicellular diazotrophs in the oligotrophic Pacific Ocean. Nature 430:1027–1032. https://doi.org/10.1038/nature02824.
11. Canfield DE, Des Marais DJ. 1993. Biogeochemical cycles of carbon, sulfur, and free oxygen in a microbial mat. Geochim Cosmochim Acta 57:3971–3984. https://doi.org/10.1016/0016-7037(93)90347-Y.
12. Falkowski PG, Fenchel T, Delong EF. 2008. The microbial engines that drive earth's biogeochemical cycles. Science 320:1034–1039. https://doi.org/10.1126/science.1153213.
13. Falkowski PG, Barber RT, Smetacek V. 1998. Biogeochemical controls and feedbacks on ocean primary production. Science 281:200–206. https://doi.org/10.1126/science.281.5374.200.
14. Capone DG, Zehr JP, Paerl HW, Bergman B, Carpenter EJ. 1997. *Trichodesmium*, a globally significant marine cyanobacterium. Science 276:1221–1229. https://doi.org/10.1126/science.276.5316.1221.
15. Appel J, Hueren V, Boehm M, Gutekunst K. 2020. Cyanobacterial *in vivo* solar hydrogen production using a photosystem I–hydrogenase (PsaD-HoxYH) fusion complex 6. Nat Energy 5:458–467. https://doi.org/10.1038/s41560-020-0609-6.
16. Ducat DC, Way JC, Silver PA. 2011. Engineering cyanobacteria to generate high-value products. Trends Biotechnol 29:95–103. https://doi.org/10.1016/j.tibtech.2010.12.003.
17. Hagemann M, Hess WR. 2018. Systems and synthetic biology for the biotechnological application of cyanobacteria. Curr Opin Biotechnol 49:94–99. https://doi.org/10.1016/j.copbio.2017.07.008.
18. Saper G, Kallmann D, Conzuelo F, Zhao F, Tóth TN, Liveanu V, Meir S, Szymanski J, Aharoni A, Schuhmann W, Rothschild A, Schuster G, Adir N. 2018. Live cyanobacteria produce photocurrent and hydrogen using both the respiratory and photosynthetic systems. Nat Commun 9:2168. https://doi.org/10.1038/s41467-018-04613-x.
19. Wijffels RH, Kruse O, Hellingwerf KJ. 2013. Potential of industrial biotechnology with cyanobacteria and eukaryotic microalgae. Curr Opin Biotechnol 24:405–413. https://doi.org/10.1016/j.copbio.2013.04.004.
20. García-Domínguez M, Reyes JC, Florencio FJ. 1999. Glutamine synthetase inactivation by protein–protein interaction. Proc Natl Acad Sci U S A 96:7161–7166. https://doi.org/10.1073/pnas.96.13.7161.
21. Saelices L, Galmozzi CV, Florencio FJ, Muro-Pastor MI. 2011. Mutational analysis of the inactivating factors, IF7 and IF17 from *Synechocystis* sp. PCC 6803: critical role of arginine amino acid residues for glutamine synthetase inactivation. Mol Microbiol 82:964–975. https://doi.org/10.1111/j.1365-2958.2011.07865.x.
22. Luque I, Flores E, Herrero A. 1994. Molecular mechanism for the operation of nitrogen control in cyanobacteria. EMBO J 13:2862–2869. https://doi.org/10.1002/j.1460-2075.1994.tb06580.x.
23. Giner-Lamia J, Robles-Rengel R, Hernández-Prieto MA, Muro-Pastor MI, Florencio FJ, Futschik ME. 2017. Identification of the direct regulon of NtcA during early acclimation to nitrogen starvation in the cyanobacterium *Synechocystis* sp. PCC 6803. Nucleic Acids Res 45:11800–11820. https://doi.org/10.1093/nar/gkx860.
24. Herrero A, Muro-Pastor AM, Flores E. 2001. Nitrogen control in cyanobacteria. J Bacteriol 183:411–425. https://doi.org/10.1128/jb.183.2.411-425.2001.
25. Herrero A, Muro-Pastor AM, Valladares A, Flores E. 2004. Cellular differentiation and the NtcA transcription factor in filamentous cyanobacteria. FEMS Microbiol Rev 28:469–487. https://doi.org/10.1016/j.femsre.2004.04.003.

26. Vega-Palas MA, Flores E, Herrero A. 1992. NtcA, a global nitrogen regulator from the cyanobacterium *Synechococcus* that belongs to the Crp family of bacterial regulators. Mol Microbiol 6:1853–1859. https://doi.org/10.1111/j.1365-2958.1992.tb01357.x.
27. Espinosa J, Forchhammer K, Burillo S, Contreras A. 2006. Interaction network in cyanobacterial nitrogen regulation: PipX, a protein that interacts in a 2-oxoglutarate dependent manner with P_{II} and NtcA. Mol Microbiol 61:457–469. https://doi.org/10.1111/j.1365-2958.2006.05231.x.
28. Forcada-Nadal A, Llácer JL, Contreras A, Marco-Marín C, Rubio V. 2018. The P_{II}-NAGK-PipX-NtcA regulatory axis of Cyanobacteria: a tale of changing partners, allosteric effectors and non-covalent interactions. Front Mol Biosci 5:91. https://doi.org/10.3389/fmolb.2018.00091.
29. Vázquez-Bermúdez MF, Herrero A, Flores E. 2002. 2-Oxoglutarate increases the binding affinity of the NtcA (nitrogen control) transcription factor for the *Synechococcus glnA* promoter. FEBS Lett 512:71–74. https://doi.org/10.1016/s0014-5793(02)02219-6.
30. Forchhammer K, Lüddecke J. 2016. Sensory properties of the P_{II} signalling protein family. FEBS J 283:425–437. https://doi.org/10.1111/febs.13584.
31. Forchhammer K, Selim KA. 2020. Carbon/nitrogen homeostasis control in cyanobacteria. FEMS Microbiol Rev 44:33–53. https://doi.org/10.1093/femsre/fuz025.
32. Heinrich A, Maheswaran M, Ruppert U, Forchhammer K. 2004. The *Synechococcus elongatus* P_{II} signal transduction protein controls arginine synthesis by complex formation with N-acetyl-l-glutamate kinase. Mol Microbiol 52:1303–1314. https://doi.org/10.1111/j.1365-2958.2004.04058.x.
33. García-Domínguez M, Reyes JC, Florencio FJ. 2000. NtcA represses transcription of *gifA* and *gifB*, genes that encode inhibitors of glutamine synthetase type I from *Synechocystis* sp. PCC 6803. Mol Microbiol 35:1192–1201. https://doi.org/10.1046/j.1365-2958.2000.01789.x.
34. Zhang H, Liu Y, Nie X, Liu L, Hua Q, Zhao G-P, Yang C. 2018. The cyanobacterial ornithine–ammonia cycle involves an arginine dihydrolase. Nat Chem Biol 14:575–581. https://doi.org/10.1038/s41589-018-0038-z.
35. Llácer JL, Espinosa J, Castells MA, Contreras A, Forchhammer K, Rubio V. 2010. Structural basis for the regulation of NtcA-dependent transcription by proteins PipX and P_{II}. Proc Natl Acad Sci U S A 107:15397–15402. https://doi.org/10.1073/pnas.1007015107.
36. Browning DF, Busby SJW. 2016. Local and global regulation of transcription initiation in bacteria. Nat Rev Microbiol 14:638–650. https://doi.org/10.1038/nrmicro.2016.103.
37. Galmozzi CV, Fernández-Avila MJ, Reyes JC, Florencio FJ, Muro-Pastor MI. 2007. The ammonium-inactivated cyanobacterial glutamine synthetase I is reactivated *in vivo* by a mechanism involving proteolytic removal of its inactivating factors. Mol Microbiol 65:166–179. https://doi.org/10.1111/j.1365-2958.2007.05773.x.
38. Klähn S, Bolay P, Wright PR, Atilho RM, Brewer KI, Hagemann M, Breaker RR, Hess WR. 2018. A glutamine riboswitch is a key element for the regulation of glutamine synthetase in cyanobacteria. Nucleic Acids Res 46:10082–10094. https://doi.org/10.1093/nar/gky709.
39. Klähn S, Schaal C, Georg J, Baumgartner D, Knippen G, Hagemann M, Muro-Pastor AM, Hess WR. 2015. The sRNA NsiR4 is involved in nitrogen assimilation control in cyanobacteria by targeting glutamine synthetase inactivating factor IF7. Proc Natl Acad Sci U S A 112:E6243–E6252. https://doi.org/10.1073/pnas.1508412112.
40. Görl M, Sauer J, Baier T, Forchhammer K. 1998. Nitrogen-starvation-induced chlorosis in *Synechococcus* PCC 7942: adaptation to long-term survival. Microbiology 144:2449–2458. https://doi.org/10.1099/00221287-144-9-2449.
41. Collier JL, Grossman AR. 1994. A small polypeptide triggers complete degradation of light-harvesting phycobiliproteins in nutrient-deprived cyanobacteria. EMBO J 13:1039–1047. https://doi.org/10.1002/j.1460-2075.1994.tb06352.x.
42. Llácer JL, Fita I, Rubio V. 2008. Arginine and nitrogen storage. Curr Opin Struct Biol 18:673–681. https://doi.org/10.1016/j.sbi.2008.11.002.
43. Watzer B, Engelbrecht A, Hauf W, Stahl M, Maldener I, Forchhammer K. 2015. Metabolic pathway engineering using the central signal processor P_{II}. Microb Cell Fact 14:192. https://doi.org/10.1186/s12934-015-0384-4.
44. Watzer B, Spät P, Neumann N, Koch M, Sobotka R, Macek B, Hennrich O, Forchhammer K. 2019. The signal transduction protein P_{II} controls ammonium, nitrate and urea uptake in cyanobacteria. Front Microbiol 10:1428. https://doi.org/10.3389/fmicb.2019.01428.
45. Muro-Pastor MI, Cutillas-Farray Á, Pérez-Rodríguez L, Pérez-Saavedra J, Vega-de Armas A, Paredes A, Robles-Rengel R, Florencio FJ. 2020. CfrA, a novel carbon flow regulator, adapts carbon metabolism to nitrogen deficiency in cyanobacteria. Plant Physiol 184:1792–1810. https://doi.org/10.1104/pp.20.00802.
46. Orthwein T, Scholl J, Spät P, Lucius S, Koch M, Macek B, Hagemann M, Forchhammer K. 2020. The novel PII-interacting regulator PirC (Sll0944) identifies 3-phosphoglycerate mutase (PGAM) as central control point of carbon storage metabolism in cyanobacteria. bioRxiv https://doi.org/https://doi.org/10.1101/2020.09.11.292599.
47. Forchhammer K. 2008. P(II) signal transducers: novel functional and structural insights. Trends Microbiol 16:65–72. https://doi.org/10.1016/j.tim.2007.11.004.
48. Fokina O, Chellamuthu V-R, Zeth K, Forchhammer K. 2010. A novel signal transduction protein P_{II} variant from *Synechococcus elongatus* PCC 7942 indicates a two-step process for NAGK–P_{II} complex formation. J Mol Biol 399:410–421. https://doi.org/10.1016/j.jmb.2010.04.018.
49. Zeth K, Fokina O, Forchhammer K. 2012. An engineered P_{II} protein variant that senses a novel ligand: atomic resolution structure of the complex with citrate. Acta Crystallogr D Biol Crystallogr 68:901–908. https://doi.org/10.1107/S0907444912016447.
50. Burillo S, Luque I, Fuentes I, Contreras A. 2004. Interactions between the nitrogen signal transduction protein P_{II} and N-acetyl glutamate kinase in organisms that perform oxygenic photosynthesis. J Bacteriol 186:3346–3354. https://doi.org/10.1128/JB.186.11.3346-3354.2004.
51. Fokina O, Herrmann C, Forchhammer K. 2011. Signal-transduction protein P_{II} from *Synechococcus elongatus* PCC 7942 senses low adenylate energy charge *in vitro*. Biochem J 440:147–156. https://doi.org/10.1042/BJ20110536.
52. Charlier D, Bervoets I. 2019. Regulation of arginine biosynthesis, catabolism and transport in *Escherichia coli*. Amino Acids 51:1103–1127. https://doi.org/10.1007/s00726-019-02757-8.
53. Cunin R, Glansdorff N, Piérard A, Stalon V. 1986. Biosynthesis and metabolism of arginine in bacteria. Microbiol Rev 50:314–352. https://doi.org/10.1128/MR.50.3.314-352.1986.
54. Chellamuthu V-R, Ermilova E, Lapina T, Lüddecke J, Minaeva E, Herrmann C, Hartmann MD, Forchhammer K. 2014. A widespread glutamine-sensing mechanism in the plant kingdom. Cell 159:1188–1199. https://doi.org/10.1016/j.cell.2014.10.015.
55. Sugiyama K, Hayakawa T, Kudo T, Ito T, Yamaya T. 2004. Interaction of N-acetylglutamate kinase with a P_{II}-like protein in rice. Plant Cell Physiol 45:1768–1778. https://doi.org/10.1093/pcp/pch199.
56. Li Y, Liu W, Sun L-P, Zhou Z-G. 2017. Evidence for P_{II} with NAGK interaction that regulates Arg synthesis in the microalga *Myrmecia incisa* in response to nitrogen starvation. Sci Rep 7:16291. https://doi.org/10.1038/s41598-017-16644-3.
57. Selim KA, Ermilova E, Forchhammer K. 2020. From cyanobacteria to Archaeplastida: new evolutionary insights into P_{II} signalling in the plant kingdom. New Phytol 227:722–731. https://doi.org/10.1111/nph.16492.
58. Leigh JA, Dodsworth JA. 2007. Nitrogen regulation in bacteria and archaea. Annu Rev Microbiol 61:349–377. https://doi.org/10.1146/annurev.micro.61.080706.093409.
59. Muro-Pastor MI, Reyes JC, Florencio FJ. 2001. Cyanobacteria perceive nitrogen status by sensing intracellular 2-oxoglutarate levels. J Biol Chem 276:38320–38328. https://doi.org/10.1074/jbc.M105297200.
60. Battchikova N, Vainonen JP, Vorontsova N, Keranen M, Carmel D, Aro E-M. 2010. Dynamic changes in the proteome of *Synechocystis* 6803 in response to CO_2 limitation revealed by quantitative proteomics. J Proteome Res 9:5896–5912. https://doi.org/10.1021/pr100651w.
61. Orf I, Klähn S, Schwarz D, Frank M, Hess WR, Hagemann M, Kopka J. 2015. Integrated analysis of engineered carbon limitation in a quadruple CO_2/HCO_3^- uptake mutant of *Synechocystis* sp. PCC 6803. Plant Physiol 169:1787–1806. https://doi.org/10.1104/pp.15.01289.
62. Zeth K, Fokina O, Forchhammer K. 2014. Structural basis and target-specific modulation of ADP sensing by the *Synechococcus elongatus* P_{II} signaling protein. J Biol Chem 289:8960–8972. https://doi.org/10.1074/jbc.M113.536557.
63. Lüddecke J, Forchhammer K. 2013. From P_{II} signaling to metabolite sensing: a novel 2-oxoglutarate sensor that details P_{II}–NAGK complex formation. PLoS One 8:e83181. https://doi.org/10.1371/journal.pone.0083181.
64. Helling RB. 1998. Pathway choice in glutamate synthesis in *Escherichia coli*. J Bacteriol 180:4571–4575. https://doi.org/10.1128/JB.180.17.4571-4575.1998.
65. Picossi S, Flores E, Herrero A. 2014. ChIP analysis unravels an exceptionally wide distribution of DNA binding sites for the NtcA transcription factor in a heterocyst-forming cyanobacterium. BMC Genomics 15:22. https://doi.org/10.1186/1471-2164-15-22.
66. Hanson TE, Forchhammer K, de Marsac NT, Meeks JC. 1998. Characterization of the *glnB* gene product of *Nostoc punctiforme* strain ATCC 29133: *glnB* or the P_{II} protein may be essential. Microbiology 144:1537–1547. https://doi.org/10.1099/00221287-144-6-1537.

67. Palinska KA, Laloui W, Bédu S, Loiseaux-de Goer S, Castets AM, Rippka R, Tandeau de Marsac N. 2002. The signal transducer P_{II} and bicarbonate acquisition in *Prochlorococcus marinus* PCC 9511, a marine cyanobacterium naturally deficient in nitrate and nitrite assimilation. Microbiology 148:2405–2412. https://doi.org/10.1099/00221287-148-8-2405.
68. Flores E, Arévalo S, Burnat M. 2019. Cyanophycin and arginine metabolism in cyanobacteria. Algal Res 42:101577. https://doi.org/10.1016/j.algal.2019.101577.
69. Steglich C, Futschik ME, Lindell D, Voss B, Chisholm SW, Hess WR. 2008. The challenge of regulation in a minimal photoautotroph: non-coding RNAs in *Prochlorococcus*. PLoS Genet 4:e1000173. https://doi.org/10.1371/journal.pgen.1000173.
70. Rippka R, Deruelles J, Waterbury JB, Herdman M, Stanier RY. 1979. Generic assignments, strain histories and properties of pure cultures of cyanobacteria. Microbiology 111:1–61. https://doi.org/10.1099/00221287-111-1-1.
71. García-Domínguez M, Lopez-Maury L, Florencio FJ, Reyes JC. 2000. A gene cluster involved in metal homeostasis in the cyanobacterium *Synechocystis* sp. strain PCC 6803. J Bacteriol 182:1507–1514. https://doi.org/10.1128/jb.182.6.1507-1514.2000.
72. Elhai J, Wolk CP. 1988. A versatile class of positive-selection vectors based on the nonviability of palindrome-containing plasmids that allows cloning into long polylinkers. Gene 68:119–138. https://doi.org/10.1016/0378-1119(88)90605-1.
73. Pinto FL, Thapper A, Sontheim W, Lindblad P. 2009. Analysis of current and alternative phenol based RNA extraction methodologies for cyanobacteria. BMC Mol Biol 10:79. https://doi.org/10.1186/1471-2199-10-79.
74. Hein S, Scholz I, Voß B, Hess WR. 2013. Adaptation and modification of three CRISPR loci in two closely related cyanobacteria. RNA Biol 10:852–864. https://doi.org/10.4161/rna.24160.
75. Reyes JC, Crespo JL, Garcia-Dominguez M, Florencio FJ. 1995. Electron transport controls glutamine synthetase activity in the facultative heterotrophic cyanobacterium *Synechocystis* sp. PCC 6803. Plant Physiol 109:899–905. https://doi.org/10.1104/pp.109.3.899.
76. Laemmli UK. 1970. Cleavage of structural proteins during the assembly of the head of bacteriophage T4 5259. Nature 227:680–685. https://doi.org/10.1038/227680a0.
77. Navarro F, Martín-Figueroa E, Florencio FJ. 2000. Electron transport controls transcription of the thioredoxin gene *trxA* in the cyanobacterium *Synechocystis* sp. PCC 6803. Plant Mol Biol 43:23–32. https://doi.org/10.1023/a:1006472018601.
78. Reinholdt O, Schwab S, Zhang Y, Reichheld J-P, Fernie AR, Hagemann M, Timm S. 2019. Redox-regulation of photorespiration through mitochondrial thioredoxin o1. Plant Physiol 181:442–457. https://doi.org/10.1104/pp.19.00559.
79. Scholl J, Dengler L, Bader L, Forchhammer K. 2020. Phosphoenolpyruvate carboxylase from the cyanobacterium *Synechocystis* sp. PCC 6803 is under global metabolic control by P_{II} signaling. Mol Microbiol 114:292–307. https://doi.org/10.1111/mmi.14512.
80. Harper S, Speicher DW. 2011. Purification of proteins fused to glutathione S-transferase. Methods Mol Biol 681:259–280. https://doi.org/10.1007/978-1-60761-913-0_14.
81. Maheswaran M, Urbanke C, Forchhammer K. 2004. Complex formation and catalytic activation by the P_{II} signaling protein of *N*-acetyl-l-glutamate kinase from *Synechococcus elongatus* strain PCC 7942. J Biol Chem 279:55202–55210. https://doi.org/10.1074/jbc.M410971200.
82. Takahara K, Akashi K, Yokota A. 2007. Continuous spectrophotometric assays for three regulatory enzymes of the arginine biosynthetic pathway. Anal Biochem 368:138–147. https://doi.org/10.1016/j.ab.2007.06.032.
83. Kumar S, Stecher G, Tamura K. 2016. MEGA7: molecular evolutionary genetics analysis version 7.0 for bigger datasets. Mol Biol Evol 33:1870–1874. https://doi.org/10.1093/molbev/msw054.
84. Altschul SF, Gish W, Miller W, Myers EW, Lipman DJ. 1990. Basic local alignment search tool. J Mol Biol 215:403–410. https://doi.org/10.1016/S0022-2836(05)80360-2.
85. Mitschke J, Georg J, Scholz I, Sharma CM, Dienst D, Bantscheff J, Voss B, Steglich C, Wilde A, Vogel J, Hess WR. 2011. An experimentally anchored map of transcriptional start sites in the model cyanobacterium *Synechocystis* sp. PCC 6803. Proc Natl Acad Sci U S A 108:2124–2129. https://doi.org/10.1073/pnas.1015154108.
86. Krasikov V, Aguirre von Wobeser E, Dekker HL, Huisman J, Matthijs HCP. 2012. Time-series resolution of gradual nitrogen starvation and its impact on photosynthesis in the cyanobacterium *Synechocystis* PCC 6803. Physiol Plant 145:426–439. https://doi.org/10.1111/j.1399-3054.2012.01585.x.
87. Schneider CA, Rasband WS, Eliceiri KW. 2012. NIH Image to ImageJ: 25 years of image analysis. Nat Methods 9:671–675. https://doi.org/10.1038/nmeth.2089.
88. Bolay P, Muro-Pastor MI, Florencio FJ, Klähn S. 2018. The distinctive regulation of cyanobacterial glutamine synthetase. Life 8:52. https://doi.org/10.3390/life8040052.

3. Publication 3 (submitted)

Research article

Rokhsareh Rozbeh & Karl Forchhammer

In vivo Detection of Metabolic Fluctuations in Real Time Using the NanoBiT Technology Based on PII Signaling Protein Interactions

2024. *International Journal of Molecular Sciences*. doi.org/10.3390

International Journal of
Molecular Sciences

MDPI

Article

In Vivo Detection of Metabolic Fluctuations in Real Time Using the NanoBiT Technology Based on PII Signalling Protein Interactions

Rokhsareh Rozbeh and Karl Forchhammer *

Interfaculty Institute of Microbiology and Infection Biology, University Tübingen, Auf der Morgenstelle 28, 72076 Tübingen, Germany; rokhsareh.rozbeh@gmail.com
* Correspondence: karl.forchhammer@uni-tuebingen.de

Abstract: New protein-fragment complementation assays (PCA) have successfully been developed to characterize protein–protein interactions in vitro and in vivo. Notably, the NanoBiT technology, employing fragment complementation of NanoLuc luciferase, stands out for its high sensitivity, wide dynamic range, and straightforward read out. Previously, we explored the in vitro protein interaction dynamics of the PII signalling protein using NanoBiT, revealing significant modulation of luminescence signals generated by the interaction between PII and its receptor protein NAGK by 2-oxoglutarate levels. In the current work, we investigated this technology in vivo, to find out whether recombinantly expressed NanoBiT constructs using the NanoLuc large fragment fused to PII and PII-interaction partners NAGK or PipX-fused to the NanoLuc Small BiT are capable of detecting the metabolic fluctuations in *Escherichia coli*. Therefore, we devised an assay capable of capturing the metabolic responses of *E. coli* cells, demonstrating real-time metabolic perturbation upon nitrogen upshift or depletion treatments. In particular, the PII-NAGK NanoBitT sensor pair reported these changes in a highly sensitive manner.

Keywords: protein-fragment complementation assay; NanoLuc; luciferase; 2-oxoglutarate; PII-interacting protein X (PipX); N-Acetylglutamate kinase (NAGK); metabolite sensor

Citation: Rozbeh, R.; Forchhammer, K. In Vivo Detection of Metabolic Fluctuations in Real Time Using the NanoBiT Technology Based on PII Signalling Protein Interactions. *Int. J. Mol. Sci.* **2024**, *25*, 3409. https://doi.org/10.3390/ijms25063409

Academic Editor: Jessica Holien

Received: 20 February 2024
Revised: 14 March 2024
Accepted: 14 March 2024
Published: 17 March 2024

1. Introduction

Protein–protein interactions (PPIs) constitute a complex network within cells, on which almost all biological processes are based, such as DNA replication, transcription, signal transduction, enzymatic reactions, cell-to-cell communication, and membrane transport [1,2]. The three-dimensional conformation and dynamic behaviours of the involved proteins predominantly regulate these interactions [3]. These interactions range from being permanent to transient in nature [1,4].

To investigate protein–protein interactions in living cells, it is desirable to employ biosensor tools that do not disrupt the native cellular context. High sensitivity and high signal to noise read out are important properties for robust and precise analysis. In this context, protein-fragment complementation assays (PCA) have successfully been developed [5]. Among the different types of PCA, the assays based on the small bioluminescence enzyme NanoLuc are of particular interest, due to the high bioluminescence output of this enzyme. Verhoef et al. (2016) developed a NanoLuc based assay where several NanoLuc fragments were generated by cleaving at different loop sites, and a particular pair comprising of the N-terminal 52-amino acid (aa) fragment and the C-terminal 119-aa fragment was selected [6]. Concurrently, Dixon et al. introduced an alternative NanoLuc-based PCA-assay system known as NanoLuc Binary Technology (often referred as split NanoLuc). A cleavage point was strategically positioned between NanoLuc residues 156 and 157, resulting in the generation of two distinct peptide fragments: an 18 kDa large fragment (termed LgBiT) and a small 11-amino acid peptide (SmBiT). To dissect specific protein–protein interactions, the

SmBiT peptide underwent engineering to minimize its inherent affinity towards the LgBiT complementation fragment. This strategy ensures that bioluminescence reconstitution, following the fusion of LgBiT and SmBiT fragments to proteins of interest, primarily relies on the interaction of the fusion partner proteins. The PCA is performed by measuring the bioluminescence after addition of suitable substrate, which can be done in vitro or in vivo. In addition to this, a different version of the NanoBiT technology uses a SmBiT fragment with high affinity to LgBiT, termed HiBiT. This system has a different purpose and is used to study protein localization and secretion [7].

In recent years, the NanoBiT technology using the low-affinity SmBiT fragment has been utilized for the precise quantitative analysis of in vitro protein–protein interactions. In mammalian systems, the NanoBiT system was successfully used to analyse the interaction of LgBiT-fused protein phosphatase 2A-B55α holoenzyme of endothelial cells with the SmBiT flotillin-1 protein [8]. To study the SARS-CoV-2 entry mechanism into human epithelial cells, the NanoBiT system was deployed by monitoring the interaction between the receptor-binding domain (RBD) and ACE2 [9]. NanoBiT technology is also increasingly in use for bacterial PPIs. For example, it was employed to verify the interaction between bacterial transcription factors NusB and NusE in *Bacillus subtilis* [10]. Similarly, the interaction RNA polymerase and initiation factor σ in *B. subtilis* was explored using NanoBiT, where the LgBiT was fused to the C-terminus of σA and SmBiT to the N-terminus of the RNA polymerase [10]. The split NanoLuc assay corroborated interactions, including those between the ribosome-associated GTPases (RA-GTPase) Era family and the 16S rRNA endonuclease YbeY, as well as the DEAD-box RNA helicase CshA in *Staphylococcus aureus* [11]. We used the NanoBiT system to accurately characterize and quantify the interaction between the PII signalling protein from the cyanobacterium *Synechocystis* sp. PCC6803 and its interaction partners, PipX and N-acetyl-L glutamate kinase (NAGK).

In addition to in vitro studies, NanoBiT has been extensively utilized for the examination of in vivo protein–protein interactions, mostly in mammalian cells [12–15]. Within bacterial cells, NanoBiT technology was employed to assess the multimerization ability of HupA, a homologue of the histone-like HU proteins, in *Clostridium difficile*, where HupA was strategically fused to the C-terminus of both SmBiT and LgBiT subunits [16]. Additionally, split NanoLuc assays were utilized to probe interactions between the transmembrane peptidase AgrB and its AgrD propeptide substrate in *Staphylococcus aureus* cells, with AgrB and AgrD being labelled with either N-terminal LgBiT, N-terminal SmBiT, C-terminal LgBiT, or C-terminal SmBiT [17]. In these cases, the primary goal of the NanoBiT technology was to demonstrate the specificity of protein interactions in vivo.

Given the impressive sensitivity and dynamic range of the NanoBiT reporter system, it presents a promising avenue for developing sensors capable of monitoring real-time metabolic changes within living cells through metabolite-dependent protein–protein interactions. The versatile PII signalling protein, with its metabolite-responsive interactions, serves as an ideal platform for such intracellular metabolite reporters. The PII protein has multitasking sensory properties by binding the effector molecules ADP, ATP or Mg-ATP-2-oxoglutarate, and transmitting metabolic information to various receptor proteins. The complex network of PII interactions is comprehensively reviewed in [18]. In cyanobacteria, among the principal interactors are the transcriptional co-activator PipX and the arginine-pathway enzyme N-Acetylglutamate kinase (NAGK) [18,19]. We and others have previously used the Förster resonance energy transfer (FRET) technology to study these interactions, whereby fluorescent proteins were fused to the C-termini of PII and the respective partner proteins [20,21]. Although these attempts led to a better understanding in PII interactions, a major drawback of the FRET system is its very narrow dynamic range and it requires precise adjustment of complex parameters such as the ratio between the partner proteins [22]. Furthermore, it suffers from high signal noise generated by background fluorescence, in particular in photosynthetic cells with high intracellular pigment concentration [23]. The NanoBiT technology avoids these restrictions.

We have previously established PII-based NanoBiT reporters for in vitro analysis of PII complex formation with its receptors PipX and NAGK and were able to precisely quantify association constants in presence of different effector molecule combinations [24]. Maximum bioluminescence signals were achieved when LgBiT was fused to the C-terminal Strep-tag of the PII protein, and SmBiT was fused to the C-terminus of either PipX or NAGK, separated by an appropriately sized flexible linker [24]. Due to the intricate properties of PII signalling proteins [19], the metabolite effects on the formation of PII-NAGK complexes differ from that for PII-PipX complexes. Presence of ATP favours formation of the PII-NAGK complex, whereas 2-oxoglutarate acts antagonistically. This response is quite robust against changes in the ATP/ADP ratio [25]. By contrast, the formation of the PII-PipX complex is favoured by ADP and antagonized by simultaneously binding Mg-ATP-2-oxoglutarate [26]. Subtle changes in the ADP concentrations already modulate the antagonistic effects of 2-oxoglutarate, such that increasing ADP concentrations strongly mitigate the antagonistic effect of 2-oxoglutarate [24,26].

The present work was carried out to find out how the NanoBiT based reporter pairs PII-NAGK or PII-PipX perform in vivo, whether they are able to respond to metabolic perturbations and if they allow in vivo detection of metabolic fluctuations. As a proof-of-concept study, the analysis was carried out in recombinant *Escherichia coli* cells, challenged by nitrogen up- and down-shift treatments, for which the posttranslational [27] and metabolic and response is well established [28].

2. Results

2.1. Establishment of PII-Based In Vivo NanoBiT Sensors

To co-express the NanoBiT sensor pairs in *Escherichia coli*, the genetic constructs shown in Figure 1 were made. As vector backbone the pACYCDuet-1 plasmid was used, which is designed for equal co-expression of two genes of interest. Briefly, the PII signalling protein was fused at its C-terminus to the large subunit of the split NanoLuc enzyme (LgBiT), connected by an 8 amino acids linker. As interaction partners, either PipX or N-Acetyl-L-Glutamate Kinase (NAGK) were used, which were fused at their C-terminal end to the SmBiT fragment, connected by an 16 amino acids linker as described previously [24]. As a control for maximal luciferase activity, which is independent of complex formation, the PII protein was fused at its C-terminus to full-length NanoLuc (PII-FL). As control for the luminescence background signal, the PII-LgBiT construct lacking a SmBiT partner was used. As a further control to proof the specificity of the PII-based protein interaction, we used a variant of the PII protein with the S49E point mutation, which strongly abrogates PII-NAGK interaction [20,24]. These plasmids were then transformed into *E. coli* BL21 (DE3) cells for bioluminescence measurements and the bioluminescence was measured, as described in the methods section.

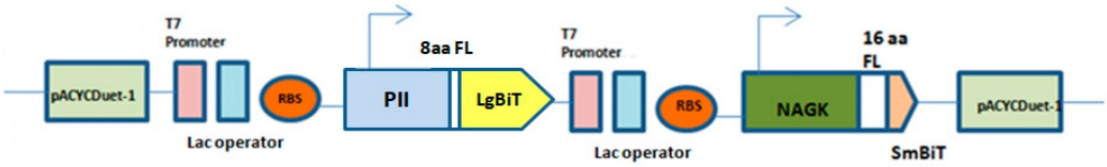

Figure 1. *Cont.*

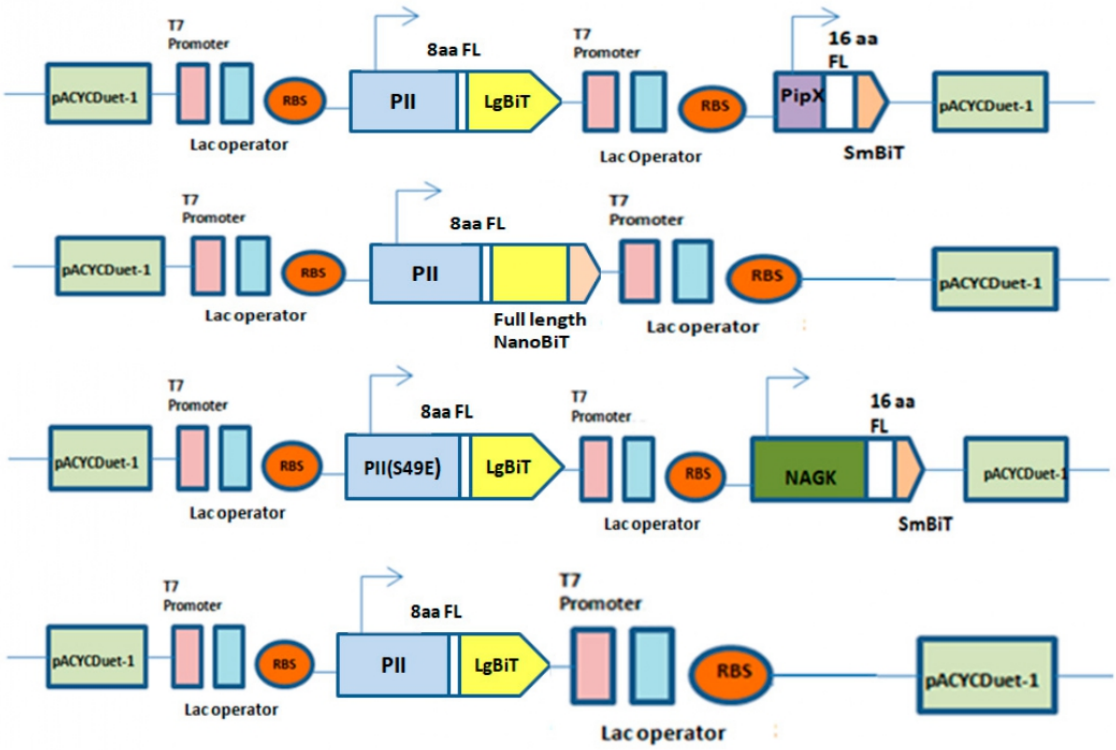

Figure 1. Expression vectors and fusion protein constructs. Schematic overview of PII-LgBiT—NAGK-SmBiT, PII-LgBiT—PipX-SmBiT, PII-Full length (FL), PII (S49E)-LgBiT—NAGK-SmBiT and PII-LgBiT proteins. Flexible linker with 8 amino acids (8aa) fused to LgBiT and flexible linker with 16 amino acids (16aa) fused to SmBiT in constructs.

The first assays were performed with either the PII-NAGK NanoBiT sensor pair or the PII-FL reporter. Following preliminary trials, we recognized the importance of precisely pre-cultivating the recombinant strains before conducting luminescence measurements, as outlined in the methods section, to ensure reproducible results. Initial experiments for assay development were done with the PII-FL reporter whose signal is independent of protein–protein interaction and only depends on the expression level of the PII-NanoLuc fusion protein. Usually, genes cloned into the pACYCDuet vectors are expressed by inducing the T7 polymerase of the host cells through the addition of IPTG. In the absence of inducer, genes are expressed at a background level. We first measured the relative luminescence signals (RLUs) from cultures, which were induced with 0.5 mM IPTG (OD600 = 0.5–0.7) and of non-induced cultures. The results are summarized in Table 1. After 60 min incubation, the RLUs were recorded. IPTG-induced cells displayed a signal of 6.8×10^7 RLU (STD = 7.2×10^6 RLU), whereas in the absence of IPTG, 4.7×10^6 RLU were recorded, which corresponds to an approximately 15-fold increase by IPTG induction. Likewise, we analysed the RLUs from the PII-NAGK NanoBiT sensor pair under induced and non-induced conditions. Here, we obtained values of 6.0×10^6 or 4.2×10^5 under induced or non-induced conditions, respectively, which corresponds to a 14-fold increase by IPTG induction, a similar fold-increase than with PII-FL. In both cases (induced and non-induced), the signals from the PII-NAGK NanoBiT constructs corresponded to approximately 9% of the signal form the full-length PII-Nanoluc sensor. This indicates the level of reconstitution of the split NanoLuc signal as compared to the signal of full-length NanoLuc enzyme. As a negative control for background noise, luminescence was recorded from cells, which

expressed only PII-LgBiT. The background luminescence was in the rage of 3–2 × 10^2 RLU, which is more than three orders of magnitude below the signal from the non-induced sensor strains. As the signal under non-induced conditions was high enough to allow precise measurement of luminescence, we decided to work under non-inducing conditions, which avoids metabolic burden to the cells. To find out if, under such conditions, the measurement is still sensitive enough to detect even very weak interactions, we used the PII-S49E variant, which previously was shown to bind to NAGK with strongly reduced affinity. In fact, a luminescence signal was detected which was well above the background level and reached approximately 5% of that of the non-mutated PII-NAGK sensor (Table 1). This is in perfect agreement with our previous in vitro PII-NAGK NanoBiT assays, which showed that the binding affinity of PII-S49E to NAGK (in presence of 2 mM ATP) is approximately 5% of that of wild-type PII [24].

Table 1. Comparison of NanoBiT signals from M9 grown reporter strains with and without IPTG induction

	(−IPTG)		(+IPTG)	
Constructs	**RLU Signal**	**%**	**RLU Signal**	**%**
PII-FL	4,721,437 ± 623,462	100	68,198,243 ± 7,174,184	100
PII-LgBiT-NAGK-SmBiT	422,034 ± 81,375	9	6,072,362 ± 545,005	9
PII(S49E)-LgBiT-NAGK-SmBiT	22,902 ± 2685	0.5	nm	nm
PII-LgBiT	254 ± 42	0.005	nm	nm

Luminescence signals (in RLU) derived from the PII-NanoLuc Full length (PII-FL) reporter, the PII-LgBiT-NAGK-SmBiT sensor pair, the PII(S49E)-LgBiT-NAGK-SmBiT sensor pair and the PII-LgBiT reporter in absence and presence of inducer IPTG after 60 min of induction. nm = not measured. Average and standard deviation of three replicates is shown.

These preliminary experiments indicated that the in vivo measurements using the PII-NAGK NanoBiT sensor yielded results compatible with the previous in vitro measurements. Since the affinity of PII-NAGK interaction is strongly modulated by the metabolic state, such that 2-oxoglutarate strongly inhibited complex formation, we next attempted to use the PII-NAGK sensor to monitor changes in metabolic states in real-time upon challenging the cells with different external stimuli.

2.2. Monitoring Metabolic Fluctuations Using the PII-NAGK Sensor

To monitor the immediate effects of metabolic perturbation, the recording of bioluminescence should start immediately after onset of the treatment. Previous rapid sampling metabolome analysis in *E. coli* showed that perturbations in nitrogen homeostasis resulted in metabolic responses in the range of seconds to minutes [28]. To establish a rapid assay, we again first used the PII-FL reporter to validate fluctuations in RLU signals. The RLUs were recorded over a period of 10 min in intervals of 10 s (5 s measurement followed by a 5 s delay). The RLU signals decreased over time, and this decrease was apparently caused by oxygen depletion in the measuring cuvette. When the samples were shaken, the luminescence briefly increased but then decreased again rapidly (see Figure 2). After approximately 5–10 min, luminescence decreased to a basal level. In principle, the same dynamics was observed with the PII-NAGK NanoBiT sensor pair. The lack of an initial stable luminescence signal prevented a simple assessment of immediate dynamic responses of the NanoBiT sensor caused by fluctuations in intracellular metabolite pools. However, we could solve this problem by normalizing the RLU response curve of treated samples to the RLU response curve of a reference sample (without perturbation). Normalization was done by dividing the RLUs from every measuring point of the treated sample by the respective RLU of the untreated sample (compare Figure 3A,B).

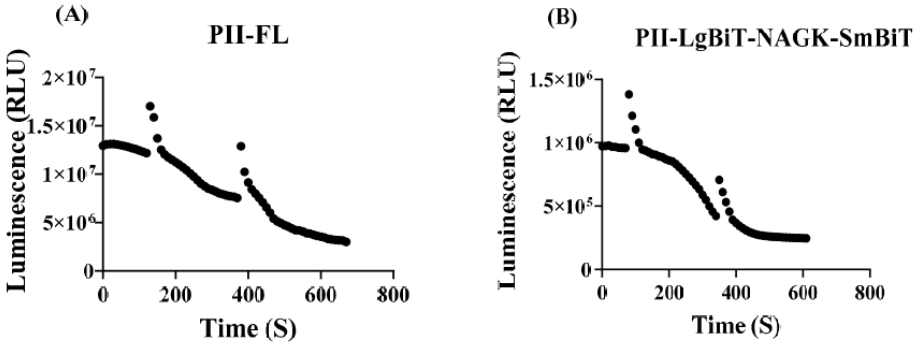

Figure 2. Sensitivity of luminescence intensity (in RLU) in the experimental set-up towards oxygen consumption during the time-course experiments. (**A**) Control measurement using the PII-FL reporter. Measurement was briefly interrupted at time 120 s and 370 s and the samples were shaken and directly measured again. (**B**) As in part (**A**) but using the PII-LgBiT—NAGK-SmBiT sensor; here, the cells were shaken at 80 s and 320 s.

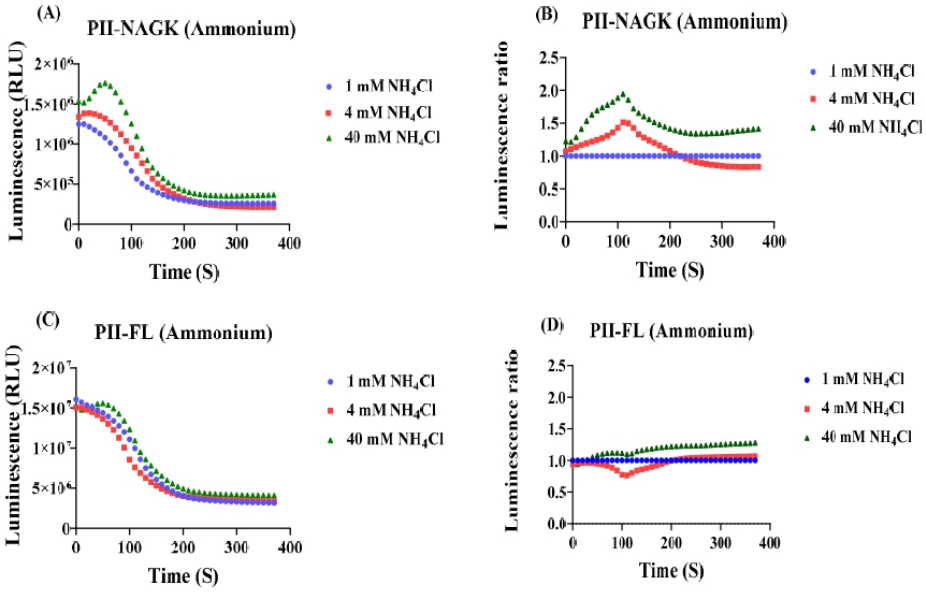

Figure 3. Luminescence response of the PII-NAGK NanoBiT sensor towards ammonium upshift treatments (**A**,**B**) and as control, of the PII-FL reporter under identical test conditions (**C**,**D**). (**A**) Time course of the luminescence signal (RLU) after addition of luminescence reagent in untreated sample (1 mM NH_4Cl), and to samples, where the NH_4Cl concentration was increased to 4 mM or 40 mM. (**B**) Normalization of the RLU response curve to the RLU response curve of the reference sample (untreated, 1 mM NH_4Cl) (**C**,**D**): as part (**A**,**B**) but using the PII-FL reporter for comparison. Average values from three measurements are shown and error bars are removed for a better comparison. The average standard deviation (STD) of each of the three replicates of the PII-NAGK sensor for ammonium treatments was less than 23%. The average standard deviation (STD) of each of the three replicates of the PII-FL sensor for ammonium treatments was less than 14%.

As a first perturbation experiment and as a proof of the measurement principle, we analysed the response of the PII-NAGK NanoBiT sensor pair towards ammonium upshift treatments. It is well established that ammonium treatment leads to a rapid reduction

in 2-oxogulatarate levels [29]. This should lead to intracellular conditions that favour PII-NAGK complex formation. Figure 3A shows the result of this experiment without normalization. In fact, the addition of 40 mM NH_4Cl led to an immediate RLU increase, but due to the baseline drift described above, luminescence decreases again after 60 s. Nevertheless, the signal remains always higher than the untreated control that was incubated at a constant concentration of 1 mM NH_4Cl. When ammonium treatment was done with 4 mM NH_4Cl, this led to less pronounced, but still clearly visible RLU increase over the untreated control. After performing the above-described normalization, it is clearly visible that the addition of 40 mM ammonium caused an immediate increase in the relative signal, which is indicative of increasing PII-NAGK interaction (Figure 3B). After approximately 2 min, a maximum of a two-fold increase was reached, followed by a slower decline and reaching a plateau that was approximately 50% over the level of the untreated sample. Treatment with 4 mM NH_4Cl showed initially a very similar dynamics, reaching a maximum after 2 min, but the signal only increased by 50%, and then rapidly returned to the initial level of the untreated sample. To reveal if this response really reflected changes in the state of the split-NanoLuc PII-NAGK complex and was not caused by indirect metabolic effects of ammonium treatment on the luminescence reaction itself, the same assay was performed with the PII-FL reporter. As shown in Figure 3C,D, the same ammonium treatment as above had almost no influence on the normalized RLU curve. This demonstrates that the relative signal increase shown by the PII-NAGK sensor pair is indeed caused by increased PII-NAGK NanoBiT assembly, indicative of dropping 2-oxoglutarate levels.

Next, the response of the PII-NAGK NanoBiT sensor pair to inhibition of nitrogen assimilation was tested. Therefore, cells were treated with either 0.1 mM or 1 mM L-methionine-sulfoximine (MSX), a specific and potent inhibitor of glutamine synthetase, or as a reference, without MSX treatment. The result is shown in Figure 4A,B: Addition of 0.1 or 1 mM MSX caused a rapid decrease in PII-NAGK NanoBiT complex formation, visible as decrease in RLU. After 6 min, the sensor signal in presence of 0.1 mM MSX or 1 mM MSX decreased to approximately 39% or 27%, respectively, of the untreated control. Again, the control experiment with the PII-FL sensor showed only a very minor response (Figure 4C). Finally, the response towards nitrogen starvation was investigated. Immediately after nitrogen step-down, the signal from the PII-NAGK NanoBiT sensor pair decreased until it reached a basal level, which corresponded to 35% of the untreated control after approximately 5–6 min and then stayed constant (Figure 4D,E). Again, the PII-FL reported did not respond to nitrogen downshift (Figure 4F), revealing that the observed signal decrease of the split-NanoLuc sensor pair represents dissociation of the PII-NAGK complex, which is expected from increasing levels of 2-oxoglutarate caused by nitrogen deprivation. Altogether, the above experiments showed that the PII-NAGK NanoBiT sensor pair was able to report in real time the dynamics of metabolic fluctuations caused by perturbing nitrogen homeostasis.

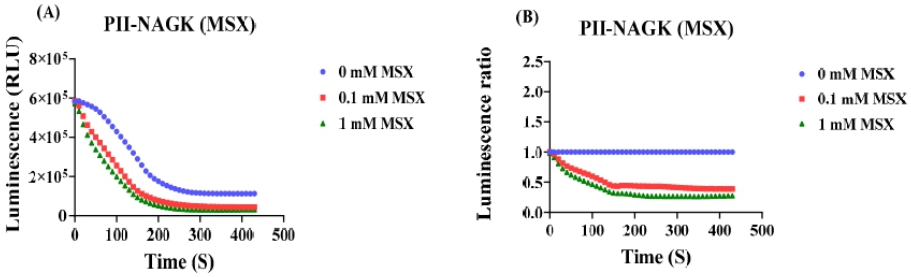

Figure 4. *Cont.*

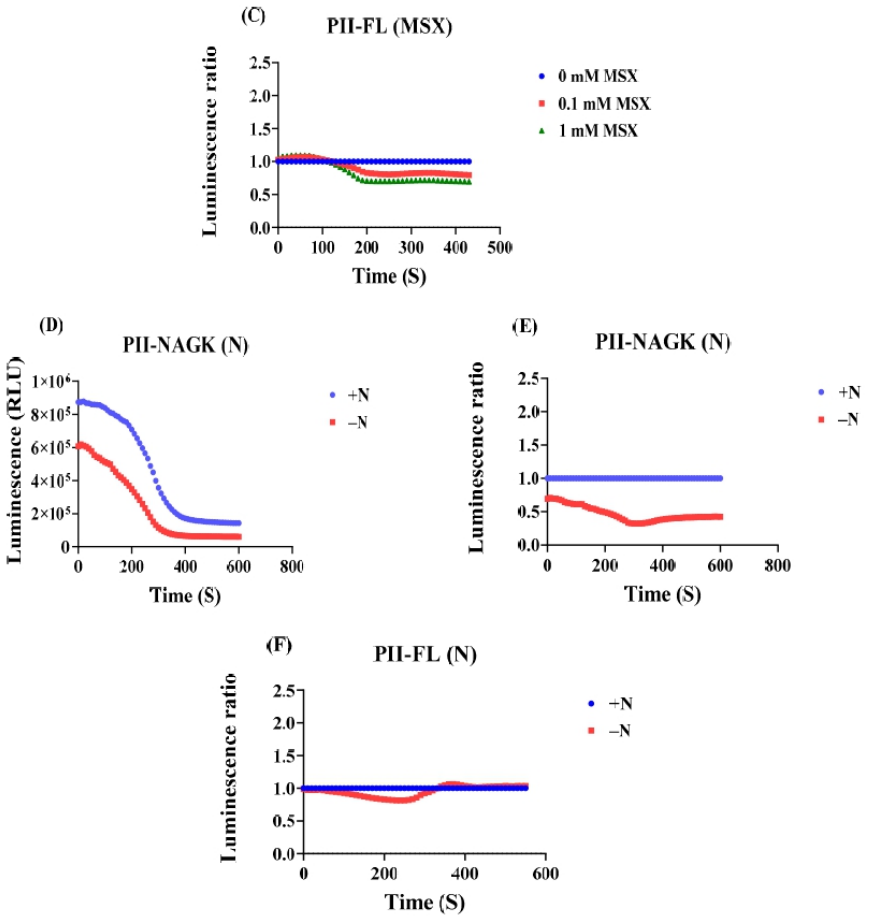

Figure 4. Luminescence response of cells carrying the PII-NAGK NanoBiT sensor following inhibition of ammonium assimilation by methionine sulfoximine (MSX) or following nitrogen starvation. For comparison, the normalized RLU curves of the PII-FL reporter subjected to the same treatments are shown (**E**,**F**). (**A**) RLU time-course measurement of the PII-NAGK NanoBiT sensor in the absence and presence of 0.1 mM and 1 mM MSX. (**B**) Normalizing the RLU response curve to the untreated reference (0 MSX). (**C**) Normalized RLU response curve upon MSX treatment using the PII-FL reporter. (**D**) RLU time-course measurement following nitrogen depletion. (**E**) Normalizing the RLU response curves shown in (**D**) to the untreated reference. (**F**) Normalized RLU response curve upon nitrogen-deprivation using the PII-FL reporter. Average values from three measurements are shown and error bars are removed for a better comparison. The average standard deviation (STD) of each of the three replicates of the PII-NAGK sensor for inhibition of ammonium assimilation by MSX and nitrogen starvation was less than 25%. The average standard deviation (STD) of each of the three replicates of the PII-FL sensor for inhibition of ammonium assimilation by MSX was less than 15%. The average standard deviation (STD) of each of the three replicates of the PII-FL sensor for nitrogen starvation was less than 13%.

2.3. Monitoring Metabolic Fluctuations Using the PII-PipX Sensor

Having confirmed the response of the PII-NAGK sensor pair to nitrogen assimilation perturbations, we subsequently employed the PII-PipX sensor pair in analogous experiments (Figure 5A–F), following the same experimental protocol as described above.

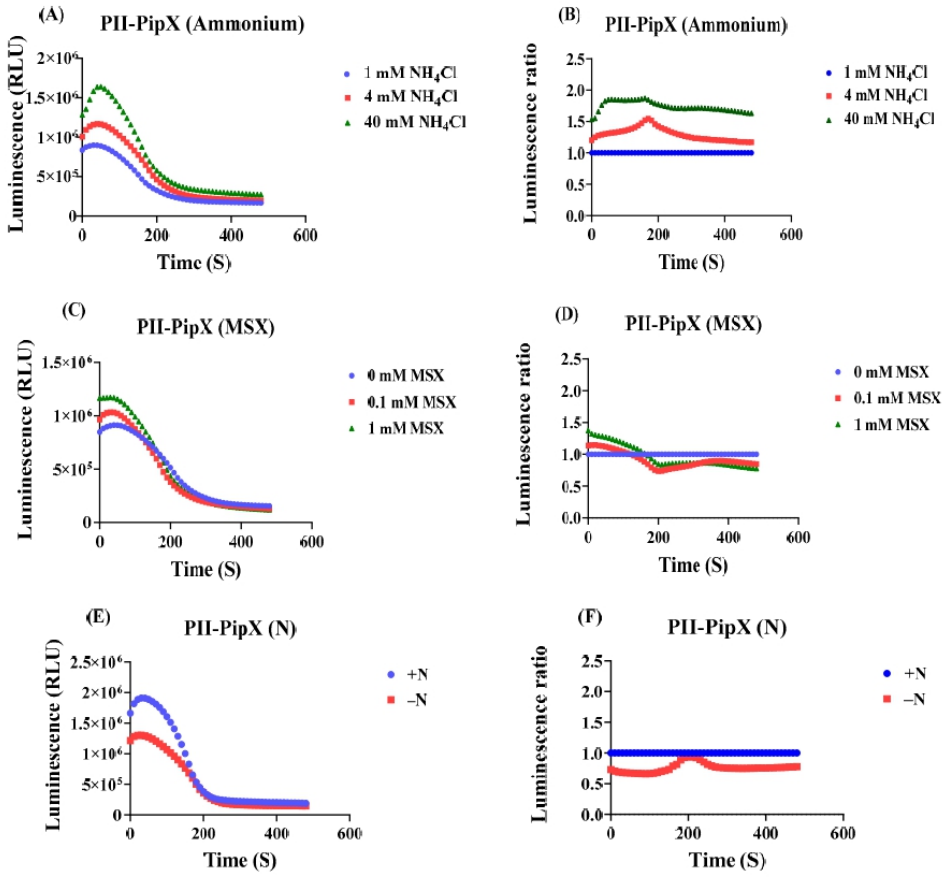

Figure 5. Effect of ammonium addition, MSX treatment and nitrogen starvation on luminescence after addition of luminescence reagent to cells carrying the PII-LgBiT—PipX-SmBiT sensor construct. (**A**) Time course of the luminescence signal (RLU) in untreated sample (1 mM NH_4Cl), and to samples, where the NH_4Cl concentration was increased to 4 mM or 40 mM. (**B**) Normalizing the RLU response curve of PII-PipX sensor to the reference sample. (**C**) RLU time course of PII-PipX NanoBiT sensor in the absence and presence of 0.1 mM and 1 mM MSX. (**D**) RLU response curves of (**C**) normalized to the reference sample. (**E**) RLU time course of PII-PipX NanoBiT sensor following nitrogen depletion. (**F**) RLU response curves of (**E**) normalized to the reference sample. Average values from three measurements are shown and error bars are removed for a better comparison. The average standard deviation (STD) of each of the three replicates of the PII-PipX sensor for ammonium treatments was less than 21%. The average standard deviation (STD) of each of the three replicates of the PII-PipX sensor for inhibition of ammonium assimilation by MSX was less than 24%. The average standard deviation (STD) of each of the three replicates of the PII-PipX sensor for nitrogen starvation was less than 23%.

In this case, the 40 mM NH_4Cl treatment caused a more rapid initial signal increase as compared to the PII-NAGK sensor and the elevated RLU remained at high level. The effect of 4 mM was delayed and reached a level between the untreated control and the 40 mM NH_4Cl treatment, similar to that which we observed for the PII-NAGK sensor pair. A quite different result was obtained in the nitrogen step-down experiments. Here, the PII-PipX sensor showed almost no response to the inhibition of nitrogen assimilation by MSX treatment. In the nitrogen step-down experiment, an immediate decrease in RLUs was observed. However, this decrease was followed by a subsequent increase to nearly

the initial RLU ratio. This clearly demonstrates that the PII-PipX NanoBiT sensor detects metabolic perturbations in a distinct manner compared to the PII-NAGK NanoBiT sensor. This agrees with the corresponding in vitro analysis of these sensor pairs, which showed that the PII-NAGK complex primarily responds to fluctuations in the 2-oxoglutarate levels, whereas PII-PipX interaction is strongly modulated by the presence of ADP.

2.4. Monitoring Metabolic Response upon Complete Nutrient Deprivation

The results obtained above suggested that in vivo fluctuations in 2-oxoglutarate levels are most sensitively detected by the PII-NAGK NanoBiT sensor. Therefore, we ultimately employed this sensor to monitor the metabolic response of *E. coli* cells towards an extremely stressful condition: shifting exponentially growing cells, cultivated in M9 medium, into distilled water: under these conditions, all nutrients are simultaneously removed.

We were curious to see the luminescence output from the PII-NAGK NanoBiT sensor. The experiment was carried out as described above and the PII-FL reporter was used as a control to monitor global effects on luminescence, which are independent on Split NanoBiT complex formation. As shown in Figure 6, the normalized signal measured with the PII-NAGK NanoBiT sensor increased immediately after the transfer and reached a 10-fold higher level 5 min after the transfer. By contrast, in the PII-FL control, only a marginal slow constant increase in relative RLU signal was visible. The strong increase detected in the PII-NAGK NanoBiT sensor cells indicates a dramatic reduction in the 2-oxoglutarate levels in response to shifting the cells to distilled water. This suggests that the cells consume the remaining TCA cycle metabolites, once nutrients are completely deprived.

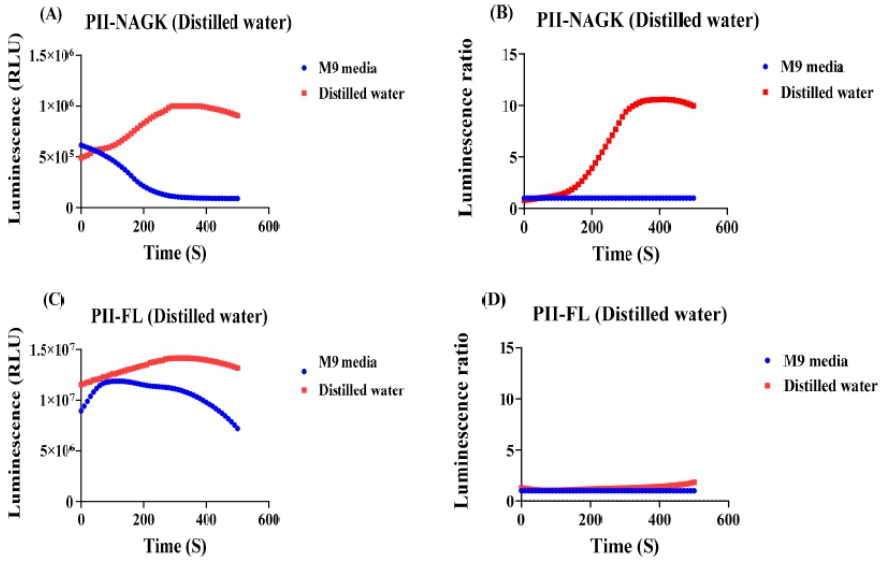

Figure 6. Detection of the metabolic response of E. coli cells shifted from M9 medium into distilled water, using the PII-LgBiT—NAGK-SmBiT sensor or as a control the PII-FL-reporter. (**A**) RLU response curve from the PII-LgBiT—NAGK-SmBiT sensor of treated sample (red) and untreated reference sample (blue) (**B**) RLU response curves of (**A**) normalized to the reference sample. (**C**) RLU response curve from the PII-FL reporter of treated sample (red) and untreated reference sample (blue). (**D**) RLU response curves of (**C**) normalized to the reference sample. Average values from three measurements are shown and error bars are removed for a better comparison. The average standard deviation (STD) of each of the three replicates of the PII-NAGK sensor for nutrient deprivation in distilled water was less than 18%. The average standard deviation (STD) of each of the three replicates of the PII-FL sensor for nutrient deprivation in distilled water was less than 11%.

3. Discussion

This work showed successful application of NanoBiT reporter constructs to follow in real-time changes in cellular 2-oxoglutarate levels. The in vivo interaction of recombinantly expressed PII-NAGK NanoBiT or PII-PipX NanoBiT sensor pairs in *E. coli* results in the reconstitution of the split NanoLuc reporter, which results in luminescence signals after adding the luminescence substrate. The background expression of the gene fusions form the pACYC-Duet vector, without addition of the inducer IPTG, was high enough to accurately measure the specific NanoBiT signals. Even low affinity interactions, such as the binding of the low-affinity PII-S49E variant to NAGK could be detected. Remarkably, a similar degree of NanoBiT reconstitution as obtained previously with purified proteins [24], demonstrating the reliability of the results.

Comparing the results with the two different PII interaction partners showed that the response of the NanoBiT sensors towards ammonium upshift yielded similar results for both, the PII-NAGK NanoBiT and PII-PipX NanoBiT senor pair. Previous metabolome analysis carried out by rapid sampling of *E. coli* cells following the addition of 10 mM NH_4Cl to nitrogen-limited cells showed a fast decline of 2-oxoglutarate levels and concomitantly to a rapid increase of glutamine levels [28]. Since the cyanobacterial PII and NAGK proteins do not respond to glutamine [19], it can be safely assumed that the observed increase in NanoBiT signals is indeed driven by the dropping 2-oxoglutarate levels. As also revealed by direct metabolite measurement, these changes occur in the range of a few minutes. After 2–3 min, the response is at its maximum [27,28].

In contrast to ammonium upshift treatments, only the PII-NAGK NanoBiT sensor was able to detect metabolic fluctuations induced by either the inhibition of nitrogen assimilation through glutamine synthetase inhibition or the removal of combined nitrogen sources. Previous metabolome analysis with *E. coli* cells revealed a rapid increase in 2-oxoglutarate levels, which would cause dissociation of PII-NAGK complexes. This agrees well with the observed rapid decline in the normalized RLU signals, which indicates dissociation of the PII-NAGK complex in vivo. Inhibition of glutamine synthetase or removal of combined nitrogen (ammonium) resulted in a similar response by the PII-NAGK NanoBiT sensor. This implies that transferring the *E. coli* cells into ammonium-free medium results in an immediate arrest of glutamine synthetase activity, like addition of the inhibitor MSX. In contrast to the PII-NAGK NanoBiT sensor, the PII-PipX NanoBiT sensor did not show a clear RLU decline. Previous in vitro analyses of PII interactions with NAGK or PipX work showed that in contrast to PII-NAGK complexes, the PII-PipX interaction is very sensitive towards subtle changes in ADP levels [25,26]. As the ADP concentrations increase, the affinity between PII and PipX increases. As shown by Zeth et al. [26], the conformation of PII in the ADP complex matches the conformation of PII in complex with PipX [26] and therefore, PipX and ADP act synergistically in binding to PII. The lack of efficient dissociation of the PII-PipX complex upon inhibition of glutamine synthetase reaction—in contrast to dissociation of the PII-NAGK NanoBiT pair imposed by increasing 2-oxoglutarate levels could be caused by subtly increasing ADP concentrations, which would prevent dissociation of PII-PipX complex but not that of the PII-NAGK complex. Dissociation of the latter complex was shown to be insensitive towards subtle fluctuations of ADP levels [26].

Overall, the PII-NAGK NanoBiT sensor described here appears to be a useful reporter to detect rapid fluctuations of cellular 2-oxoglutarate levels, both for increasing or decreasing levels. In our final experiment, we used this sensor to monitor the cellular response upon transferring exponentially growing cells into completely nutrient-free water. The reporter showed a maximal signal increase indicating full association of PII and NAGK, indicating extremely low 2-oxoglutarate levels. This metabolic response appears reasonable: in the absence of nutrients, the metabolites of the TCA cycle would be completely consumed for respiration until reaching a minimum. In a similar way, this reporter construct, cloned into appropriate expression plasmids, could provide easy and fast detection of real-time metabolic responses of bacterial cells towards various conditions. Eventually, when

cloned into appropriate expression plasmids, the sensor may also be applied for metabolite sensing in other cellular systems, like eukaryotic cell cultures, as NanoBiT reporters have extensively been used in mammalian cells [12–15].

4. Materials and Methods

Cloning of NanoBiT constructs: to create the split NanoLuc constructs for in vivo study, we used as vector backbone the pACYCDuet-1 plasmid (Addgene, Watertown, MA, USA), which is designed for the coexpression of two target genes [30]. Therefore, the vector contains two multiple cloning sites, into which the two NanoBiT partner constructs were cloned. Each cloning site is preceded by a T7 promoter, lac operator and ribosome binding site. The same NanoBiT gene fusions were used as previously described for in vitro investigation of PII interactions with its target proteins [24]. The gene encoding PII-LgBiT was cloned in the linearized vector with *Nco*I (New England Biolabs, Frankfurt am Main, Germany) in the first cloning site. NAGK-SmBiT or PipX-SmBiT were cloned into the *Nde*I (New England Biolabs, Frankfurt am Main, Germany) second cloning site for pACYCDuet vector following the protocol described by Gibson cloning previously [31]. The plasmid DNA was transformed into *E. coli* DH10β, and cultivated at 37 °C overnight on agar plates using the chloramphenicol antibiotic with the final concentration of 25 mg/mL for selection. Positive colonies were detected using colony PCR (Labcycler Basic, SensoQuest, Göttingen, Germany). These were then moved to Lysogeny broth (LB) [32] enriched with the chloramphenicol antibiotic and allowed to grow overnight at 37 °C. The plasmid DNA was extracted from the cells utilizing the Monarch Plasmid Miniprep Kit (New England Biolabs, Frankfurt am Main, Germany) following the guidelines provided by the manufacturer. The DNA sequences were confirmed by the GATC LIGHTRUN sequencing services (Eurofins Genomics, Ebersberg, Germany). After verification, the plasmids were transformed into electrocompetent *E. coli* BL21 (DE3) cells [33].

Cultivation of NanoBiT Expressing Cells and Luminescence Measurement

Cells from LB agar plates with the appropriate NanoBiT constructs were first cultivated overnight in LB with chloramphenicol antibiotic, from where an aliquot was removed to inoculate cells in M9 mineral salts medium supplemented with 0.4% glucose to an initial optical density (OD600) of 0.07. Cells were allowed to grow at 37 °C until an OD600 of 0.9 was reached, from where a second transfer of cells into M9 medium occurred, yielding a starting OD600 of 0.1. Cultivation was continued until an OD600 between 0.5 to 0.7 was reached. At this point, 500 µL aliquots of the culture were removed and used for bioluminescence recording, immediately after adding the bioluminescence reagent (Promega, Walldorf, Germany) together with the specific treatment that should result in metabolic perturbation. To assess the effects of various substances and inhibitors on live *E. coli* cells using real-time bioluminescence measurement, 20 µL of the selected concentration of the component was combined with 10 µL of Nano-Glo® Live Cell Reagent (made by mixing 1 part of Nano-Glo® Live Cell Substrate with 19 parts of Nano-Glo® LCS Dilution Buffer) (Promega, Walldorf, Germany) in a luminescence reaction tube. Following this, 500 µL of the bacterial culture was introduced to this mixture. The resulting luminescence was then measured for 5 s. with 5 s. delay using a Sirius Luminometer (from Berthold Detection System, Bad Wildbad, Germany) operated by FB12 Sirius Software, version 3.2 (Berthold Technologies, Bad Wildbad, Germany) for the indicated length of time. Measurement was immediately started by closing the luminometer's door. For each tested condition, at least three independent measurements (biological replicates) were carried out, from which the average RLU and the standard deviation at each time point were calculated. The graphs show the average value at each measured time point. For clarity of the presentation, the error bars are not shown. However, the average values of the standard deviations at any time point were calculated and the value is given in the legends to the figures.

For nitrogen depletion experiments, cells were cultivated as described above in M9 media until they reached an OD600 of approximately 0.6. Then, a 500 µL aliquot was

harvested by centrifugation for 60 s at 10,000 rpm (Thermo Scientific Pico 17 Microcentrifuge, Sindelfingen, Germany). Following the removal of the supernatant, the pellet was resuspended in 500 µL of M9 media without a combined-nitrogen source, and luminescence was immediately measured as described above.

5. Conclusions

We report here how the metabolite-sensitive protein interactions of the PII signalling protein were used to develop a sensor for real-time monitoring of metabolic fluctuations within living *Escherichia coli* cells. The PII-interactions reconstitute bioluminescence, sensitive towards metabolic perturbations, from in vivo expressed NanoBiT reporter constructs. We established an assay at negligible background luminescence, where the signals exhibit exceptional sensitivity and dynamic capabilities. Interaction of PII with its receptor NAGK in particular offers a robust platform for the detection of intercellular 2-oxoglutarate fluctuations. We could monitor the rapid metabolic responses of *E. coli* with a resolution of ten seconds in response to changing nitrogen supply. This study lays the groundwork for broader applications in metabolic studies, which should be possible in all organisms, in which the NanoBiT constructs can be expressed in vivo.

Author Contributions: R.R.: performed experiments, data analysis and visualization, preparation of tables and figures, writing preliminary drafts; K.F.: conceptualization and supervision, data analysis, manuscript writing. All authors have read and agreed to the published version of the manuscript.

Funding: This work was supported by the DFG funded collaborative research project FOR 2816 (FO195/16-2) and DFG grant Fo195/21-1 and by infrastructural funding via the Cluster of Excellence (EXC2124) "Controlling Microbes to Fight Infections".

Data Availability Statement: Data are contained within the article.

Acknowledgments: We acknowledge the contribution of Carmen Jerez Garcia in initial assay development.

Conflicts of Interest: The authors declare no conflict of interest.

References

1. Nooren, I.M.; Thornton, J.M. Diversity of protein–protein interactions. *EMBO J.* **2003**, *22*, 3486–3492. [CrossRef] [PubMed]
2. Keskin, O.; Tuncbag, N.; Gursoy, A. Predicting protein–protein interactions from the molecular to the proteome level. *Chem. Rev.* **2016**, *116*, 4884–4909. [CrossRef] [PubMed]
3. Liddington, R.C. Structural basis of protein-protein interactions. *Protein-Protein Interact. Methods Appl.* **2004**, *261*, 3–14.
4. Keskin, O.; Gursoy, A.; Ma, B.; Nussinov, R. Principles of protein− protein interactions: What are the preferred ways for proteins to interact? *Chem. Rev.* **2008**, *108*, 1225–1244. [CrossRef]
5. Blaszczak, E.; Lazarewicz, N.; Sudevan, A.; Wysocki, R.; Rabut, G. Protein-fragment complementation assays for large-scale analysis of protein–protein interactions. *Biochem. Soc. Trans.* **2021**, *49*, 1337–1348. [CrossRef]
6. Verhoef, L.G.; Mattioli, M.; Ricci, F.; Li, Y.-C.; Wade, M. Multiplex detection of protein–protein interactions using a next generation luciferase reporter. *Biochim. Biophys. Acta (BBA)-Mol. Cell Res.* **2016**, *1863*, 284–292. [CrossRef]
7. Westerhausen, S.; Nowak, M.; Torres-Vargas, C.E.; Bilitewski, U.; Bohn, E.; Grin, I.; Wagner, S. A NanoLuc luciferase-based assay enabling the real-time analysis of protein secretion and injection by bacterial type III secretion systems. *Mol. Microbiol.* **2020**, *113*, 1240–1254. [CrossRef] [PubMed]
8. Thalwieser, Z.; Király, N.; Fonódi, M.; Csortos, C.; Boratkó, A. Protein phosphatase 2A–mediated flotillin-1 dephosphorylation up-regulates endothelial cell migration and angiogenesis regulation. *J. Biol. Chem.* **2019**, *294*, 20196–20206. [CrossRef]
9. Yang, X.; Liu, L.; Hao, Y.; So, E.; Emami, S.S.; Zhang, D.; Gong, Y.; Sheth, P.M.; Wang, Y. A bioluminescent biosensor for quantifying the interaction of SARS-CoV-2 and its receptor ACE2 in cells and in vitro. *Viruses* **2021**, *13*, 1055. [CrossRef]
10. Tsang, T.F.; Qiu, Y.; Lin, L.; Ye, J.; Ma, C.; Yang, X. Simple method for studying in vitro protein–protein interactions based on protein complementation and its application in drug screening targeting bacterial transcription. *ACS Infect. Dis.* **2019**, *5*, 521–527. [CrossRef]
11. Wood, A.; Irving, S.E.; Bennison, D.J.; Corrigan, R.M. The (p)ppGpp-binding GTPase Era promotes rRNA processing and cold adaptation in Staphylococcus aureus. *PLoS Genet.* **2019**, *15*, e1008346. [CrossRef]
12. Pipchuk, A.; Yang, X. Using Biosensors to Study Protein–Protein Interaction in the Hippo Pathway. *Front. Cell Dev. Biol.* **2021**, *9*, 660137. [CrossRef]

13. Cooley, R.; Kara, N.; Hui, N.S.; Tart, J.; Roustan, C.; George, R.; Hancock, D.C.; Binkowski, B.F.; Wood, K.V.; Ismail, M. Development of a cell-free split-luciferase biochemical assay as a tool for screening for inhibitors of challenging protein-protein interaction targets. *Wellcome Open Res.* **2020**, *5*, 20. [CrossRef] [PubMed]
14. Sicking, M.; Jung, M.; Lang, S. Lights, Camera, Interaction: Studying Protein–Protein Interactions of the ER Protein Translocase in Living Cells. *Int. J. Mol. Sci.* **2021**, *22*, 10358. [CrossRef] [PubMed]
15. Kashima, D.; Kageoka, M.; Kimura, Y.; Horikawa, M.; Miura, M.; Nakakido, M.; Tsumoto, K.; Nagamune, T.; Kawahara, M. A Novel Cell-Based Intracellular Protein–Protein Interaction Detection Platform (SOLIS) for Multimodality Screening. *ACS Synth. Biol.* **2021**, *10*, 990–999. [CrossRef] [PubMed]
16. Paiva, A.M.O.; Friggen, A.H.; Qin, L.; Douwes, R.; Dame, R.T.; Smits, W.K. The bacterial chromatin protein HupA can remodel DNA and associates with the nucleoid in Clostridium difficile. *J. Mol. Biol.* **2019**, *431*, 653–672. [CrossRef] [PubMed]
17. Bardelang, P.; Murray, E.J.; Blower, I.; Zandomeneghi, S.; Goode, A.; Hussain, R.; Kumari, D.; Siligardi, G.; Inoue, K.; Luckett, J. Conformational analysis and interaction of the Staphylococcus aureus transmembrane peptidase AgrB with its AgrD propeptide substrate. *Front. Chem.* **2023**, *11*, 1113885. [CrossRef] [PubMed]
18. Forchhammer, K.; Selim, K.A.; Huergo, L.F. New views on PII signaling: From nitrogen sensing to global metabolic control. *Trends Microbiol.* **2022**, *30*, 722–735. [CrossRef]
19. Forchhammer, K.; Lüddecke, J. Sensory properties of the PII signalling protein family. *FEBS J.* **2016**, *283*, 425–437. [CrossRef]
20. Lüddecke, J.; Forchhammer, K. From PII signaling to metabolite sensing: A novel 2-oxoglutarate sensor that details PII-NAGK complex formation. *PLoS ONE* **2013**, *8*, e83181.
21. Chen, H.L.; Bernard, C.S.; Hubert, P.; My, L.; Zhang, C.C. Fluorescence resonance energy transfer based on interaction of PII and PipX proteins provides a robust and specific biosensor for 2-oxoglutarate, a central metabolite and a signalling molecule. *FEBS J.* **2014**, *281*, 1241–1255. [CrossRef]
22. Remy, I.; Michnick, S.W. Application of protein-fragment complementation assays in cell biology. *Biotechniques* **2007**, *42*, 137–145. [CrossRef]
23. Lüddecke, J.; Francois, L.; Spät, P.; Watzer, B.; Chilczuk, T.; Poschet, G.; Hell, R.; Radlwimmer, B.; Forchhammer, K. PII protein-derived FRET sensors for quantification and live-cell imaging of 2-oxoglutarate. *Sci. Rep.* **2017**, *7*, 1437. [CrossRef]
24. Rozbeh, R.; Forchhammer, K. Split NanoLuc technology allows quantitation of interactions between PII protein and its receptors with unprecedented sensitivity and reveals transient interactions. *Sci. Rep.* **2021**, *11*, 12535. [CrossRef] [PubMed]
25. Fokina, O.; Herrmann, C.; Forchhammer, K. Signal-transduction protein PII from Synechococcus elongatus PCC 7942 senses low adenylate energy charge in vitro. *Biochem. J.* **2011**, *440*, 147–156. [CrossRef] [PubMed]
26. Zeth, K.; Fokina, O.; Forchhammer, K. Structural basis and target-specific modulation of ADP sensing by the Synechococcus elongatus PII signaling protein. *J. Biol. Chem.* **2014**, *289*, 8960–8972. [CrossRef] [PubMed]
27. Radchenko, M.V.; Thornton, J.; Merrick, M. Association and dissociation of the GlnK–AmtB complex in response to cellular nitrogen status can occur in the absence of GlnK post-translational modification. *Front. Microbiol.* **2014**, *5*, 124255. [CrossRef] [PubMed]
28. Yuan, J.; Doucette, C.D.; Fowler, W.U.; Feng, X.J.; Piazza, M.; Rabitz, H.A.; Wingreen, N.S.; Rabinowitz, J.D. Metabolomics-driven quantitative analysis of ammonia assimilation in *E. coli*. *Mol. Syst. Biol.* **2009**, *5*, 302. [CrossRef] [PubMed]
29. Yuan, J.; Bennett, B.D.; Rabinowitz, J.D. Kinetic flux profiling for quantitation of cellular metabolic fluxes. *Nat. Protoc.* **2008**, *3*, 1328–1340. [CrossRef] [PubMed]
30. Merck. *pACYCDuet™-1 DNA—Novagen*; Merck: Darmstadt, Germany, 2024.
31. Addgene. *Gibson Assembly Cloning*; Addgene: Watertown, MA, USA, 2024.
32. Bertani, G. Studies on lysogenesis I: The mode of phage liberation by lysogenic *Escherichia coli*. *J. Bacteriol.* **1951**, *62*, 293–300. [CrossRef] [PubMed]
33. Studier, F.W.; Daegelen, P.; Lenski, R.E.; Maslov, S.; Kim, J.F. Understanding the differences between genome sequences of *Escherichia coli* B strains REL606 and BL21 (DE3) and comparison of the *E. coli* B and K-12 genomes. *J. Mol. Biol.* **2009**, *394*, 653–680. [CrossRef] [PubMed]

X. ACKNOWLEDGMENTS

I would like to express my deepest gratitude to all individuals who contributed to the completion of this thesis.

First and foremost, I extend my heartfelt thanks to my supervisor, Prof. Karl Forchhammer, for his invaluable mentorship, persistent encouragement, and insightful feedback throughout my research journey. His expertise and dedication have profoundly enriched my academic experience. My special thanks also go to my second supervisor, Christiane Wolz, for accepting the responsibility of assessing this work.

Furthermore, I would like to thank Iris for her valuable contributions to our research group and for her guidance during the course of my thesis work. Many thanks to Jörg for his supervision and assistance during the initial stages of my PhD, and to Adrian and Khaled for their helpful suggestions and constructive feedback, which have enhanced the quality of my work.

I extend my deepest gratitude to my friends Ritu, Sofia, Ana, and Tchini for creating a supportive atmosphere in the lab. Their friendship and encouragement during challenging times have been invaluable, and I am truly grateful for their presence in my academic journey. Additionally, I want to thank my coworkers Markus and Michael for their collaboration and for making an enjoyable atmosphere in our lab.

I am thankful to Nike, Janette, Nelli, Niels, Moritz, Björn, Anka, Eva, Johanna, Antje, Alex, Philip, Klaus, and Tim for being wonderful colleagues. Our cheerful moments during breaks were cherished, and their willingness to offer assistance throughout this project was greatly appreciated.

I would like to extend my appreciation to our secretaries and technicians Michaela, Claudia, Carolina, Louisa, Eva, and Hainz for their administrative support and technical assistance.

I am deeply thankful to my friends Aida, Nasrin, Elnaz, Elaheh, Raheleh, and Saeed for always being positive and staying by my side like a family. Their presence has made this journey more enjoyable and smoother.

A special acknowledgment goes to my friend Ali for his support during the ups and downs of this period. His encouragement has been a source of inspiration.

I am forever grateful to my family, especially my parents, my brothers, Mohammad and Hossein, and my sister, Reihaneh. I owe a debt of gratitude for their unwavering support and encouragement from afar. Their love and encouragement have been a constant source of strength throughout this journey.

I am sincerely grateful to anyone else who has contributed to my academic and personal growth.